2005

MICROELECTRODE ARRAY STUDIES OF NORMAL AND DISEASE-ALTERED L-GLUTAMATE REGULATION IN THE MAMMALIAN CENTRAL NERVOUS SYSTEM

Brian Keith Day
University of Kentucky

ABSTRACT OF DISSERTATION

Brian Keith Day

The Graduate School
University of Kentucky
2005

MICROELECTRODE ARRAY STUDIES OF NORMAL AND DISEASE-ALTERED L-GLUTAMATE REGULATION IN THE MAMMALIAN CENTRAL NERVOUS SYSTEM

ABSTRACT OF DISSERTATION

A dissertation submitted in partial fulfillment of the
requirements for the degree of Doctor of Philosophy in the
College of Medicine
at the University of Kentucky

By
Brian Keith Day

Lexington, Kentucky

Director: Dr. Greg A. Gerhardt, Professor of Anatomy and Neurobiology

Lexington, Kentucky

2005

ABSTRACT OF DISSERTATION

MICROELECTRODE ARRAY STUDIES OF NORMAL AND DISEASE-ALTERED L-GLUTAMATE REGULATION IN THE MAMMALIAN CENTRAL NERVOUS SYSTEM

L-glutamate (Glu) is the major excitatory neurotransmitter in the mammalian central nervous system. Monitoring extracellular Glu is critical to understanding Glu regulation to discriminate physiological and pathological roles. To overcome the limitations of previous *in vivo* extracellular Glu studies, we developed Glu selective microelectrode arrays with better spatial and temporal resolutions than commonly used techniques like microdialysis. We used these microelectrode arrays to characterize basal and potassium-evoked Glu neurotransmission in the normal rat brain. We then investigated disease-related Glu alterations in a rat model of Parkinson's disease and normal Glu regulation in young and aged rhesus monkeys. In the normal anesthetized rat striatum and frontal cortex, basal Glu was regulated by active release and uptake mechanisms, fully TTX-dependent, and measured at ~2 micromolar levels. Potassium-evoked Glu kinetics were fast, concentration-dependent, and rapidly reproducible at 15-20 seconds intervals. In the unilateral 6-hydroxydopamine-lesioned rat, there were significant bilateral increases in potassium-evoked Glu release in the striatum and frontal cortex compared to hemisphere-matched non-lesioned rats. Ipsilateral striatal effects may have been related to DA loss, while contralateral striatal effects and the bilateral frontal cortical

effects may have resulted from parkinsonian neurotransmitter changes or bilateral neuranatomical connectivity, especially in the cortex. There were also alterations in Glu kinetics in the nucleus accumbens in both non-lesioned and lesioned rats. With appropriate technological and methodological modifications, we successfully recorded normal Glu signaling in anesthetized nonhuman primates in the operating room. Fast potassium-evoked Glu signals were recorded in the motor cortex of all monkeys, and Glu ejections showed robust Glu uptake in the motor and frontal cortices of all monkeys. These findings are comparable to initial rat studies. Slow evoked Glu kinetics and high basal Glu levels with oscillatory behavior were recorded in the frontal cortex. The primary age-related differences between monkeys were the nearly ten-fold increases in the volumes of Glu ejected needed in the aged monkey to achieve amplitude-matched signals in the motor and frontal cortices and a decreased uptake rate in the motor cortex. Preliminary work with excised human tissue and future plans for patient-oriented research and clinical applications are discussed.

KEYWORDS: Glutamate, Microelectrode, Voltammetry, Rat, Nonhuman primates

Brian Keith Day

06/27/05

MICROELECTRODE ARRAY STUDIES OF NORMAL AND DISEASE-ALTERED L-GLUTAMATE REGULATION IN THE MAMMALIAN CENTRAL NERVOUS SYSTEM

By

Brian Keith Day

Greg A. Gerhardt
Director of Dissertation

Douglas Gould
Director of Graduate Studies

06/27/05

RULES FOR THE USE OF DISSERTATIONS

Unpublished dissertations submitted for the Doctor's degree and deposited in the University of Kentucky Library are as a rule open for inspection, but are to be used only with due regard to the rights of the authors. Bibliographical references may be noted, but quotations or summaries of parts may be published only with the permission of the author, and with the usual scholarly acknowledgments.

Extensive copying or publication of the dissertation in whole or in part also requires the consent of the Dean of the Graduate School of the University of Kentucky.

A library that borrows this dissertation for use by its patrons is expected to secure the signature of each user.

Name Date

DISSERTATION

Brian Keith Day

The Graduate School
University of Kentucky
2005

MICROELECTRODE ARRAY STUDIES OF NORMAL AND DISEASE-ALTERED L-GLUTAMATE REGULATION IN THE MAMMALIAN CENTRAL NERVOUS SYSTEM

DISSERTATION

A dissertation submitted in partial fulfillment of the
requirements for the degree of Doctor of Philosophy in the
College of Medicine
at the University of Kentucky

By
Brian Keith Day

Lexington, Kentucky

Director: Dr. Greg A. Gerhardt, Professor of Anatomy and Neurobiology

Lexington, Kentucky

2005

Dedicated to my wife Misty, parents Judy and Fred, and friends

ACKNOWLEDGMENTS

This work would not have been possible without the insight and direction of many people. First, I would like to thank my Dissertation Advisor, Dr. Greg A. Gerhardt, for providing guidance, encouraging independence, and thinking big. François Pomerleau, Peter Huettl, and Jason Burmeister were instrumental in my early training and always gave me honest feedback. Robin Lindsay provided steadfast support. Jorge Quintero provided experimental support and dissertation assistance. Indeed, all of the Gerhardt lab personnel were committed to advancing science in a fun environment. I also wish to thank our collaborators: Lotta Granholm, Ph.D. and Lauren Willis (MUSC, lesioned rat study); Richard Grondin, Ph.D., Zhiming Zhang, M.D., Liming Luan, M.D., and Eric Forman (UK, rhesus macaque study); and Craig van Horne, M.D., Ph.D. and Beth Noll (Harvard University, excised human tissue study). Furthermore, I would like to thank my Dissertation Advisory Committee and outside reader: Drs. Don M. Gash, James W. Geddes, Linda Dwoskin, Subbu Apparsundaram, and James Flesher. Their advice has challenged my thinking, planning, and execution, and, in doing so, contributed to my professional growth and to the quality of this dissertation. I would also like to thank the members of the UK M.D./Ph.D. program and Charlie Snow, Ph.D. (director) for their guidance and support. Finally, I would like to thank my early mentors who encouraged me to pursue a career in science and medicine, especially Kirkland Housemaster Don Pfister, Ph.D. and U.S. Army Col. Geoffrey S.F. Ling, M.D., Ph.D.

The personal support of family and friends was also invaluable. I would like to thank my wife Misty for her encouragement, understanding, and emotional and intellectual support. My mother and father, Fred and Judy Day, taught me dedication to always do my best and the rewards of hard work. They believed in me and expected great things. My friends, from Boston to Lexington, always stood by me as I pursued my goals but stayed quick to remind me to relax and find balance. Thanks John, Luke, Ray, Todd, Washington, Phil, Matt, Justin, Erin, and Kevin.

TABLE OF CONTENTS

LIST OF TABLES

LIST OF FIGURES

Chapter One: Introduction

A Brief Introduction to Intracranial Electrode Applications

This dissertation documents continuing work towards the long-term goal of clinically using implanted microelectrode arrays that detect specific neurochemicals to positively impact the management of human neurological diseases. Although the concept of putting electrodes into the human brain may sound like science fiction or at least an extreme medical approach, in fact, neurosurgeons routinely use a wide variety of intracranial electrodes to care for patients in the modern era. Both recording and stimulating electrode protocols have become standards of care or good alternative approaches for patients suffering from brain disorders such as Parkinson's disease (PD) and epilepsy (Starr, Vitek, and Bakay, 1998, Wyler and Abson-Kraemer, 1994). Ultimately, we hope that microelectrodes coupled with electrochemical detection will provide similar benefit and take their place alongside other intracranial electrodes used to monitor, diagnose, and treat human nervous system disorders.

Both recording and stimulating electrodes are used in the surgical treatment of PD, a progressive neurodegenerative disease which primarily affects movement. When the symptoms are no longer well-controlled by standard medications, advanced PD patients may elect to ablate or stimulate different subcortical areas of their brains. These approaches attempt to alter signals emerging from the basal ganglia or thalamus to alleviate some parkinsonian symptoms. Targeting deep brain nuclei usually begins with an imaging study (computed tomography (CT) and/or magnetic resonance imaging (MRI)) but is routinely accompanied by intraoperative electrophysiological brain recordings that use implanted electrodes. Because the patterns of spontaneous neuronal firing predictably differ between discrete brain nuclei, electrodes can be used to precisely locate brain areas of interest. Typically tungsten or platinum-iridium microelectrodes are used to record single-unit, extracellular action potentials for

this type of mapping. In addition or as an alternative, stimulation protocols can be followed which use these microelectrodes (microstimulation) and/or macroelectrodes (macrostimulation) and rely on reported or observed changes in visual, motor, or sensory responses to localize electrode placement. In the case of ablation, alternating current can be passed in a monopolar fashion from the electrode to a dispersive grounding pad on the patient's skin to lesion the targeted area, a technique known as radiofrequency thermocoagulation. In fact, pallidotomies and thalamotomies (ablative surgeries which target the globus pallidus internal segment (GPi) and motor thalamus, respectively) most often use this technique (Krauss and Jankovic, 1996, Starr, Vitek, and Bakay, 1998, Krack et al., 2000).

PD patients who decide with their physicians that permanent lesioning is not the best option may elect to have a chronic indwelling stimulating electrode, called a deep brain stimulator (DBS), implanted in one or both brain hemispheres (Starr, Vitek, and Bakay, 1998). Again, confirming placement of the DBS electrode may involve initial microelectrode mapping or microstimulation, and the DBS electrode itself can be used for localizing macrostimulation prior to final placement. Although some clinical researchers have questioned the benefit of extensive microelectrode mapping, it is highly accepted that some form of recording or stimulation is absolutely critical for electrode placement (Eskandar et al., 2000, Guridi et al., 2000, Pollak et al., 2002). An extension wire is tunneled under the patient's skin and connected to a battery-powered pulse generator implanted in the patient's upper chest. A physician programs the stimulation parameters of the pulse generator using a wireless controller, and the patient can turn the stimulator on or off as needed. Early applications of DBS electrodes targeted the thalamus; however, the GPi and subthalamic nucleus (STN) are becoming increasingly popular targets (Olanow, Brin, and Obeso, 2000). Exactly how deep brain stimulation works to alleviate PD symptoms is unknown; functional lesioning and altering basal ganglia signaling are leading theories (Starr, Vitek, and Bakay, 1998, Benazzouz and Hallett, 2000).

A wide variety of electrodes are also used in the surgical management of patients with intractable epilepsy, a brain disorder characterized by multiple seizures caused by abnormal cerebral electrical activity. The goal is to identify and remove epileptogenic foci, which are local networks of hyperactive neurons that burst-fire continuously, often at levels sufficient to initiate an epileptic seizure. Strip, grid, and depth electrodes are all useful intra- and post-operative tools that aid in the search for epileptogenic foci (Wyler and Abson-Kraemer, 1994). Strip and grid electrodes are both implanted in the epidural or subdural spaces in close contact with the cortical surface and differ primarily in their geometry. Strip electrodes have 2-16 circular contacts arranged in a linear fashion on a flexible, flat plastic strip. Grid electrodes are two-dimensional arrays that have 40-64 circular contacts and are basically parallel rows of strip electrodes. Depth electrodes have 6 cylindrical contacts fabricated along flexible tubing similar to a catheter that can be implanted into deep brain structures using a rigid guide cannula (McCarthy, Spencer, and Riker, 1991). All three types of electrodes are used to make electroencephalographic (EEG) recordings of brain activity, and epileptogenic foci can be localized in relation to EEG findings from the multiple recording sites (Olivier and Boling, Jr., 1994). Sometimes it is necessary to determine the relationship of an epileptogenic focus to functional cortex using a technique known as cortical mapping. This requires using an implanted grid electrode with bipolar stimulation to determine the functional significance of cortical regions near the area targeted for resection. In this way, cortex that, if removed, would severely impair the patient is identified (Wyler and Abson-Kraemer, 1994). Epileptogenic foci tend to be surgically removed not ablated as previously discussed (Kim and Spencer, 1994).

Clearly, intracranial electrode applications such as electrophysiological recordings and the ability to stimulate brain regions are common, valuable tools used to monitor and manipulate the intracranial environment to benefit patient care; however, physicians and scientists alike have been interested in complementing these techniques with the ability to monitor specific neurochemicals in the intact brain. Neurochemicals, such as neurotransmitters,

are key components of the nervous system because the major communication system between neurons is chemical signaling (Cooper, Bloom, and Roth, 1996). Advancing the techniques employed to investigate neurochemicals will deepen our insight and understanding of the biology, pathology, and pharmacology of the nervous system. Currently the most widely used technique to study neurochemicals is intracerebral microdialysis (Timmerman and Westerink, 1997). However, the limitations of this technique (discussed later) have motivated some scientists to develop new technologies to monitor molecules in the intracranial environment. In the last decade, our group has developed enzyme-coated ceramic-based microelectrode arrays capable of recording specific neurochemicals and created exciting new tools for basic scientific research. Already these high-quality devices are routinely used in animal models and may soon record Glu from an intact human brain. This dissertation documents how we have pushed this technology from the lab bench to the veterinary operating room and beyond on a course to advance and diversify the ways that we study the brain and possibly manage patients in the 21st century.

The Evolution of Enzyme-Coated Ceramic-Based Microelectrode Arrays

The idea of coupling enzyme reactions with electrodes to measure biologically active molecules extends at least as far back as 1966 when Kajihara and Hagihara reported measuring serum glucose levels using an oxygen electrode coupled with glucose oxidase. Other groups were also working with the concept; Updike and Hicks (1967) reviewed “The enzyme electrode” in *Nature* the following year. By 1970, Guilbault and Hrabankova had expanded the list of measurable chemicals to include the amino acids, but it was not until 1987 that Korenbrot, Perry, and Copenhagen reported an enzyme electrode specifically for the measurement of L-glutamate. Work continued, but the new technologies suffered from slow response times, poor selectivities, inadequate sensitivities, and limited *in vivo* applications. In the early 1990’s, the first reports of Glu

recordings in the intact brain emerged (Tamiya and Karube, 1992, Hu et al., 1994). Although it would take many more years to improve the quality and reproducibility of electrode fabrication and performance, the technology was beginning to move beyond the development stages and enter the exciting era of *in vivo* applications.

The electrode design and performance of Hu et al. (1994), in particular, surpassed the rest and served as one of the predecessors to our group's enzyme-coated ceramic-based microelectrode arrays. Their electrode consisted of a Teflon-coated platinum-iridium wire stripped at the end and epoxyed at the tip to create a ~700 micron long sensing cavity. Nafion™ and cellulose acetate coatings, applied first, provided electrostatic repulsion of anionic interferents, while subsequent application of L-glutamate oxidase and L-ascorbate oxidase in a bovine serum albumin/glutaraldehyde protein matrix provided sensitivity to Glu and further selectivity against ascorbic acid. Sealed in glass, starting 8-12 mm behind the sensing cavity, the electrode was rigid enough for stereotactic implantation into the brain of anesthetized rats. Beyond what we now recognize as several time-tested design elements, the electrode performed exceptionally well, using high-speed amperometry to record Glu signals not just *in vitro* but *in vivo*. In the rat hippocampus, they investigated Glu uptake with exogenous challenges as well as both potassium-evoked and electrically stimulated Glu release. With average sensitivity, selectivity, limit of detection, and response speed on par with even today's standards, their enzyme-based electrode truly set the bar.

However, there was room for improvement. Demonstrating reproducibility of evoked Glu signals required a 20 minute rest interval presumed by the authors to be necessary for neurotransmitter replenishment. This was despite the fact that the recorded Glu signals lasted only ~1 minute, and intracellular Glu levels were known to be sufficiently high to make a lengthy rest period for replenishment unlikely. Furthermore, the electrode lost on average over 50% sensitivity following brain exposure. It was a hand-made electrode that could not easily be mass-produced for distribution or readily fabricated by other

investigators. Despite its reported *in vitro* selectivity, the singular nature of the electrode left the identity of its signal as Glu open to criticism without difficult placement of a second, Glu-insensitive but otherwise identical, electrode within microns of the first.

While enzyme-based techniques were advancing our ability to use electrodes to detect specific chemicals, new electrode materials were being developed, in parallel, to create semi-conductor based, multisite microelectrodes as early as the 1970's (Sreenivas et al., 1996, Burmeister, Moxon, and Gerhardt, 2000). Multisite microelectrodes had many potential advantages over single electrodes including reproducible recording sites, spatially defined sites for layered brain structures, and the possibility of simultaneous electrophysiological and electrochemical recordings using the same microelectrode. They might also offer distinctly configured recording sites for multiple analytes or monitoring interferences. It also might be possible to supply investigators with a highly reproducible, affordable recording device. By the mid 1990's, micromachining, integrated circuit technologies, thin-film deposition techniques, and photolithographic patterning had advanced the field tremendously. However, the initial silicon-based sputtered-carbon microelectrode arrays that our group developed suffered from an undesirable electrical conductance of the silicon substrate, which was likely the cause of a high background current and poor signal-to-noise characteristics seen in initial studies (Sreenivas et al., 1996). To remedy these problems, the silicon was replaced by an inert ceramic substrate with polyimide insulation, which was also used to improve strength, diminish cross talk, provide greater versatility, and lower production costs (Burmeister, Moxon, and Gerhardt, 2000). Because carbon will not stick to ceramic without extensive surface modifications, the recording site material was changed to sputtered platinum. This also provided a better surface to detect the products of enzyme-based chemical reactions.

In the late 1990's and early 2000's, our refined ceramic-based multisite microelectrode arrays demonstrated fast and reliable Glu detection with low detection limits (0.25 – 0.50 μM Glu), enhanced sensitivity, good selectivity

(>100:1 versus ascorbic acid), fast response times (90% rise times = 1 second), and superior spatial and temporal resolutions (Burmeister, Moxon, and Gerhardt, 2000, Burmeister and Gerhardt, 2001). We used procedures modified from Hu et al. (1994) to prepare our microelectrodes (full description in Chapter Two) and began using them routinely for *in vivo* studies (Burmeister et al., 2002, Pomerleau et al., 2003). Our lab's commitment to technology development has continued to improve the quality and versatility of the recording capabilities. At the same time, we have broadened our focus to explore biological applications. Currently, our microelectrode arrays have been used to record Glu in anesthetized mice and rats, freely-moving rats, rat brain slices, anesthetized monkeys, and excised human brain tissue. They have also been used for electrophysiological and electrochemical (Glu) recordings in the awake, behaving monkey, and using other enzyme coatings, have been reconfigured to characterize other neurotransmitters using electrochemical detection including glucose, aspartate, choline, acetylcholine, and lactate (Burmeister and Gerhardt, 2001, Parikh et al., 2004, Burmeister, Palmer, and Gerhardt, 2005). This dissertation documents my role in this team effort to advance how we can use this technology to investigate normal and disease-altered biology and contribute to both science and medicine.

Microelectrode Arrays vs. Microdialysis for Studying L-Glutamate

Microelectrode-based recording techniques are not the only approaches used to monitor the chemical composition of the extracellular space of the brain. In fact, the most widely used techniques are based on intracranial microdialysis, which produces dialysate fluid samples for analysis (Khan and Shuaib, 2001). The main advantage of microdialysis methods is the ability to couple sampling with highly sensitive detection systems, such as high performance liquid chromatography and electrochemical or fluorescence detection. The detection limits of these systems for Glu are in the nanomolar to femtomolar range (Zhang

et al., 2005, Smolders et al., 1995, Rowley, Martin, and Marsden, 1995). Another advantage of microdialysis is the ability to measure multiple chemicals from each sample. Often *in vivo* microdialysis studies will profile multiple amino acids (e.g. Glu, γ-aminobutyric acid (GABA), glycine, aspartate, taurine) or other neurochemicals over the time course of the experiment (Qureshi et al., 2003, Qu et al., 1998). These capabilities certainly make this technique attractive for many applications.

Nonetheless, there are disadvantages to microdialysis-based techniques that limit their usefulness in certain cases. Many of these limitations stem from the microdialysis probe and the way in which it creates samples for analysis. Microdialysis probes basically are constructed of two steel tubes (inlet and outlet) connected at the tip by a semipermeable dialysis membrane. Once implanted in the brain, perfusion fluid is slowly pumped through the probe (typical flow rate: 1-2 µl/minute) allowing bidirectional exchange of small molecules across the membrane (Berners, Boutelle, and Fillenz, 1994). Because molecules will move along their concentration gradients, microdialysis probes can be used for local drug application (reverse microdialysis) as well as for sampling from the extracellular fluid (Khan and Shuaib, 2001). Volumes of dialysate are collected at the end of the outlet tube outside of the brain and typically frozen for off-line analysis. During sampling, concentrations of extracellular molecules do not completely equilibrate with the artificial medium. In fact, *in vitro* recovery testing is a routine part of most microdialysis studies. As a result, microelectrode recordings have the distinct advantage over microdialysis-coupled detection methods of actually measuring molecules in the extracellular fluid.

Other advantages of microelectrodes over microdialysis probes are their size and spatial resolution. A typical cylindrical microdialysis probe (CMA/11, CMA Microdialysis AB, North Chelmsford, MA) has a 1-4 mm long dialysis membrane with a 0.24 mm outer diameter. Comparatively, the implantable 0.005 ± 0.0005” (~130 ± 13 µm) thick ceramic portion of a microelectrode array is 10 mm long, with a triangular shape that tapers from 1 mm at the base to 2-5 µm at the tip (Burmeister et al., 2002). The center of the array is positioned 1.0 mm

from the tip, and the length of the array is 766 μm (length includes all four 15 x 333 μm recording sites and 100 μm front-to-back spacing). Based on these dimensions, both the volumes of displacement and the surface areas at the sampling/recording interfaces can be calculated and compared. A typical microdialysis probe displaces approximately 5 to 18 times as much brain tissue along the interface length as compared to our microelectrode arrays (0.05 - 0.18 mm^3 vs. ~0.01 mm^3). Furthermore, the described dialysis membrane makes contact with about 150 – 600 times as much brain tissue as one microelectrode recording site (0.75 – 3.02 mm^2 vs. 4995 μm^2). In the era of using electrophysiological data in conjunction with neurochemical detection, the impetus with respect to size has been to develop smaller devices and interfaces that will potentially be less disruptive, closer to the synapse, and in contact with fewer cells. This may be especially important for studying Glu, which is thought to be tightly regulated perisynaptically (Danbolt, 2001). Although both techniques measure extrasynaptic Glu, microelectrodes are smaller and have much better spatial resolution.

Probably the single greatest advantage of using microelectrodes over typical microdialysis is better temporal resolution (800 msec vs. typically 5-20 min). The highly sensitive detection systems used for microdialysis require adequate sample volumes (~10-20 nl). Flow rates greater than 2 μl/minute would create these volumes more quickly, but this approach is impractical because of poorer relative recovery, potential for creating non-physiological conditions around the probe, and possible tissue damage (Rossell, Gonzalez, and Hernandez, 2003). As such, a typical off-line microdialysis study might perfuse fluid at 1-2 μl/minute with dialysate fractions collected every 5-20 minutes. Because it is widely recognized that small or rapid changes in neurochemicals might be missed altogether using microdialysis as described, proponents of the technique have pushed to improve the temporal resolution of the methods. Primarily, investigators have reported improved temporal resolution by combining dialysate outflow with on-line sample separation and subsequent small volume detection methods (both on- and off-line). The best example to date would be the

use of capillary (zone) electrophoresis separation and laser-induced fluorescence detection (CE-LIFD) employed by several groups who report temporal resolution of only a few seconds (Tucci et al., 1997, Lada, Vickroy, and Kennedy, 1997, Rossell, Gonzalez, and Hernandez, 2003). The Hernandez group, in particular, couples microdialysis on-line with derivatization reactions in a cellulose-based capillary collection tube, which is cut into small sections, and claims 1 second time resolution corresponding to the length of each section. Under this logic, they could lower the temporal resolution of their method simply by cutting smaller sections of the collection tube. However, the true temporal resolution of microdialysis methods is limited by the number of seconds required for small molecule diffusion and equilibration across the microdialysis membrane. As such, temporal resolution of only a few seconds achieved by investigators such as the Kennedy group may realistically be the lower limit of microdialysis methods. In addition, microdialysis-based measurements are time-delayed from the actual intracranial events by minutes to days, even with on-line detection. In contrast, our microelectrodes sample the extracellular fluid and record Glu every 800 msec. Furthermore, Glu signals are displayed as they happen in the brain on a second-by-second basis. In fact, we have recently developed software capable of recording average Glu measurements forty times per second, although recordings made at that speed are not yet routine. Clearly, our temporal resolution is much better than typical off-line microdialysis methods and continues to outperform the best on-line adaptations.

A commonly underreported aspect of using implanted devices for measuring small concentrations of molecules under physiological conditions is tissue trauma. This consideration is especially important for measuring Glu, which is present at very high amounts inside all brain cells (10 mM, Meldrum, Akbar, and Chapman, 1999), because traumatized cells could leak Glu into the extracellular space and obscure experimental findings. It is widely known that inflammation follows microdialysis probe implantation, and there is increased glucose metabolism and decreased blood flow around the probe within the first 24 hours. Using both light and electron microscopy to observe microdialysis-

sampled brain tissue, several ultrastructural changes were reported. Tissue disruption was apparent up to 1.4 mm from the probe tract, there was asymmetric (glutamatergic) synapse loss and decreased neuron density up to 400 μm from the implantation site, and swollen mitochondria and endoplasmic reticulum were observed (Clapp-Lilly et al., 1999, Khan and Shuaib, 2001, Drew et al., 2004). Although a full analysis of tissue damage related to implanting our microelectrode arrays has not been conducted, initial work has revealed minimal trauma even with microelectrodes implanted for 2 months. Strong indirect evidence comes from recent electrophysiological recordings made with our microelectrodes demonstrating that the neurons remain functionally intact following implantation for up to 6 months (Deadwyler and Gerhardt, unpublished data). Although further work is needed, these results support that our microelectrodes may produce less tissue trauma due to their size, tapered design with smooth edges, and means of operation.

The shortcomings of microdialysis for the measurement of Glu and GABA have come under particular scrutiny. Glu and GABA measures in microdialysis studies are often reported to have non-classical neurotransmitter characteristics. In short, tetrodotoxin (TTX) applications and calcium removal, conditions which should inhibit neuronal vesicular release of neurotransmitters, are widely reported to have no effect on basal Glu and GABA measures (Shiraishi et al., 1997, Timmerman and Westerink, 1997). As a result, many investigators have concluded that basal levels of these neurochemicals originate purely from non-neuronal sources such as uptake reversal and glial metabolism. However, Timmerman and Westerink (1997) and more recently Drew et al. (2004) have questioned the significance of these findings. This is in light of the knowledge that the molecules sampled by microdialysis are far removed from the synapse and mounting evidence that some neurotransmitters, such as Glu and GABA, are “faster” than others (i.e. more tightly regulated perisynaptically). They argue that the non-classical nature may not be purely biological but a failure of the microdialysis-coupled technologies to detect changes near the synapse, due to

limitations with respect to size, spatial resolution, temporal resolution, and tissue trauma.

In summary, our ceramic-based microelectrode arrays with electrochemical detection have several advantages over microdialysis-coupled detection techniques for the measurement of Glu. Our microelectrodes are smaller and have better spatial resolution (15 x 333 μm vs. ~250 μm x 1-4 mm). They have better temporal resolution (800 msec vs. typically 5-20 min) and display the intracranial events as they happen on a second-by-second basis. They measure Glu in the extracellular space and not an artificial medium. They may also create less tissue trauma. Though our limit of detection (LOD: 0.25 – 0.50 μM Glu) does not rival those of the highly sensitive detection systems used for microdialysis studies, current measures of basal and evoked Glu in the mammalian brain are in the micromolar range, above our LOD (Hu et al., 1994, Lada, Vickroy, and Kennedy, 1998, Kulagina, Shankar, and Michael, 1999, Baker et al., 2002, Burmeister et al., 2002, Pomerleau et al., 2003). These advantages are especially important for measuring fast neurotransmitters like Glu because, unlike microdialysis probes, our microelectrode arrays are designed to be closer to the synapse and maximize opportunities for detecting changes in extrasynaptic Glu that may reflect synaptic events.

The Glutamatergic System in the Normal Mammalian CNS

The vast majority of synapses in the mammalian central nervous system use Glu as a neurotransmitter to create fast neuronal excitation. Glu neuron cell bodies can be found throughout the brain and spinal cord but are mainly concentrated in the cerebral cortex, hippocampus, cerebellum, thalamus, and dorsal horn of the spinal cord. Glutamatergic synapses are widely distributed throughout the mammalian CNS with the highest density found in the hippocampus, cortex, lateral septum, striatum, and molecular layer of the cerebellum (Nakanishi, 1992, Hudspith, 1997, Siegel et al., 1994). While the

neuroanatomy of Glu neurons was emerging, investigators were also exploring the function of Glu in the brain. Today we understand that Glu plays a central role in a wide variety of normal CNS functions including cognition, learning, memory, sensation, and movement (Meldrum, 2000, Feldman et al., 1997, Riedel et al., 2003).

Despite its ubiquitous nature, Glu is able to contribute to many different CNS functions in part because of multiple Glu receptors, broadly classified as ionotropic and metabotropic (Figure 1.1). Ionotropic Glu receptors (iGluRs) are ligand-gated ion channels represented by N-methyl-D-aspartate (NMDA), α-amino-3-hydroxy-5-methyl-4-isoxazole-proprionic acid (AMPA), and kainate (KA) receptors, named according to their specific agonists. In addition to being ligand-gated, NMDA receptors are also voltage-gated (to relieve magnesium blockade) and require the co-agonist glycine. The iGluRs are responsible for fast synaptic transmission with the fast component of the excitatory post-synaptic current (EPSC) attributed to sodium influx through AMPA receptors and the slow component of the ESPC resulting from the slightly delayed inward movement of both sodium and calcium through NMDA receptors. NMDA receptors have also been shown to be important for intracellular calcium signaling responsible for synaptic plasticity (long-term potentiation (LTP) and long-term depression (LTD)). The role of KA receptors is less well known; however, they are densely distributed in the CA3 region of the hippocampus and have been demonstrated to participate in non-NMDA receptor-dependent LTP there (Bortolotto et al. 2003). IGluR subunits are encoded by different genes, have splice variants, undergo post-transcriptional (mRNA) editing, and assemble in multiple combinations for additional functional diversity (Siegel et al., 1994, Feldman et al., 1997).

In addition, there are three groups of ligand-gated G-protein-coupled Glu receptors called the metabotropic Glu receptors (mGluRs). These receptors are not involved in fast neurotransmission but are thought to modulate the activities of neurons and glia through intracellular second messenger signaling. Group I mGluRs (mGluR1,5) couple with G_q11 proteins to increase phospholipase C

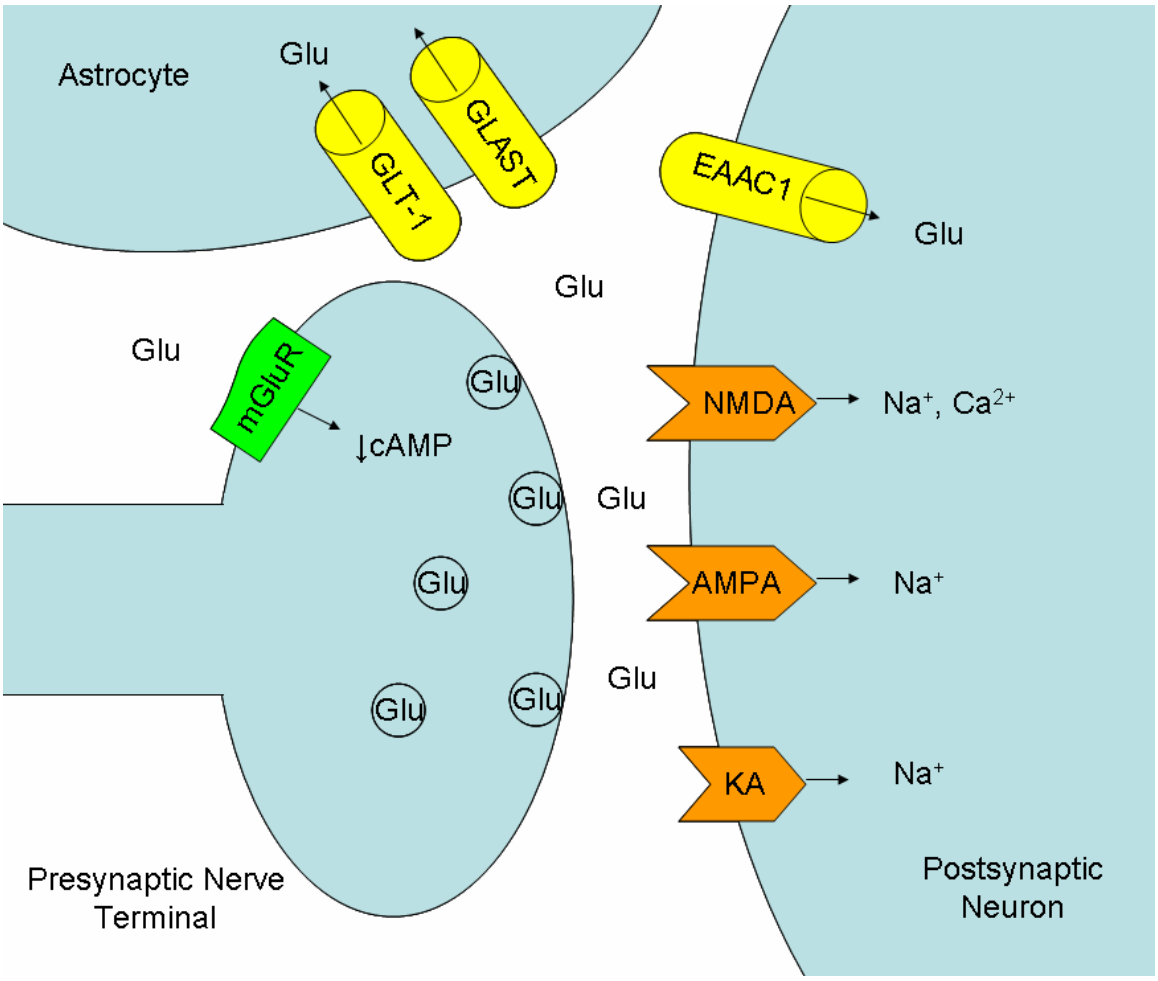

Figure 1.1 The Glutamatergic Synapse

Both ionotropic Glu receptors (orange chevrons) and metabotropic Glu receptors (mGluR) contribute to the diversity of functions attributed to the major excitatory neurotransmitter Glu in the mammalian CNS. Glu released from the presynaptic nerve terminal is primarily removed from the extracellular space by EAAT's (yellow cylinders). See text for further details.

activity, phosphoinositide hydrolysis, and intracellular inositol triphosphate (IP_3) and diacylglycerol (DAG) signaling. This group has been shown to increase Glu release. Groups II and III mGluRs (mGluR2,3 and mGluR4,6-8, respectively) link with G_i/G_o proteins to decrease adenylate cyclase activity and lower cyclic AMP. Both groups, but especially group II mGluRs, have autoreceptor function, providing inhibitory feedback to Glu presynaptic nerve terminals to decrease Glu release. Several studies on the mGluRs to learn more about their distribution, additional neuronal and glial functions, and potential as therapeutic targets are currently underway (Watkins, 2000, Cartmell and Schoepp, 2000, Danbolt, 2001).

Glu neurotransmission is terminated by sodium-dependent excitatory amino acid transporters (EAATs) (Figure 1.1). Three different EAATs are present in the rat brain (Glu Aspartate Transporter (GLAST), Glu Transporter-1 (GLT-1), and Excitatory Amino Acid Carrier 1 (EAAC1)), while five have been discovered in humans (EAAT1-5). Most Glu uptake is accomplished by glial Glu transporters (rat GLAST and GLT-1, homologous to human EAAT1 and EAAT2, respectively), while some is performed by postsynaptic neuronal transporters (rat EAAC1, homologous to human EAAT3). The presence of a presynaptic EAAT has long been postulated; however, its identity and physiological relevance remain disputed. In the rat forebrain, glial Glu uptake is dominated by GLT-1, while GLAST is the predominant Glu transporter in the rat cerebellum (Meldrum, Akbar, and Chapman, 1999). EAAC1 can be trafficked to the membrane surface, and this action has been associated with protein kinase C activity. Perisynaptically, these transporters can be present in densities on the order of $10^4/\mu m^3$ membrane and account for the rapid return of extracellularly released Glu to basal levels. Glu uptake is important to maintain low basal levels for fast signaling (good signal-to-noise) and to avoid overexposing cells to Glu, which has been shown to be neurotoxic (excitotoxicity) (Danbolt, 2001).

Microelectrode arrays configured to record Glu allow us to investigate Glu neurotransmission close to the synapse where Glu receptors and transporters are localized. As an action potential travels along a glutamatergic axon,

propagated by voltage-gated sodium channels, the wave of depolarization ultimately reaches the presynaptic nerve terminal. There, voltage-gated calcium channels are activated, and calcium moves into the terminal allowing the docking of Glu-filled synaptic vesicles. Glu is released into the synaptic cleft where it binds AMPA and NMDA receptors in the post-synaptic density to create fast neuronal excitation (Hudspith, 1997, Meldrum, 2000). The concentrations in the synaptic cleft rise very quickly (estimated ~1 mM, Meldrum, Akbar, and Chapman, 1999) and almost immediately Glu begins to diffuse into the extrasynaptic extracellular space. Glu transporters, located primarily on glial processes opposed to the synaptic cleft and perisynaptically on the postsynaptic neuron, quickly begin to actively remove Glu from the extracellular space (Danbolt, 2001). Some Glu molecules escape immediate uptake and diffuse farther extrasynaptically where they can act on both ionotropic and metabotropic Glu receptors located on nearby neurons and glia. It is most likely this fraction of vesicular Glu which we currently have methods to study. However, information gained from studying extrasynaptic Glu may reflect Glu signaling in the synaptic cleft.

The considerable knowledge that already exists about Glu biology has stimulated intense interest in directly measuring Glu signaling in the intact brain. In some of the present studies, we focused on investigating normal Glu neurotransmission in the anesthetized rat and monkey brain and had very straightforward aims. We questioned how basal Glu is regulated, what we could learn about its origin, and how we could measure its levels. We also wanted to study evoked Glu kinetics, or in other words, to directly measure endogenous Glu as it is released from the presynaptic terminals and cleared from the extracellular space by the Glu transport system. In some studies, we extended this aim by applying exogenous Glu and specifically investigating the limits and responsiveness of the uptake system. *We wanted to conduct these studies because no technology has ever before been able to reliably make these measurements in the intact brain as fast or as close to the synapse.* We also wanted to define some of the normal characteristics of Glu signaling to provide a

basis to hypothesize and test for alterations in Glu neurotransmission which may underlie many brain disorders.

The Role of L-Glutamate in Parkinson's Disease

While much of this work attempts to understand Glu regulation at the synaptic level, it may be equally important to place those findings in context of a large neural network with much higher levels of complexity. In fact, this is always the case in the intact brain where, in any particular brain region, there are multiple neurotransmitter and neuromodulatory influences not just on dendrites and soma to manipulate membrane potentials but also on presynaptic terminals and glial cells to affect neurotransmitter release and uptake kinetics. The connectivity of networks is perhaps best demonstrated when there is a failure, sometimes of just one circuit, which disrupts the entire system. Parkinson's disease unfolds in a similar fashion, and studying the many changes that occur in the brain following disease onset is an interesting and important task.

Idiopathic PD is an age-related chronic neurodegenerative disorder that is classically characterized by resting tremor, cogwheel muscular rigidity, and slowness or loss of movement (bradykinesia or akinesia) (Lang and Lozano, 1998). PD patients also tend to have postural instability, a shuffling gait, and masked facies (facial expression). The pathophysiology of Parkinson's disease clearly begins with the loss of dopamine neurotransmission along the nigrostriatal pathway from the substantia nigra pars compacta (SNc) to the striatum (caudate and putamen) (Wichmann and DeLong, 2003). However, from a network perspective, the downstream effects of dopamine denervation on brain circuitry are far reaching, affecting Glu, GABA, acetylcholine, and many other neurotransmitter systems (Starr, 1995, Wichmann and DeLong, 2003) (Figure 1.2). With the role of dopamine and dopamine-based treatments exhaustively investigated, many investigators have turned to studying other neurotransmitter

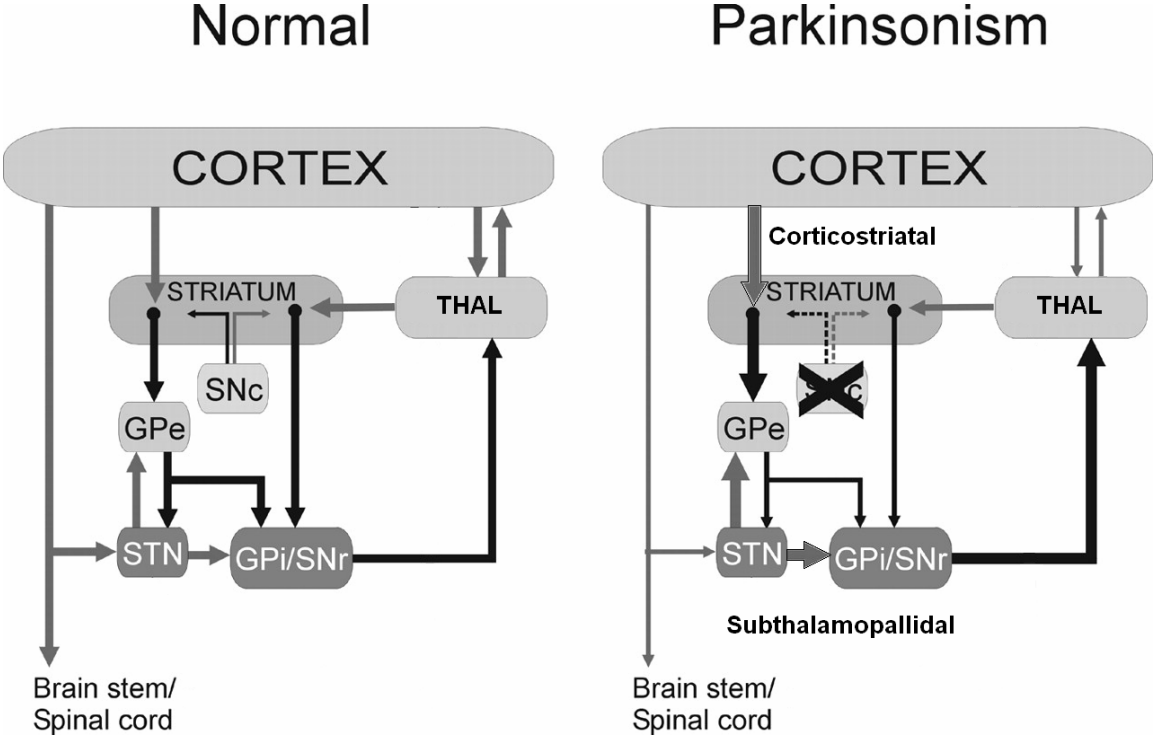

Adapted from Wichmann and DeLong (2003)

Figure 1.2 Normal and Disease-Altered Basal Ganglia-Thalamocortical Circuitry

In the normal brain, excitatory influences (gray arrows) and inhibitory influences (black arrows) act in a balanced fashion to help control movement. In the parkinsonian brain, the loss of DA from the SNc along the nigrostriatal pathway alters many neuronal pathways within the basal ganglia-thalamocortical loops. Progressively, this results in an inhibition of voluntary movement consistent with the symptoms of PD. Alterations in Glu regulation include hyperactivity along the corticostriatal and subthalamopallidal pathways. Abbreviation not defined in the text: globus pallidus external segment (GPe).

changes in hopes of a greater understanding of PD and finding new therapeutic targets.

One of the results stemming from this change of focus has been the widely accepted redefinition of PD as a disease of secondary Glu hyperactivity along a number of involuntary motor pathways. Specifically, glutamatergic projections from the cortex (the corticostriatal pathway) and thalamus (THAL) provide the major driving force to the medium spiny neurons and cholinergic interneurons, respectively, in the striatum, which embodies the major input nuclei of the involuntary motor pathways. Furthermore, the subthalamic nucleus (STN) transmits Glu to the major output structures of the involuntary motor pathways, namely the internal segment of the globus pallidus (GPi) and the substantia nigra pars reticulata (SNr) (Wichmann and DeLong, 2003). Evidence supports that both the corticostriatal pathway and subthalamic nucleus projections are overactive in PD (Bergman, Wichmann, and DeLong, 1990, Calabresi et al., 1993, Greenamyre, 2001). Understanding Glu signaling in the parkinsonian brain may provide insight into the pathophysiology and progression of PD, the mechanism of action of currently used medications and surgical treatments, and potentially new therapeutic approaches.

We were interested in using our microelectrodes to study differences in Glu regulation in an animal model of PD, namely the 6-hydroxydopamine (6-OHDA)-lesioned rat, which is thought to model the late stages of PD. We recorded potassium-evoked endogenous Glu release and uptake kinetics in the striatum, nucleus accumbens, and frontal cortex of both unilaterally-lesioned hemiparkinsonian rats and normal rats in the same age range. We then compared results between the groups and within the lesioned group for significant differences. This study largely focused on the corticostriatal pathway. We would liked to have also investigated Glu signaling near the cell bodies and terminals of the subthalamic nucleus; however, it is a much more difficult target in the rat brain and more suitable for future studies.

The Role of L-Glutamate in Epilepsy

Epilepsy is a brain disorder characterized by multiple seizures, each of which is an episodic motor, sensory, and/or psychic disturbance caused by abnormal cerebral electrical activity that can be recorded using electroencephalography (EEG). The study of epilepsy may benefit from the second-by-second monitoring made possible by our microelectrodes because Glu neurotransmission is central to its pathophysiology. Alterations in excitatory and inhibitory influences may underlie this brain disorder (During and Spencer, 1993). Throughout the mammalian CNS and especially in the cerebral cortex, Glu is the major excitatory neurotransmitter and GABA is the major inhibitory neurotransmitter. Changes in the regulation of either of these chemicals in an epileptic brain can alter the balance toward uncontrolled excitation and the potential for seizure onset. The prominent role of these neurochemicals is evidenced by the fact that many anticonvulsant medications work by enhancing GABA activity while most animal models of epilepsy work by chemically, electrically, or genetically altering Glu regulation.

Both animal and human studies support the strong relationship between Glu and epilepsy. Intracellular recordings from rat hippocampal slices demonstrate that Glu is responsible for paroxysmal depolarizing shifts characteristically associated with epileptic burst discharges (Meldrum, Akbar, and Chapman, 1999). Glu receptor agonists (e.g. kainate and NMDA) can chemically induce seizures in rats and mice. Genetically altering Glu receptor subunits or transporters in mice can create epileptic phenotypes, and Glu receptors and their subunits often display changes in protein levels in electrically or chemically induced rat models of epilepsy. Studies of resected epileptic brain tissue from humans reveal alterations in mRNA and protein levels of Glu receptors and Glu receptor subunits (Meldrum, Akbar, and Chapman, 1999). Of particular interest to our group are recent data collected from human subjects demonstrating that

there are increases in extracellular Glu levels that occur immediately before and during seizures and higher basal Glu in the epileptogenic foci of some patients in the time period between seizures (During and Spencer, 1993, Ronne-Engstrom et al., 1992, Wilson et al., 1996, Thomas et al., 2003, Cavus et al., 2005).

Considering the future of intracranial Glu recording microelectrodes, it has become clear that the first human applications would most likely come from the neurosurgical arena and specifically from human epilepsy research, where implanted devices are commonly used intra- and post-operatively to monitor electrical activity and neurochemicals (During and Spencer, 1993, Engel, Jr., 1998, Fried et al., 1999, Cavus et al., 2005). Our attempts to bridge the worlds of basic science, technology development, and patient-oriented research have proven to be a difficult task, however, and not enough experimental work was completed to merit a full chapter. Nonetheless, important progress and many plans for the future have been made. The appendix documents how we may introduce our microelectrode arrays into the human operating room, presents preliminary recordings from excised human tissue from an epileptic brain, discusses additional technological changes that need to be implemented, and explains how we believe microelectrode arrays may someday benefit patients who suffer from epilepsy and potentially many other brain disorders.

Chapter Two: Methods

Microelectrode Array Design

Fabrication

Microelectrode arrays were constructed in conjunction with Thin-Film Technologies, Inc. (Buellton, CA, USA). For a full description of microelectrode array fabrication, see Burmeister, Moxon, and Gerhardt, 2000 and Burmeister and Gerhardt, 2001. Because the microelectrode arrays are fabricated using photolithography, multiple geometries (number, size, shape, and arrangement) of the microelectrode array's recording sites are routinely available. For consistency, most studies used the S2 geometry defined as microelectrode arrays with four platinum (Pt) recording sites (15 x 333 μm) geometrically arranged as two pairs of recording sites with 100 μm spacing between pairs and 30 μm spacing between paired sites (Figure 2.1). Microelectrode arrays with a different geometry (serial recording sites, see Appendix Figure A.1) were provided to our collaborators at the Brigham Hospital in Boston.

Layer-Dependent Glu Selectivity

Two chemical layers were applied to make the microelectrode array selective for Glu, one for exclusion and one for sensitivity. First, the Pt recording sites were coated with Nafion™, which electrostatically repels anionic interferents such as L-ascorbic acid (AA) and DOPAC (Gerhardt et al., 1984). Thereafter, the sites were coated with a protein matrix layer (bovine serum albumin (BSA)/glutaraldehyde (GLUT)) containing the enzyme L-glutamate oxidase (GluOx). The GluOx layer permits the detection of Glu by enzymatically degrading it into α-ketoglutarate and H_2O_2. As H_2O_2 diffuses through the Nafion™

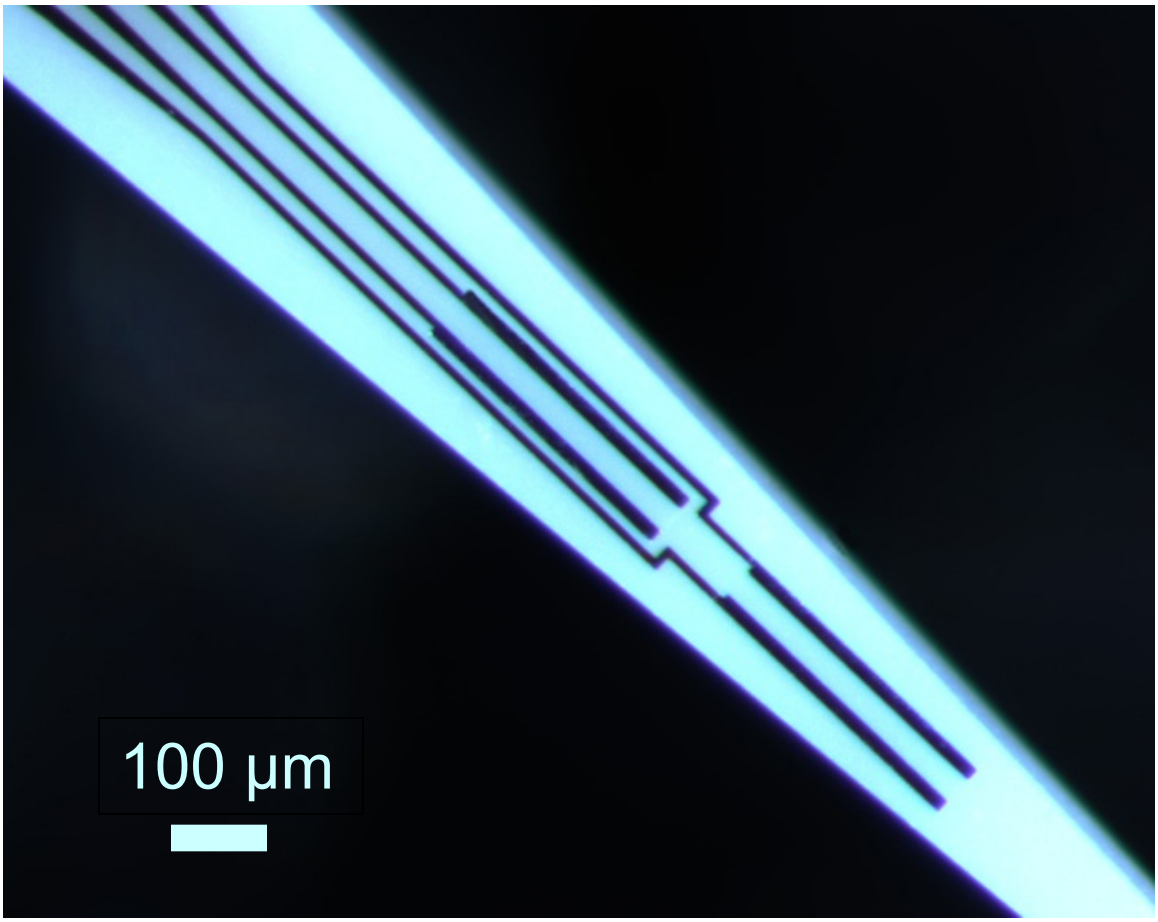

Figure 2.1 Ceramic-Based Pt Microelectrode Array (S2 Geometry)

The ceramic-based microelectrode array (pictured) has four Pt recording sites (15 x 333 µm ea.), which are designed as two pairs of adjacent recording sites (30 µm spacing) arranged 100 µm apart.

layer and contacts the Pt surface, it is oxidized at an applied voltage of +0.7 V versus Ag/AgCl reference. This reaction frees 2 electrons per H_2O_2 molecule to flow through our electrochemical detection system and record the presence of Glu (Figures 2.2 and 2.3).

Self-Referencing Configuration

To configure a microelectrode array to record Glu in self-referencing recording mode, the recording sites were prepared as previously described except one pair of recording sites was coated with an enzyme-free protein matrix layer (BSA/GLUT) to provide similar small molecule diffusion and detection characteristics without the ability to detect Glu (Figure 2.4). Signals on self-referencing or “sentinel” recording sites may be used qualitatively to verify the identity of signals as Glu on Glu recording sites or quantitatively to subtract away background signals, noise, interferences, or artifacts.

Electrode Preparation and Use

Silver/Silver Chloride (Ag/AgCl) Reference Electrodes

All of our studies were conducted using constant potential amperometry in 2 electrode configuration to record Glu *in vitro* (calibration) and *in vivo*. This method requires both a working electrode (microelectrode array) and a silver/silver chloride (Ag/AgCl) reference electrode. Reference electrodes are critical for several reasons. First, applying a potential (voltage) at the working electrode requires having an electrical reference point, which is provided by the reference electrode. Second, to measure electrical current related to electrochemical events occurring at the working electrode, there must be a physical path of electron flow connected to a balanced (equal and opposite) electrochemical event at the reference electrode. Finally, the relationship between the working electrode and the reference electrode is thermodynamically stable, which is necessary for electrochemical recordings.

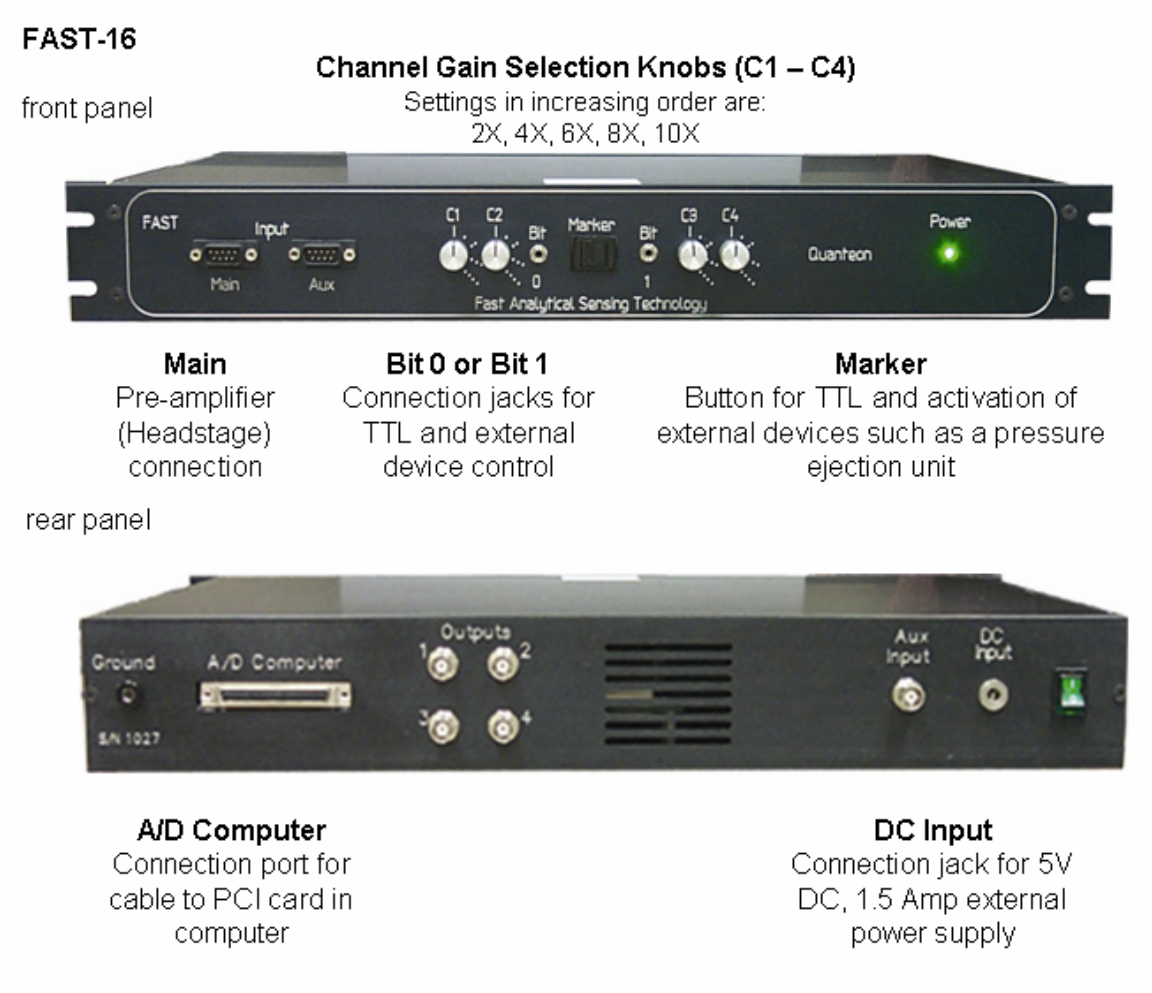

Figure 2.2 The FAST-16 Electrochemical Recording System

Front and rear views of the FAST-16 potentiostat box are shown. Additonal information about features, controls, and connections is included. The FAST-16 is used to create a potential difference between the working electrode (microelectrode array) and the reference electrode to promote electrochemical reactions. In conjunction with other hardware elements, including the headstage (pre-amplifier) and PCI card in the computer, the FAST-16 also amplifies the signal (electrical current) and digitizes it. The FAST-16 software creates second-by-second data files based on this information.

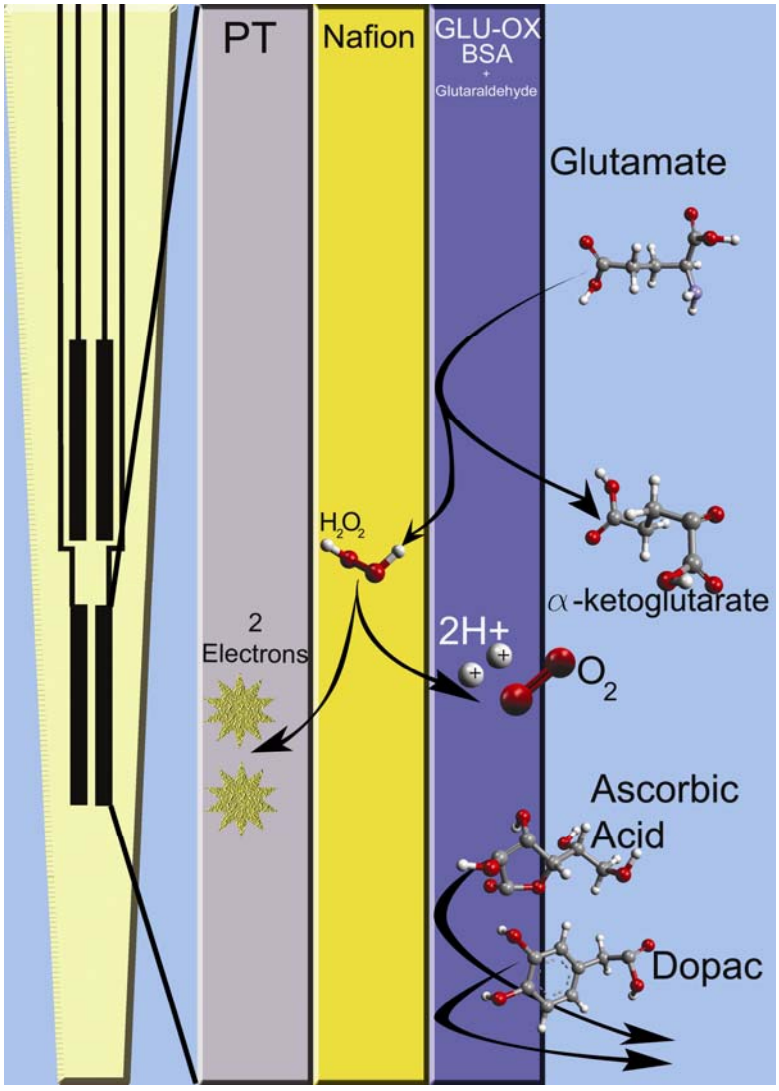

Figure 2.3 Layer-Dependent Glu Selectivity

Microelectrode arrays are made selective for Glu by coating layers of polymers on the Pt surface. Nafion™ is first applied to electrostatically repel anionic interferents (e.g. AA and DOPAC). Then, a protein matrix layer (BSA/glutaraldehyde) containing the enzyme GluOx is applied. GluOx degrades Glu to produce H_2O_2 and α-ketoglutarate. H_2O_2 can be electrochemically detected on Pt (+0.7 V vs. Ag/AgCl reference). Other abbreviations: oxygen (O_2) and proton (H^+).

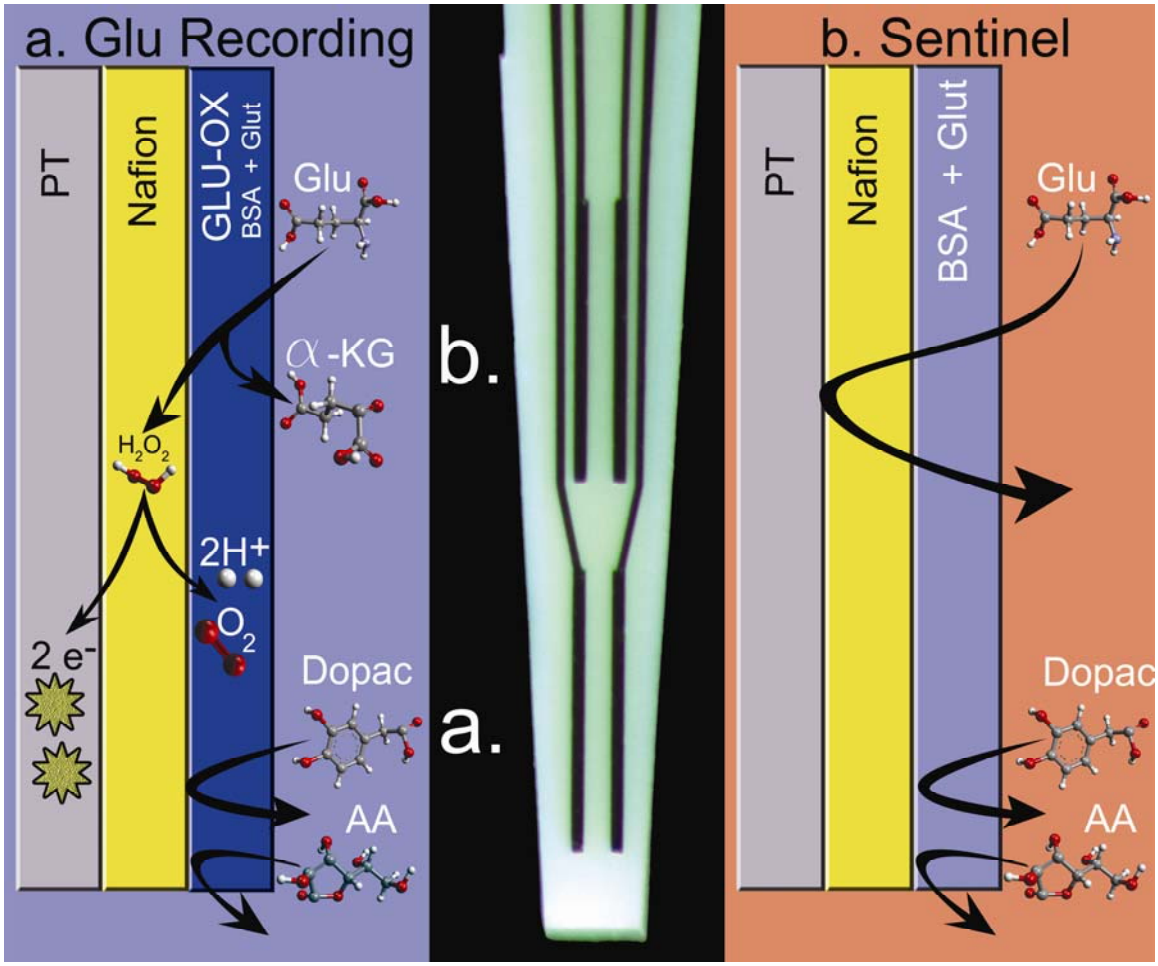

Figure 2.4 Microelectrode Array Configured for Self-Referencing Glu Recordings

Refer to Figure 2.3 for a detailed explanation of layer-dependent Glu selectivity on Glu recording sites. A protein matrix layer (BSA/glutaraldehyde (GLUT)) with GluOx was coated on one pair to configure Glu recording sites (a). A similar protein matrix layer without GluOx was coated on the other pair to create self-referencing or "sentinel" sites (b). Enzyme-free sites are not configured to detect Glu. Other abbreviations: α-ketoglutarate (α-KG), electron (e^-).

Two types of Ag/AgCl reference electrodes were used. Glass-bodied reference electrodes (RE-5b, Bioanalytical Systems, Inc.) require minimal preparation. On arrival, these electrodes are stored in 3 M NaCl. The quality of these electrodes can be tested against a known good Ag/AgCl reference electrode using a voltmeter; the potential difference should not exceed ±10 mV. This type of reference electrode is routinely used during microelectrode array calibration. The glass-bodied type is also preferred for some *in vivo* electrochemical recordings because an implanted bare wire Ag/AgCl reference electrode can damage brain tissue. An RE-5b was used to allow Glu recordings in the anesthetized nonhuman primates. This is possible because during each experiment the reference electrode maintained ionic contact with the animal's brain.

Bare wire Ag/AgCl reference electrodes were prepared for acute anesthetized rat experiments. Teflon-coated silver wire was cut to length (10-20 cm), and roughly 5 mm of Teflon was stripped from both ends. One end was soldered to an amphenol gold pin connector. The other end was placed in a saturated chloride solution (1 M HCl supersaturated with NaCl) along with a stainless steel wire. A modified power supply (9 V DC) was plugged into a 120 V wall outlet, the negative lead was connected to the stainless steel wire, and the positive lead was connected to the silver wire. AgCl was allowed to electroplate onto the exposed silver wire for 5-10 minutes. The prepared Ag/AgCl end of the reference electrode was implanted in the rat's brain, and the amphenol connector was plugged into the FAST-16 hardware.

Microelectrode Arrays

The microelectrode arrays were coated to make them selective for Glu. Clean microelectrode arrays were dipped into fresh, stock Nafion™ and oven-dried at 175 ^{o}C for 4 minutes. A 10 µL solution containing 1% (w/v) GluOx, 1% (w/v) BSA, and 0.125% (w/w) glutaraldehyde in ddH_2O was prepared. Under a dissecting microscope, a microsyringe (model 80100, Hamilton Co.) was used to

coat the recording sites with the enzyme solution. A small drop of the solution (~0.1 µL) suspended at the tip of the microsyringe needle was put in contact with the recording sites and removed. The coating was allowed to air dry, and 2-4 additional coatings were applied at one minute intervals to achieve appropriate thickness. When required, microelectrode arrays were configured for self-referencing recordings by leaving one or more adjacent recording sites uncoated and similarly applying an enzyme-free solution containing 1% BSA and 0.125% glutaraldehyde to these sites as a second coating step (Figure 2.4). All coatings were permitted to cure (overnight to two weeks) at room temperature in a clean environment prior to *in vitro* testing.

To calibrate the microelectrode arrays, constant voltage amperometry was performed using a FAST-16 high-speed electrochemistry instrument (Quanteon, L.L.C.) using software (Fast Analytical Sensor Technology (FAST), Quanteon, L.L.C.) written for simultaneous four-channel recordings. Typically, measurements were carried out using an applied potential of +0.7 V vs. Ag/AgCl reference (Bioanalytical Systems, Inc., RE-5b). Some microelectrodes were calibrated at +0.7 V and separately at +0.25 V for particular experiments. For calibrations, the microelectrode recording sites were soaked for 45-60 minutes in a solution of 0.05 M phosphate-buffered saline (PBS) at room temperature, pH 7.4. The microelectrode was then connected to the FAST-16 hardware, and the recording sites were lowered into 40 ml of PBS at 37 °C in a 50 ml beaker. The PBS was slowly stirred without creating a vortex, using a 10 x 3 mm magnetic stir bar. A battery-operated stir plate (Barnant Co.) was used to mix the solution and to reduce AC (60 Hz) interference. The buffer's temperature was maintained using a recirculating water bath (Quanteon, LLC). A combination headstage gain (2 nA/V) and secondary gain of 10X (200 pA/V final gain) was used for all amperometric recordings. Aliquots of stock solutions of 20 mM AA, 20 mM Glu, 2 mM DA, and 8.8 mM H_2O_2 were sequentially added to the buffer to produce the following final concentrations: 250 µM AA, 20, 40, 60 & 80 µM Glu, 2 µM DA, and 8.8 µM H_2O_2. Amperometric measurements were taken for each addition. Selectivity ((ΔI/ µM Glu):(ΔI/ µM AA), where I = current), slope (sensitivity, (ΔI/

μM Glu)), limit of detection (LOD, signal-to-noise = 3), and linearity (R^2) of the regression line of current vs. Glu concentration were calculated for each recording site. We have high confidence in the accurate measurement of Glu concentrations below the lower limit of our calibration range (i.e. <20 μM Glu) because of the excellent linearity of the response to the Glu reporter molecule H_2O_2 by Nafion™-coated microelectrode array recording sites (R^2 > 0.999 ± 0.000, Burmeister, Moxon, and Gerhardt, 2000).

Most experiments required delivering drugs or chemicals intracranially. When not required, the following steps were omitted. A Kopf model 700C pipette puller (David Kopf Instruments, Tujunga, CA) was used to pull single barrel glass capillary micropipettes (1.0 mm × 0.58 mm, 6", A-M Systems, Inc., Everett, WA, USA). The pulled glass micropipettes were bumped until the inner tip diameter was 10-15 μm. The micropipette tip was placed central to all recording sites and between 50 μm and 100 μm from the recording surface and attached to the microelectrode array's ceramic paddle using Sticky Wax (Kerr Brand).

With or without an attached micropipette, the microelectrode was stored with the recording sites in PBS until the *in vivo* studies. Rats were anesthetized and surgically prepared for electrochemical recordings as described in the Animal Preparation for *In Vivo* Electrochemical Recording section (below). For intracranial ejections, a solution was loaded into the single-barrel micropipette using a custom-made, pulled stainless steel needle (30 gauge, Popper and Sons, Inc., New Hyde Park, NY, USA) attached to a sterile syringe filter (0.22 μm pore size, Costar, Corning, NY, USA) and a 1 cc syringe. The fully prepared microelectrode array was implanted into the animal's brain. A fifteen minute equilibration period per brain region was allowed prior to beginning each experiment. Volumes of the solutions were ejected from the micropipette using a Picospritzer III (Parker Hannifin Corp., General valve operation, 5 to 40 PSI over 0.2 to 2.0 seconds) and monitored using a stereomicroscope fitted with a reticule (Friedemann and Gerhardt, 1992). The FAST-16 recording system was used to record *in vivo* Glu. Specific details regarding recorded brain structures and their coordinates, intracranially applied drugs and chemicals, changes in recording

parameters, and data analysis are included with the corresponding experiments described in chapters three, four, and five and the appendix. See Burmeister et al. (2002) for additional details (e.g. microelectrode fabrication, microelectrode cleaning and re-use).

The Durability of L-Glutamate Oxidase

It is important for *in vivo* applications of enzyme-based detection technologies that the enzyme used is resistant to being denatured by changing experimental conditions. Reduced enzyme activity by the loss or altered conformation of enzyme active sites would impair the microelectrode array's sensitivity and limit of detection. Though we had never noted experimental findings that lead us to hypothesize that GluOx activity was changing due to denaturation, we did not appreciate the durability of this enzyme until we attempted to denature it ourselves to create an inactivated form of GluOx (iGluOx). These efforts were made in an attempt to match our protein matrices on Glu recording and sentinel/referencing sites more closely (BSA/Glut/GluOx vs. BSA/Glut/iGluOx, respectively). L-glutamate oxidase (EC 1.4.3.11) is a 140 kD protein composed of three subunits arranged in a hexameric structure ($\alpha_2\beta_2\gamma_2$) (Kusakabe et al., 1983). Several attempts to inactivate the enzyme were conducted as follows.

In initial testing, 5 µl (5 units) of stock enzyme solution were placed in a microcentrifuge tube and heated in a water bath at 80 °C for 15 minutes. The resulting condensed pellet, which was lighter in color and reduced in volume, was reconstituted with ddH_2O to a final volume of 5 µl to bring it back to stock solution concentration. This solution was used in place of the normal GluOx stock solution to create a potentially heat-inactivated enzyme coating for the sentinel recording sites. Two microelectrode arrays were prepared using this coating and calibrated as described in the preceding section. It should be noted that the potentially-inactivated enzyme coating contained visible aggregates of enzyme unlike the typical homogenous appearance of normal enzyme coatings. Sentinel

recording sites on both microelectrode arrays responded well to Glu additions during calibration demonstrating that the heated enzyme had retained activity.

Four additional methods were attempted to inactivate samples of the enzyme. Four 2 µl samples (2 units each) of stock enzyme solution were placed in separate microcentrifuge tubes and subjected to one of the following conditions: heated in a water bath at 100 °C for 15 minutes, heated by heat block at 100 °C for 15 minutes, microwaved at maximum power in a 1.1 kW output microwave oven for 1 minute, and cycled through one freeze-thaw cycle (-80 °C to room temperature). All samples were capped and sealed with both Parafilm and tape to prevent the escape of water vapor from the sample. Heated samples were immediately cooled down in an ice-cold water bath and allowed to rest for at least 15 minutes prior to activity testing. All samples were tested for activity using an uncoated microelectrode array as a H_2O_2 detector. The FAST-16 hardware and software was used to perform a H_2O_2 calibration (a.k.a. peroxide test) of the microelectrode array exactly as calibrations are described in the preceding section except no AA, Glu, or DA was used and 8.8 mM H_2O_2 was added to create the following sequence of final volumes: 8.8, 17.6, 26.4, and 35.2 µM H_2O_2. This peroxide test was not done specifically to produce a calibration factor but qualitatively to confirm that the microelectrode array had good sensitivity for H_2O_2. Also, the microelectrode tip was rinsed thoroughly with ddH_2O between enzyme activity tests.

To prepare each sample for testing, the tape and Parafilm were removed, any water vapor that had condensed in the top was shaken down, and the tube was uncapped. Then, the sample was diluted with ddH_2O (1:10) to a final volume of 20 µl to provide an adequate volume and vertical clearance for the microelectrode tip. The enzyme sample was agitated by a pipettor and/or spun using a vortexer if it did not readily mix with the added water. Portions of the microcentrifuge tube were carefully cut and removed until there was only a ~1 cm portion of the bottom of the tube remaining, which was the reservoir for the sample. This miniature reservoir was securely held in place by modeling clay to hold it upright. A bare wire Ag/AgCl reference electrode, prepared as described

in the preceding section, was placed in the enzyme sample solution, and the microelectrode tip was lowered stereotaxically until all sites were submerged. Amperometric recordings (+0.7 V vs. Ag/AgCl reference) were made in the solution as up to 5 additions of Glu (20 mM, 1 µl) were added. This procedure has been used to verify GluOx activity in the past to troubleshoot non-responsive prepared microelectrodes, and it was known that normal stock enzyme would produce maximum detectable current with one addition of Glu even without stirring.

None of the methods used to inactivate GluOx completely eliminated enzyme activity. The enzyme subjected to the 100 °C water bath displayed activity at the third addition of Glu, and after 5 additions showed ~30% of maximum detectable current. The enzyme placed in the 100 °C heat block did not show activity until the fifth addition, which produced ~50% of maximum response. Both microwaved and freeze-thawed enzyme samples showed maximal detectable current after the first addition of Glu. In summary, we have not developed methods to inactivate GluOx for use on sentinel recording sites of microelectrode arrays configured for self-referencing. Instead, we have found that GluOx is an extremely durable enzyme, which is an advantage for acute use, chronic implantation, and future sterilization procedures. The long-term stability of purified or solubilized GluOx has not been fully determined by any research group or commercial entity. Initial studies conducted by our group investigating exogenous Glu detection in the brains of chronically implanted freely-moving rats indicate that GluOx in our cured protein matrix is active for up to 50 days *in vivo*.

Animal Preparation for *In Vivo* Electrochemical Recordings

All animals were handled and cared for using protocols approved by the institutional animal care and use committees (IACUC) of the University of Kentucky Chandler Medical Center (UKMC) and the Medical University of South

Carolina (MUSC). Both institutions are fully accredited by AAALACI (Association of Assessment and Accreditation of Laboratory Animal Care International).

Normal Young Fischer 344 Rats

Male Fischer 344 rats (3-6 months old, 200-300 g) were used to study normal Glu regulation and as non-lesioned control animals for the unilateral 6-OHDA lesion study. The Fischer 344 rat, an inbred strain of rats, was chosen for these studies to limit the biological variability between animals. Coordinates used for stereotaxic surgery and microelectrode implantation were calculated from *bregma* using the rat brain atlas of Paxinos and Watson (1986). Rats were anesthetized with urethane (1.25 mg/kg, i.p.) in three divided doses. First, a loading dose approximately equal to one-half of the total dose was administered; the remaining urethane was given in two more injections over the course of up to 1 hour as the rat became sedated. Partially anesthetized rats were weighed shortly before the second injection to ensure proper dosing. Urethane-injected rats were rested on a 37 °C heating pad as they approached the surgical plane of anesthesia. A rat was considered to be fully anesthetized when he was non-responsive to toe pinch; rats reflexive to noxious stimuli two hours after the initial loading dose were given additional doses of urethane (0.1 cc of 25% (w/v), i.p.) at 15 minute intervals until they no longer responded to toe pinch. Anesthetized rats were placed in a stereotaxic frame (incisor bar: -2.3 mm) and rested on a 37 °C heating pad.

The top of the rat's head was visualized through a zoom-capable stereomicroscope (10x eyepiece, 0.5x objective, 0.7 to 4.5 zoom) on a boom stand. A midline, longitudinal incision (~4 cm) was made through the scalp overlying the skull. The skin and fascia were reflected bilaterally and held in retraction by clamps. Throughout the surgery, bleeding was controlled by cauterization, and the surgical field was cleaned of blood and loose tissue using physiological (0.9%) saline irrigation, surgical gauze (2 x 2's), and cotton-tipped applicators. Identification of skull landmarks (sagittal suture, coronal suture,

lambdoidal suture, *bregma*, and *lambda*) helped guide surgical bone removal; in particular, *bregma* was permanently marked prior to drilling. Section(s) of skull overlying the brain areas of interest were outlined. Perimeters were cut nearly or completely to the dural surface using a Dremel hand-held drill (Model 395, Racine, WI) with an engraving cutter drill bit (Dremel bit #105, 106, or 107, Racine, WI). The resulting bone flap was removed. The dura was carefully incised and dissected away to expose the cortical surface of the rat brain. A small burr hole was drilled through the skull at a remote location from the primary surgical area(s) for Ag/AgCl reference electrode implantation. Starting from bregma, prepared microelectrode arrays were stereotaxically aligned and lowered until the center of the recording sites were at the cortical surface. Microelectrode arrays were advanced into the brain to record different depths by a microdrive (Narishige, MO-8) (Figure 2.5).

Unilateral 6-Hydroxydopamine-Lesioned Young Fischer 344 Rats

Unilateral 6-hydroxydopamine (6-OHDA)-lesioned male Fischer 344 rats (5-9 months old, 250-350 g) were used to study the effects of striatal dopamine denervation on potassium-evoked Glu kinetics. Coordinates used for stereotaxic surgery and microelectrode implantation were calculated from *bregma* using the rat brain atlas of Paxinos and Watson (1986).

Lesioning and rotational testing were performed by Lauren Willis in the lab of Anne-Charlotte Granholm, Ph.D. (Department of Physiology and Neurosciences, Medical University of South Carolina). Rats were anesthetized with chloral hydrate (400 mg/kg in 0.9% NaCl, i.p.) and stereotaxically lesioned in the right medial forebrain bundle with 9 μg/4 μl of 6-OHDA in normal saline containing 0.02% ascorbate (coordinates -4.4 mm AP, +1.3 mm ML, and -7.8 mm DV from the dural surface; see Granholm et al., 1997). The 6-OHDA neurotoxin was administered over 4 minutes followed by a 2-minute delay period prior to needle withdrawal to allow for toxin absorption into the brain tissue. Animals were

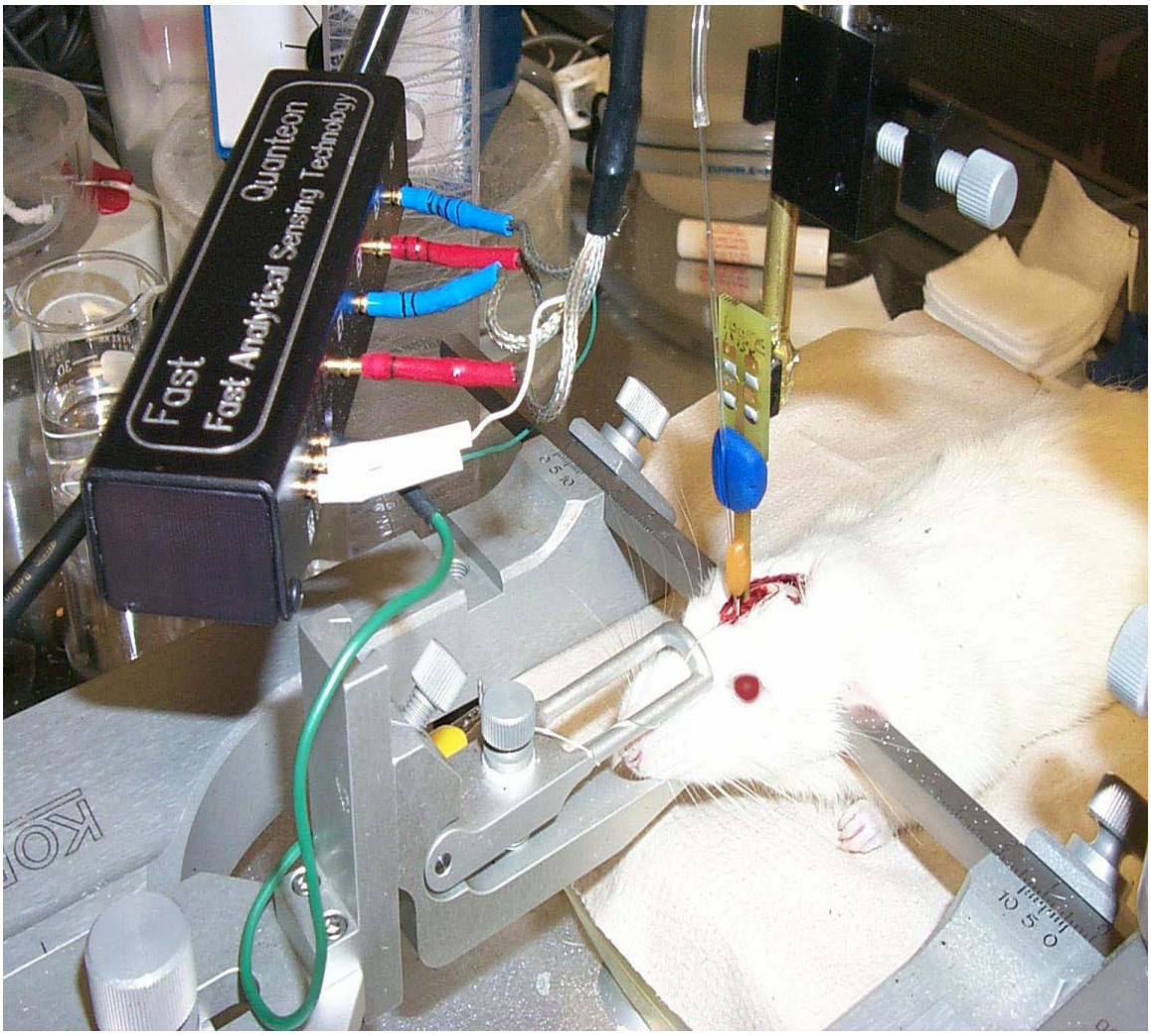

Figure 2.5 The *In Vivo* Glu Recording Setup for Anesthetized Rat Studies

provided with acetaminophen in their drinking water for 24 hours to alleviate potential post-surgical discomfort.

Lesioned animals were evaluated for apomorphine-induced rotational behavior beginning one week following 6-OHDA administration and tested once a week thereafter for a total of 4 weeks. Briefly, animals were placed in rotometer bowls (Hudson et al., 1993) and secured to the counting sensor by a thoracic harness. Subjects were allowed to acclimate to the environment for 10 minutes, and then administered a subcutaneous injection of apomorphine (0.05 mg/kg). Subsequent rotational behavior was recorded for one hour. Following rotational testing, animals were released from their harnesses, removed from the rotometer bowls, and returned to their cages.

A group of rats which responded to apomorphine with average contralateral rotations ≥300 times/hour were transferred to the University of Kentucky for *in vivo* electrochemical recordings. At least three months was allowed for the lesion to stabilize before recordings were made. Animals were anesthetized, surgically prepared, and implanted with electrodes exactly as described in the preceding section.

Normal Anesthetized Rhesus Monkeys (*Macaca mulatta*)

Three female normal rhesus monkeys (8, 25, and 28 years old) were used to characterize normal Glu regulation in the motor cortex and frontal cortex of young and aged nonhuman primates. Several methodological modifications were required to conduct recordings in the veterinary operating room. Because method refinement was part of the aims of conducting this study, a full methodological description is presented in Chapter Four.

Drugs and Chemicals

All chemicals were used as received unless otherwise stated. All solutions were prepared using distilled, deionized water.

Chemicals for Microelectrode Preparation and Calibration

Nafion™ (5% (w/v) in a mixture of aliphatic alcohols and water), BSA, glutaraldehyde (25% (w/w) in water), AA, Glu monosodium salt, and DA were obtained from Sigma-Aldrich Corp. (St. Louis, MO, USA) (Figure 2.6). GluOx was purchased from Seikagaku America, Inc. (East Falmouth, MA, USA). The 3% H_2O_2 solution was purchased from a local retailer. Sodium chloride, sodium phosphate monobasic, and sodium phosphate dibasic (used to make 0.05 M PBS) were obtained from Fisher Scientific (Fair Lawn, NJ, USA). The DA stock solution was prepared in 1% perchloric acid for prolonged stability. Glutaraldehyde was stored at -20 ºC. Special care was taken to ensure that the stock Nafion™, BSA, and glutaraldehyde solutions were only used for 1-2 months.

Intracranially-Applied Drugs and Chemicals

Solutions used for intracranial injections were prepared in 0.9% saline, adjusted to pH 7.2-7.4, and filtered before use using a sterile syringe filter (0.22 µm pore size, Costar, Corning, NY, USA). Sodium chloride, potassium chloride, and calcium chloride dihydrate (used for 0.9% saline and high potassium solutions) were obtained from Fisher Scientific (Fair Lawn, NJ, USA). Glu monosodium salt and tetrodotoxin (TTX) were obtained from Sigma-Aldrich Corp. (St. Louis, MO, USA). D,L-*threo*-β-benzyloxyaspartate (TBOA) was obtained from Tocris Cookson Inc. (Ellisville, MO, USA) (Figure 2.6).

Anesthetics and Special-Use Drugs and Chemicals

Injectable anesthetics used in rat studies were prepared in 0.9% saline; sodium chloride was obtained from Fisher Scientific (Fair Lawn, NJ, USA). Urethane, chloral hydrate, 6-OHDA, apomorphine, and AA (used to delay the oxidation of the previous two drugs in solution) were obtained from Sigma-Aldrich

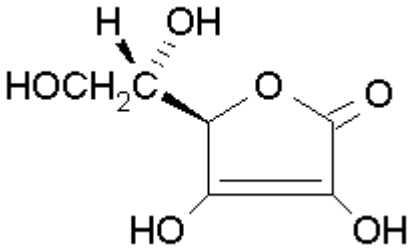

L-ascorbic acid (AA)

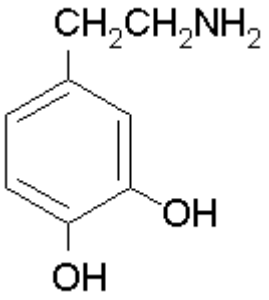

Dopamine (DA)

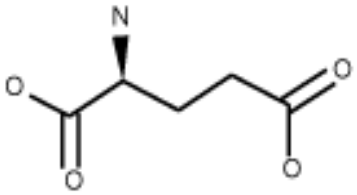

L-glutamic acid (Glu)

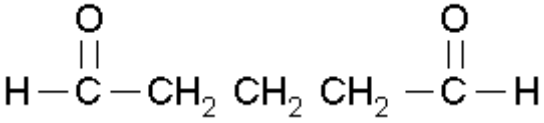

Glutaraldehyde (GLUT)

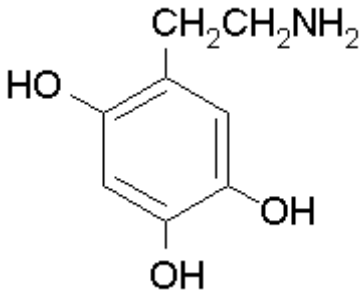

6-Hydroxydopamine (6-OHDA)

Figure 2.6 Molecular Structures of Selected Drugs and Chemicals

Figure 2.6 (continued)

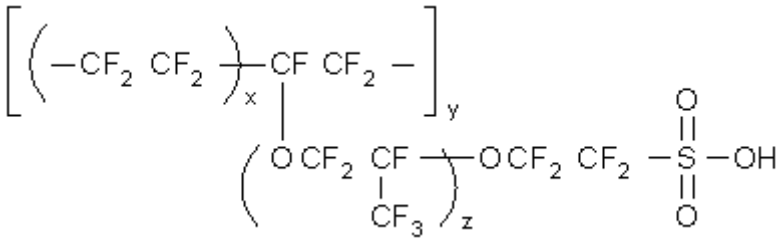

Nafion™

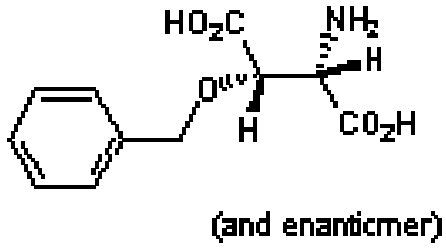

D,L-*threo*-β-benzyloxyaspartate (TBOA)

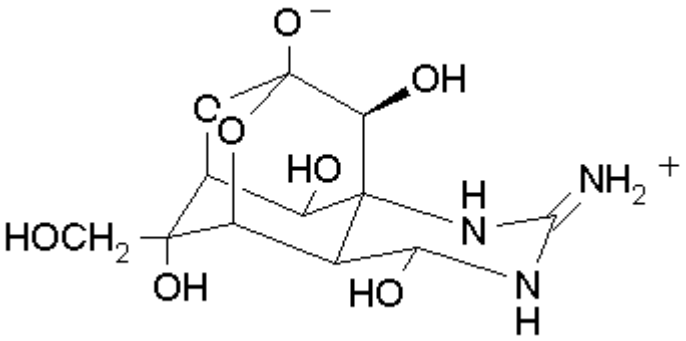

Tetrodotoxin (TTX)

Corp. (St. Louis, MO, USA) (Figure 2.6). While recovering, 6-OHDA-lesioned rats were given acetaminophen, which was provided by the hospital pharmacy at the Medical University of South Carolina (Charleston, SC). The following drugs and chemicals were used to prepare the nonhuman primates for anesthesia, magnetic resonance imaging, and surgery. Ketamine hydrochloride and chlorhexidine diacetate were obtained from Fort Dodge Animal Health (Fort Dodge, IA). Atropine sulfate was obtained from Butler Company (Columbus, OH). Sodium pentobarbital was obtained from Ovation Pharmaceuticals, Inc. (Deerfield, IL). Isoflurane was obtained from Baxter Healthcare Corporation (Deerfield, IL). Betadine® was obtained from Purdue Frederick Company (Stamford, CT). The 70% isopropyl alcohol solution was obtained from Hydrox Laboratories (Elgin, IL). Chronically-studied nonhuman primates were also given post-operative pain medication and prophylactic antibiotics. Buprenorphine was obtained from Reckitt Benckiser Health Care (Richmond, VA). Penicillin G Benzathine and Penicillin G Procaine were obtained from G. C. Hanford Manufacturing Company (Syracuse, NY).

Data Analysis

Glu Signal Parameters

Glu signals, produced by evoked Glu release or exogenous Glu applications, are described by concentration and time measurements, which are then used to calculate additional signal parameters. Figure 2.7 depicts an example of a spike-shaped signal and some of the signal parameters that may be used to describe it. These include amplitude (the maximum change in concentration (μM Glu)), rise time (T_R, the time *from onset* (stimulation or exogenous application of Glu) until peak amplitude (sec)), and total signal duration (T_{Total}, the time *from onset* until complete return to baseline (sec)). Other signal parameters are time measurements related to signal decay. Although abbreviated similarly, they should be considered separately from T_R and T_{Total}.

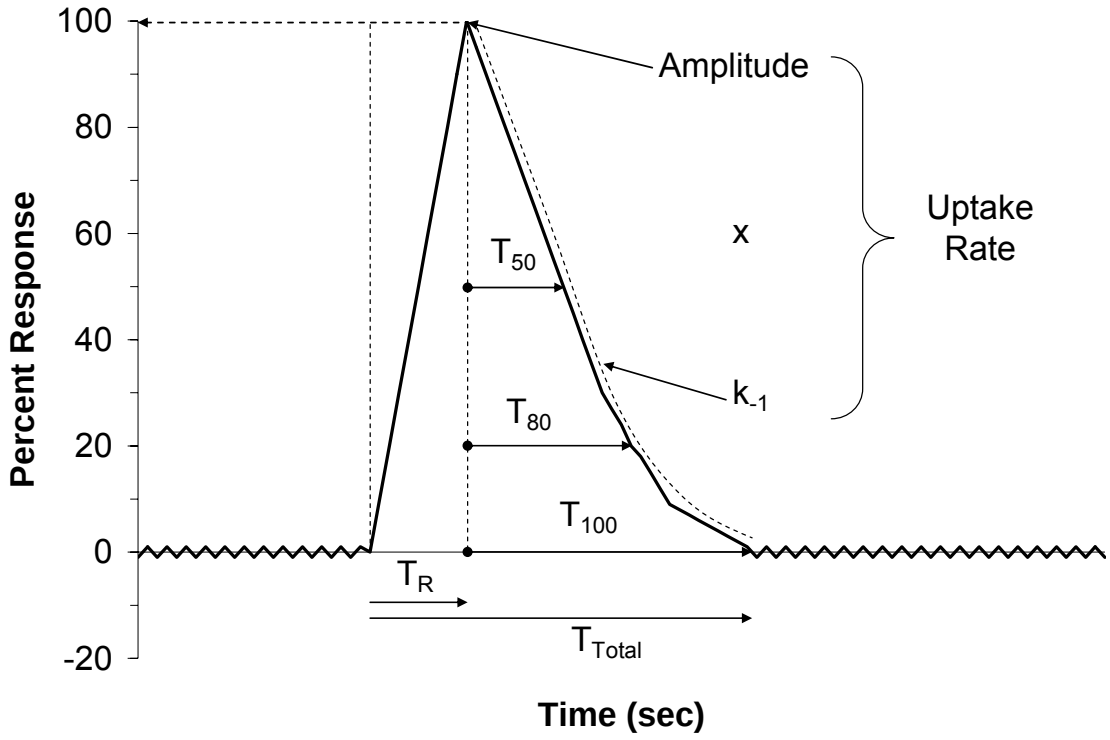

Figure 2.7 Glu Signal Parameters

A schematic example of a spike-shaped Glu signal is shown to illustrate how different signal parameters are measured and calculated. See text for details. Typically Glu signals are plotted as concentration versus time. The y-axis has been changed to percent response to clarify the definitions of certain signal parameters.

These often include T_{50}, T_{80}, and T_{100}, and follow the general format of T_D (sec), where T refers to the time *from peak amplitude* for the signal to decay by D percent. Next, k_{-1} (sec^{-1}) is a rate constant (first-order exponential rate of fit) related only to the decay portion of the curve. The constant k_{-1} is the slope of the linear regression of the natural log transformation of this data over time. Finally, uptake rate (μM Glu/sec) is calculated by multiplying peak amplitude by k_{-1}.

Repeated potassium-evoked Glu releases and Glu ejection signals were collected at one or more depths within each brain region of interest. Individual parameters for each signal were pooled across animals by brain region. Each signal is considered an independent event under the assumption that the variability of responses within an animal is much greater than the variability of responses between animals, as has been stated for similar studies of other neurotransmitters, such as DA (see Cass et al., 1995). The number of data points (n) used for statistical analyses is the number of Glu signals recorded; however, the number of animals is also reported for consideration (e.g. n=40 signals in 4 rats).

Other Analytical Approaches

Data analyses with respect to basal Glu regulation (effects of TTX and TBOA) and basal Glu measures are described in detail in Chapter Three.

Chapter Three: Normal L-Glutamate Regulation in the Anesthetized Rat Brain

Introduction

The work presented in this chapter focuses on basal and potassium-evoked Glu release in the brains of normal young anesthetized rats. Previous work by our group had established many characteristics of *in vivo* Glu dynamics including fast signaling driven by rapid Glu uptake, limited dose-dependence of potassium-evoked Glu responses, robust dose-dependence of locally-applied exogenous Glu, and the reproducible nature of potassium-evoked Glu responses (Burmeister, Moxon, and Gerhardt, 2000, Burmeister and Gerhardt, 2001, Burmeister et al., 2002). Nonetheless, the speed and reproducibility of potassium-evoked Glu signals needed to be more extensively analyzed and fully documented. In particular, the effects of varying the concentration of potassium and shortening the time interval between potassium stimulations are reported.

Though we had conducted many Glu kinetics studies, work had not yet been completed to study basal Glu. Conducting basal Glu studies was especially important because our technology works much faster and closer to the synapse than microdialysis and might reveal significant and novel findings. These studies were delayed, in part, because our technology is especially good at detecting relative changes in Glu concentration from a defined baseline, an advantage which we readily used to study basal Glu regulation, but determining the concentration of Glu that contributed to that baseline is more difficult and required both technological refinement and new analytical approaches. The baseline signal (i_B) presented a challenge because it is composed of multiple components, the background current (i_{BKD}) and the current generated by electrochemical detection of molecules on the Pt surface ($i_B = i_{BKD} + i_X + i_Y + i_Z + \cdots$). The background current may differ between microelectrodes and changes over time during an amperometric recording. After equilibration, it is nearly

constant over a short period of time for all similarly designed, fabricated, and prepared recording sites within a microelectrode array, but you cannot know exactly what it is at a particular time point. The latter fact explains why we could not simply subtract away the background current from the baseline signal to ultimately calculate basal Glu concentrations. In fact, we conceptually had a solution for many years, which was self-referencing, but we had not yet carried out the experiments to test the hypothesis that we could use self-referencing subtraction methods to quantitate basal Glu levels.

The studies presented in this chapter were conducted in the striatum and frontal cortex to expand our knowledge of potassium-evoked Glu release and break new ground into investigations of basal Glu. The high temporal and spatial resolution of our microelectrode arrays allowed us to study *in vivo* Glu faster and closer to synaptic events than previously possible. Furthermore, the self-referencing capabilities of our microelectrode-based technology produced data that we could use in new experimental and analytical approaches to determine basal Glu measures. One of these new approaches utilized the versatility of our technology by varying the applied voltage (versus Ag/AgCl reference electrode) at the recording surface. Finally, we used the combination of a self-referencing recording mode and varying the applied voltage to further confirm that Glu is the source of our amperometric signal because signal identity is the most cited potential disadvantage of voltammetric-based microelectrode studies (see Gerhardt and Burmeister, 2000, Obrenovitch and Zilkha, 2001).

Methods

Refer to Chapter Two for full details. In the Animal Preparation for *In Vivo* Electrochemical Recordings section, the Normal Young Fischer 344 Rats subsection is relevant to studies presented in this chapter.

Stereotaxic Implantation and Glu Recordings

Microelectrode arrays, with or without attached single-barrel micropipettes, were stored with the recording sites in PBS until the *in vivo* studies. For experiments in which one or more intracranial ejections were required, an appropriate solution (described below) was loaded into the micropipette. After aligning the center of the recording sites at the cortical surface, the microelectrode array was advanced into the brain using a hydraulic microdrive (Narishige MO-8). Recordings were made in the striatum (AP +1.0, ML -2.5, DV -5.0 mm) and in the frontal cortex (AP +2.7, ML -1.5, DV -2.0 mm). The microelectrode tip was thoroughly rinsed with physiological saline between regional recordings. A fifteen minute equilibration period per brain region was allowed prior to beginning each experiment. The FAST-16 recording system, software, and recording parameters previously described were used to record *in vivo* Glu unless otherwise noted. To study basal Glu regulation, one of the following solutions was loaded into the micropipette for ejection: physiological (0.9%) saline, a 100 μM TTX solution, or a 100 μM TBOA solution (barrel concentrations). To measure basal Glu, microelectrodes configured for self-referencing Glu recordings were typically used without attached micropipettes. Passive recordings were made to determine basal Glu at a constant potential (+0.7 V vs. Ag/AgCl) and varied potentials (+0.25 V compared to +0.7 V, vs. Ag/AgCl reference). To study evoked Glu release, a potassium solution (70 mM KCl, 79 mM NaCl, 2.5 mM $CaCl_2 \bullet 2H_2O$, pH 7.4 or 120 mM KCl, 29 mM NaCl, 2.5 mM $CaCl_2 \bullet 2H_2O$, pH 7.4) was locally applied at 10 second to 5 minute intervals.

Data Analysis

For the basal Glu regulation data, a single channel subtraction approach was used. Following a 15 minute equilibration period to allow the signal to establish a baseline, pretreatment and post-treatment baselines were defined as the baseline signals during the 5 minute periods immediately before and after local intracranial drug applications. An averaged 10 second portion of the

pretreatment baseline was compared to the maximum averaged 10 second portion of the post-treatment baseline to determine the change in signal due to treatment. The change in signal was converted into apparent change in Glu concentration using a recording site-specific calibration factor. Apparent changes in Glu concentration due to TTX or TBOA were compared to apparent changes in Glu concentration due to normal saline for each brain region by an unpaired, two-tailed t-test (α=0.05). Average TTX- and TBOA-dependent Glu levels were calculated by subtracting the average apparent change in Glu concentration due to saline from each apparent change in Glu from individual TTX and TBOA experiments. Descriptive statistics were used to characterize the new data sets.

To determine basal Glu measures, paired channel subtraction approaches were used. A 15 minute equilibration period was allowed for the signals to attain their baselines. Simultaneously recorded signals on paired channels of the microelectrode array (enzyme-coated (+GluOx) versus enzyme-free (-GluOx)) were compared. Using a constant voltage method (+0.7 V vs. Ag/AgCl reference), resulting differences were converted to Glu concentration using the +GluOx calibration factor (slope m_{+GluOx} = ΔI/μM Glu) from the enzyme-coated site, calculated from a typical calibration at +0.7 V vs. Ag/AgCl reference. We can use this slope because the slope calculated from the enzyme-free sentinel site during the same calibration was approximately zero for all microelectrodes that were used to measure basal Glu (Figures 3.1 and 3.2). Additionally, using a varied voltage method, each brain region was recorded at +0.25 V and +0.7 V (both vs. Ag/AgCl reference) and the voltage-dependent signal changes across individual channels were compared between +GluOx and -GluOx channels. Signal differences were converted to Glu concentration using a calibration factor equal to the difference in +GluOx calibration factors calculated at both +0.25 V and +0.7 V (both vs. Ag/AgCl reference) (Figure 3.3). Resulting measures from the two paired channel subtraction methods as well as average calculated TTX-dependent changes in Glu concentrations were compared by a 1-way ANOVA with Bonferroni post-hoc tests (α=0.05) for each brain region.

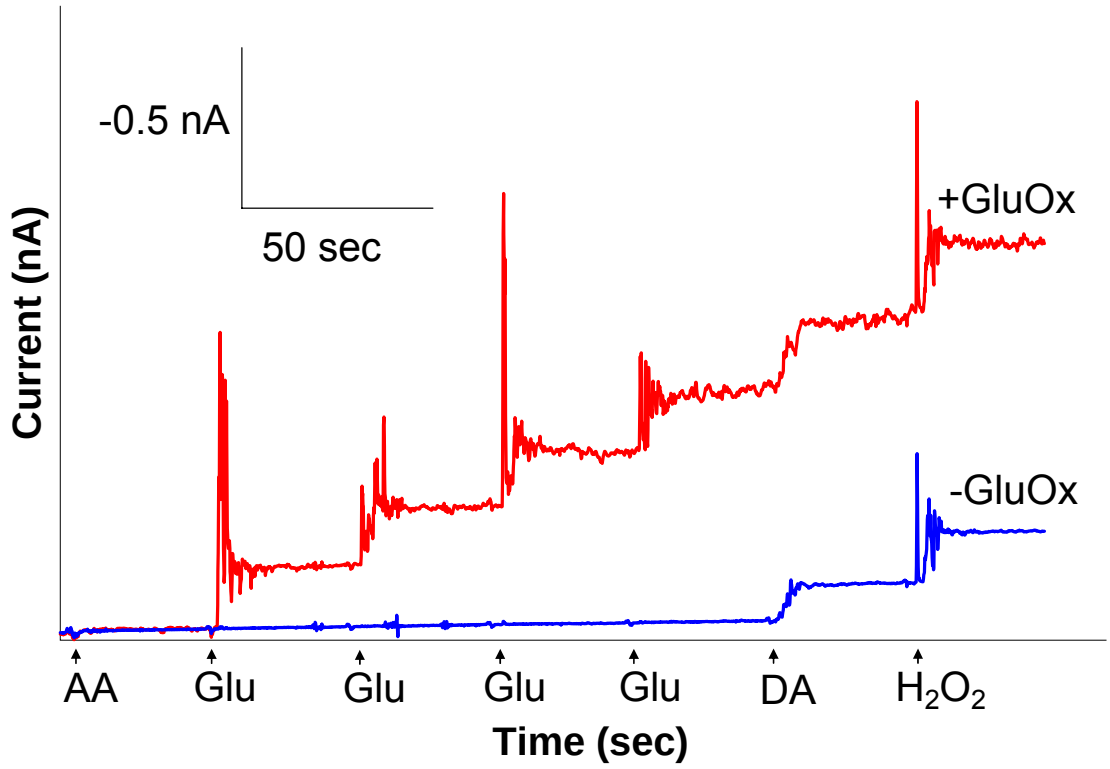

Figure 3.1 Typical Calibration of a Microelectrode Array Configured for Self-Referencing Glu Recordings

During calibration, a standard sequence of chemicals was added to determine each recording site's sensitivity to Glu, selectivity for Glu over AA, and responsiveness to other non-anionic electroactive molecules (e.g. DA and H_2O_2). An enzyme-coated Glu recording site (+GluOx) responds well to Glu and some electroactive molecules. An enzyme-free sentinel site (-GluOx) does not respond to Glu but shows similar responses to the same electroactive molecules. Final concentrations of each addition shown above: 250 μM AA, 20, 40, 60, and 80 μM Glu, 2 μM DA, and 8.8 μM H_2O_2.

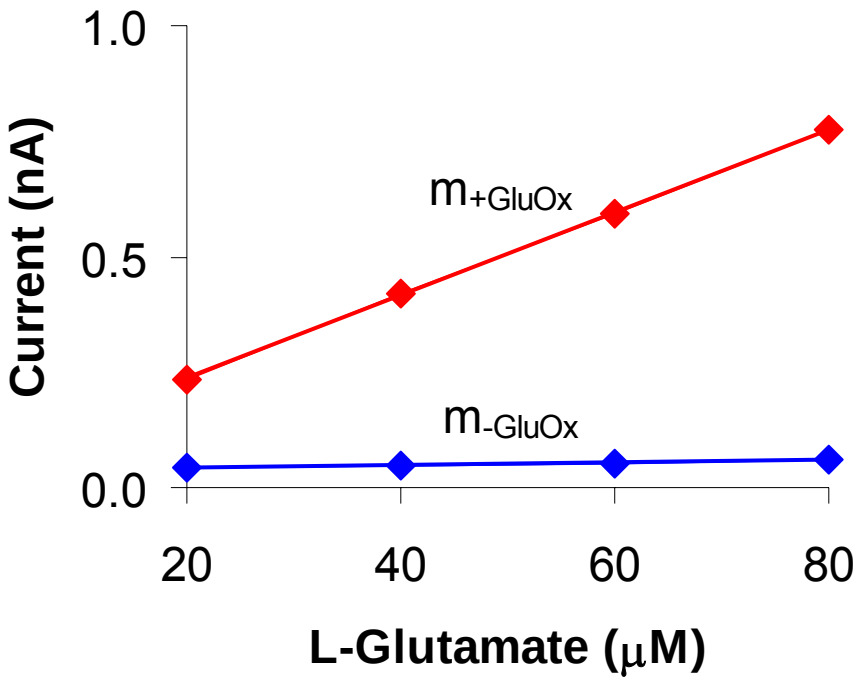

Figure 3.2 Slopes of Glu Recording Sites and Sentinel Sites under Normal Calibration Conditions

Data from a representative calibration are shown. Though calibrations can be graphed as current versus time (Figure 3.1), the data can also be replotted to show the average current at each Glu concentration. The slope of the linear regression of this plot produces our calibration factor (ΔI/μM Glu) for each recording site. When we subtract raw current data between paired channels to use self-referencing recordings quantitatively (i.e. I_{+GluOx} minus I_{-GluOx}), the proper calibration factor to determine Glu concentration is the difference between the slopes from the paired channels (i.e. m_{+GluOx} minus m_{-GluOx}). Because enzyme-free sites do not respond to Glu, $m_{-GluOx} \approx 0$, and the calibration term simplifies to m_{+GluOx}. In short, $\Delta Glu = (I_{+GluOx} - I_{-GluOx})/ m_{+GluOx}$, where ΔGlu = the change in Glu concentration between the two paired channels at constant potential (+0.7 V vs. Ag/AgCl reference).

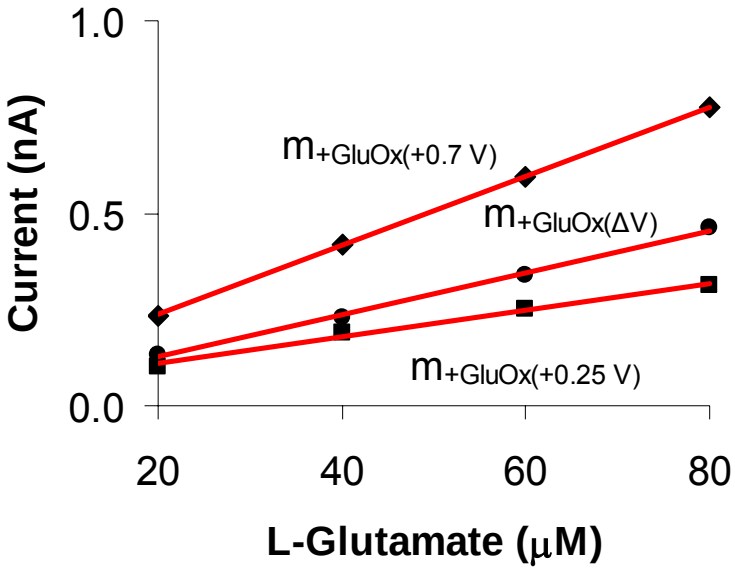

Figure 3.3 Slopes of Glu Recording Sites Calibrated at Two Different Applied Potentials

To use a varied voltage analytical approach to measure basal Glu, we calibrated the same microelectrode arrays at two different applied potentials (vs. Ag/AgCl reference). Current versus Glu concentration plots are shown for a representative enzyme-coated recording site calibrated at +0.7 V (diamonds) and +0.25 V (squares). A voltage-dependent change in current on an enzyme-coated channel ($\Delta I_{+GluOx(\Delta V)} = I_{+GluOx(+0.7\ V)} - I_{+GluOx(+0.25\ V)}$) minus a voltage-dependent change in current on an enzyme-free channel ($\Delta I_{-GluOx(\Delta V)} = I_{-GluOx(+0.7\ V)} - I_{-GluOx(+0.25\ V)}$) produces the change in current due to Glu revealed by a change in applied potential ($\Delta I_{Glu(\Delta V)}$). The proper calibration factor to convert this current into Glu concentration is the difference between the slopes calculated for an enzyme-coated recording site calibrated at the different applied potentials ($m_{+GluOx(+0.7\ V)} - m_{+GluOx(+0.25\ V)} = m_{+GluOx(\Delta V)}$, circles). Again, enzyme-free slopes are very close to zero and do not contribute to the calculations. In summary, $\Delta Glu(\Delta V) = \Delta I_{Glu(\Delta V)} / m_{+GluOx(\Delta V)}$, where $\Delta Glu(\Delta V)$ = the change in Glu concentration between the two paired channels (enzyme-coated and enzyme-free) using a varied applied potential approach.

Each potassium-evoked Glu signal was described by the following parameters: amplitude (μM Glu), rise time (T_R (sec)), and total signal duration (T_{Total} (sec)). Refer to the Data Analysis section of Chapter Two for detailed explanations of these signal parameters. Average parameters were compared for each potassium concentration using an unpaired, two-tailed t-test with Welch's correction (α=0.05).

Results

Basal Glu Regulation: Effects of TTX and TBOA

The potent voltage-dependent sodium channel blocker tetrodotoxin (TTX) was locally applied to inhibit action potential-dependent vesicular release in the recording area (Figure 3.4A). TTX applications (100 μM barrel concentration, ~100 nl) produced a rapid drop in our signal in both the rat striatum (n=17 recordings in 5 rats) and frontal cortex (n=17 recordings in 5 rats). The observed decreases were significantly greater than the dilution artifact produced by physiological saline ejection (striatum: n=11 recordings in 4 rats, frontal cortex: n=10 recordings in 4 rats). The average TTX-dependent changes in Glu concentration were 1.9 ± 0.7 μM and 2.0 ± 0.8 μM (mean ± SEM) in the striatum and frontal cortex, respectively (Figure 3.4B). We also investigated the effects of the potent, competitive, non-transportable excitatory amino acid transporter (EAAT) inhibitor D,L-threo-β-benzyloxyaspartate (TBOA). Local applications of TBOA (100 μM barrel concentration, ~100 nl) caused a transient but detectable signal increase compared to physiological saline ejection within 5 minutes in both the rat striatum (n=54 recordings in 3 rats) and frontal cortex (n=44 recordings in 4 rats) (Figure 3.5A). The average TBOA-dependent changes in Glu concentration were 1.6 ± 0.1 μM and 2.8 ± 0.4 μM (mean ± SEM) in the striatum and frontal cortex, respectively (Figure 3.5B).

A.

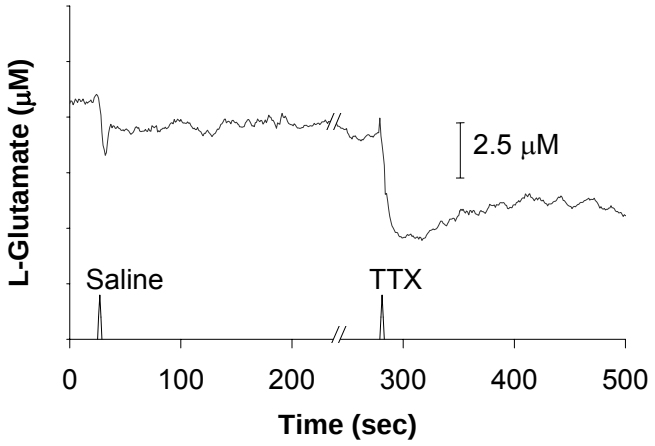

B.

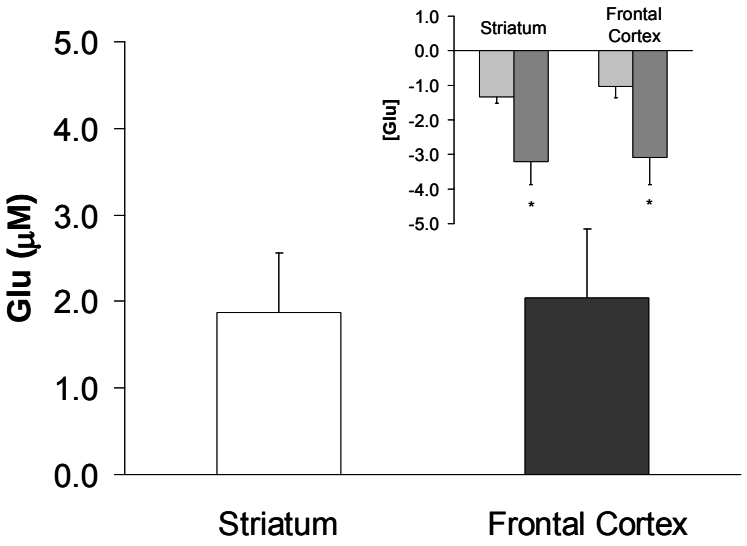

Figure 3.4 The Effects of TTX on Basal Glu Recordings

A) The composite trace demonstrates the typical effects of locally applied physiological saline and TTX (100 μM, ~100 nl) in the rat brain. B) The average decrease in apparent Glu concentration was significantly larger for TTX (dark gray bars) than saline applications (light gray bars) in the striatum and frontal cortex (inset, *$p<0.05$). Subtracting the apparent change in Glu due to saline (dilution artifact) from the apparent change in Glu due to TTX, the TTX-dependent Glu concentration was approximately 2 μM in both brain regions.

A.

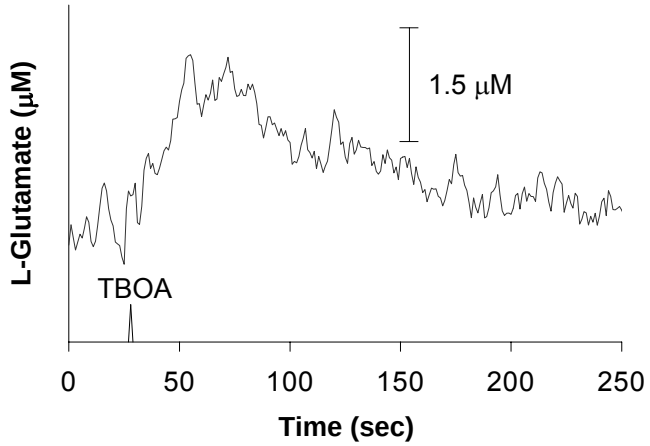

B.

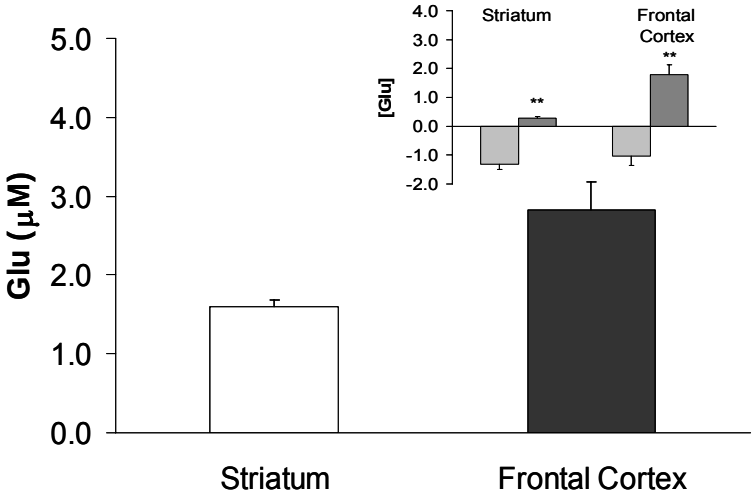

Figure 3.5 The Effects of TBOA on Basal Glu Recordings

A) The recording trace demonstrates a transient increase in signal following local application of the potent, general EAAT inhibitor TBOA (100 μM, ~100 nl). B) The average maximal change in apparent Glu concentration was significantly different following TBOA application (dark gray bars) compared to saline (light gray bars) in the striatum and frontal cortex (inset, **p<0.0001). Correcting for dilution, the average TBOA-dependent Glu concentration ranged from 1-3 μM in these brain regions.

Basal Glu Measures

Based on the TTX-dependent Glu levels that we observed, we were interested in determining overall steady-state basal Glu levels in the anesthetized rat striatum and frontal cortex. Investigating this question by analyzing channels individually is not possible because the baseline signal on each enzyme-coated channel is not a pure measurement of basal Glu. Instead, we recorded Glu in a self-referencing mode (see Burmeister and Gerhardt, 2001) to quantify basal Glu levels. We used two different methods based on comparing signals from paired enzyme-coated (+GluOx) and enzyme-free (-GluOx) channels; hereafter referred to simply as paired channels. First, we compared paired channel recordings at a constant applied potential (+0.7 V vs. Ag/AgCl) (Figure 3.6A). Calculated average signal differences were then converted to Glu concentration using an appropriate calibration factor (Figures 3.2 and 3.6B). Using this method, we measured an average basal Glu level of 1.4 ± 0.2 μM (n=16 recordings in 8 rats) in the striatum and 1.6 ± 0.3 μM (n=13 recordings in 8 rats) in the frontal cortex (Figure 3.6C). We also used a second approach that employed our ability to record at different applied potentials. By calibrating and conducting *in vivo* recordings separately at two different applied potentials (+0.25 V vs. +0.7 V, vs. Ag/AgCl reference), we could compare voltage-dependent signal changes between paired channels. Differences on enzyme-free channels primarily reflect changes in the background current due to the change in applied voltage. This change in background current also occurs on enzyme-coated channels. However, the voltage-dependent differences also reflect an increased ability to detect Glu (Figure 3.7A). Once again, average signal differences are converted to Glu concentration using an appropriate calibration factor (Figures 3.3 and 3.7B). Using this approach, we measured an extracellular Glu level of 1.8 ± 0.3 μM (n=16 recordings in 8 rats) in the striatum and 1.8 ± 0.4 μM (n=15 recordings in 8 rats) in the frontal cortex (Figure 3.7C). There was no significant difference in brain region-specific average basal Glu measures between the constant potential and varied potential methods. Recall that our TTX-saline comparisons revealed a TTX-dependency of

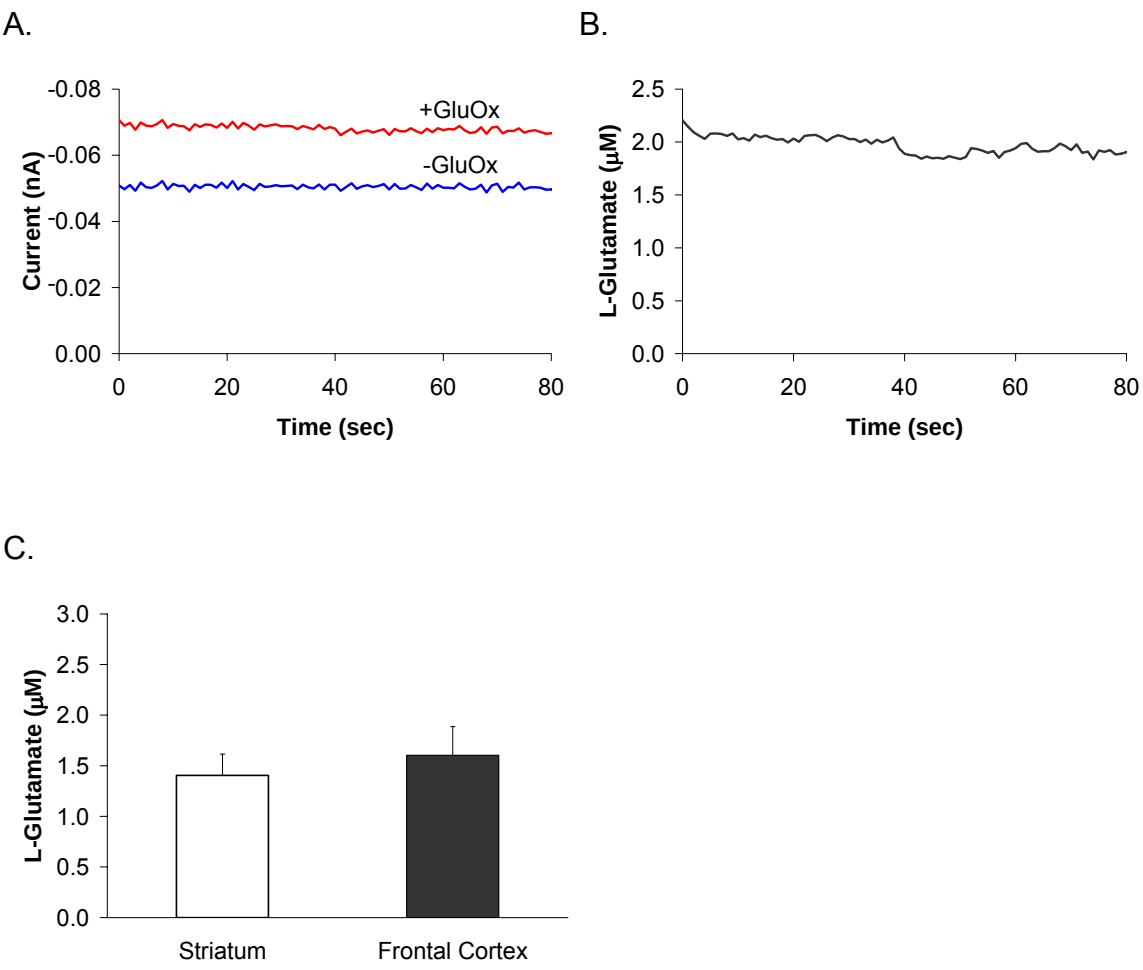

Figure 3.6 Basal Glu Measures Using a Constant Applied Potential Method

Passive simultaneous recordings from paired channels (enzyme-coated and enzyme-free) were compared and signal differences were converted to average Glu concentrations using appropriate calibration factors (see Figure 3.2). A) Recording in a self-referencing mode at a constant potential (+0.7 V vs. Ag/AgCl) allowed the detection of basal Glu on the enzyme-coated channel (+GluOx) which increases the baseline signal compared to the simultaneous response on the enzyme-free channel (-GluOx). B) The product of sychronized signal subtraction and conversion to Glu concentration is demonstrated. C) Average basal Glu measures for the striatum and frontal cortex were 1.4 ± 0.2 and 1.6 ± 0.3 (µM Glu, mean ± SEM), respectively.

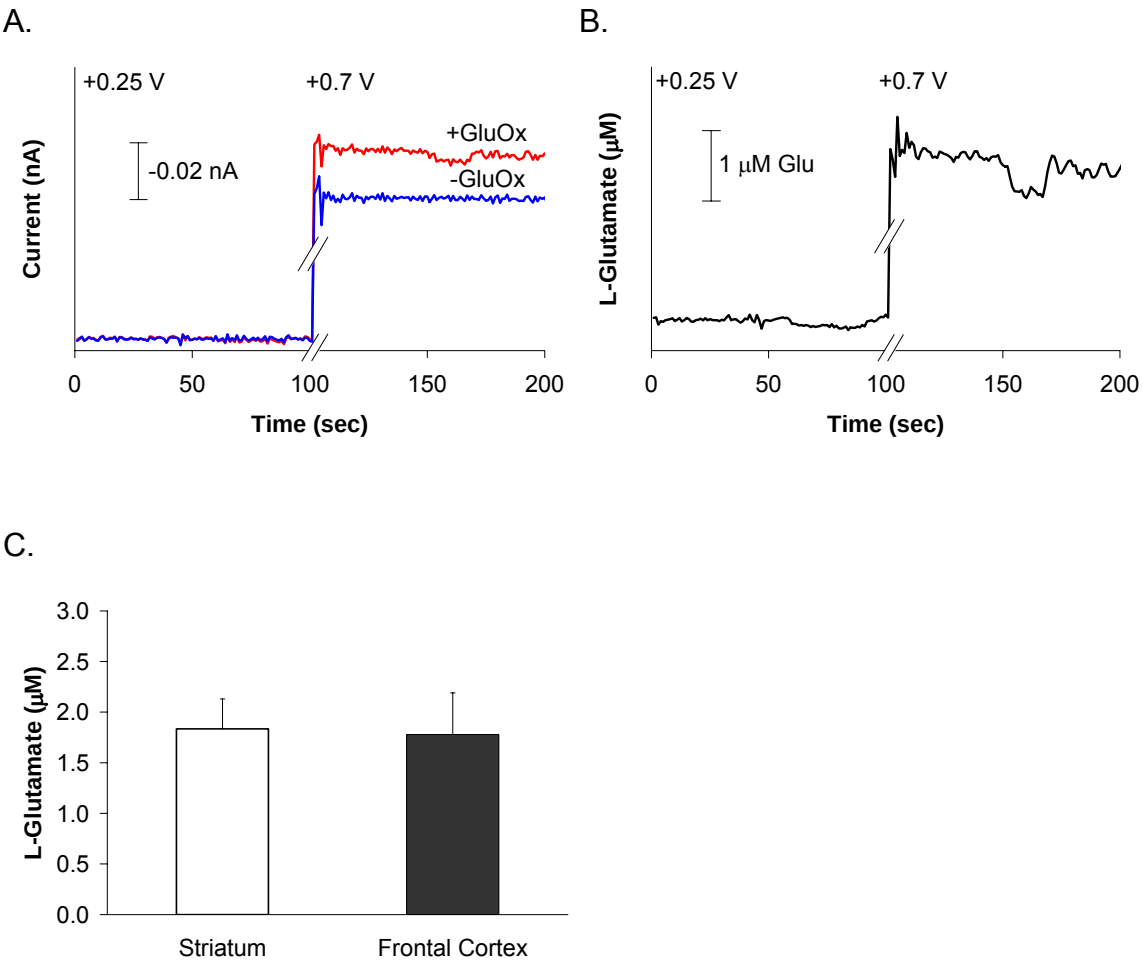

Figure 3.7 Basal Glu Measures Using a Varied Applied Potential Method

A) Self-referencing signal analysis was used in conjunction with varied applied potential (+0.25 V vs. +0.7 V, vs. Ag/AgCl) to measure basal Glu. Recording at +0.25 V nearly eliminated the detection of the Glu reporter molecule H_2O_2. At +0.7 V, H_2O_2 detection is restored. Aligned voltage-dependent signal changes from paired channels showed a universal increase due to heightened background current. The +GluOx channel increase was larger due to additional Glu detection. B) The result of sychronized signal subtraction and conversion to Glu concentration is shown. The appropriate calibration factor was previously described (Figure 3.3). C) Average basal Glu measures for the striatum and frontal cortex were 1.8 ± 0.3 and 1.8 ± 0.4 (µM Glu, mean ± SEM), respectively. Basal Glu measures did not significantly differ by method (c.f. Figure 3.6).

1.9 ± 0.7 μM in the striatum and 2.0 ± 0.8 μM in the frontal cortex (Figure 3.4). These differences did not significantly differ from our paired channel subtraction determinations of average basal Glu measures for either brain region. Taken together, our data support the hypothesis that basal Glu levels in two regions of the urethane-anesthetized rat brain are fully TTX-dependent and likely arise from neuronal vesicular release.

Potassium-Evoked Glu Release

To further explore potassium-evoked Glu release, we examined Glu responses under different depolarizing conditions and focused on their reproducibility. Pressure ejections of both 70 mM and 120 mM KCl solutions (50-275 nl, average volume 113 nl) evoked reproducible Glu release in the anesthetized rat striatum and frontal cortex (Table 3.1). The 120 mM KCl stimulations produced Glu signals with larger peak amplitudes (μM Glu) than 70 mM KCl in both the striatum (13.3 ± 0.9 vs. 5.7 ± 0.3, mean ± SEM, $p<0.0001$) and frontal cortex (15.9 ± 0.9 vs. 8.4 ± 0.5, $p<0.0001$). Rise times (T_R in seconds) were slightly longer for 120 mM KCl versus 70 mM KCl in the striatum (2.8 ± 0.2 vs. 1.6 ± 0.1, mean ± SEM, $p<0.0001$) but were not significantly longer in the frontal cortex (2.0 ± 0.1 vs. 1.7 ± 0.1, N.S.). Signal durations (T_{Total} in seconds) were also significantly longer after 120 mM KCl compared to 70 mM KCl in the striatum (13.0 ± 0.3 vs. 9.7 ± 0.3, mean ± SEM, $p<0.0001$) and frontal cortex (13.4 ± 0.3 vs. 9.6 ± 0.3, $p<0.0001$). In Figure 3.8A, local stimulations (70 mM KCl, 100 nl) in the anesthetized rat striatum produced signals that rose to peak amplitude in 1-4 seconds and lasted approximately 10-20 seconds. Evoked Glu signals in the frontal cortex maintained similar amplitudes and durations at stimulation intervals as short as 15 seconds (120 mM KCl, 100 nl, Figure 3.8B) and began to overlap with extracellular Glu accumulation at intervals of 10 seconds (Figure 3.8C). Other neurotransmitters, such as DA, fail to show readily reproducible potassium-evoked responses when stimulated at rapid intervals (see Gerhardt, Rose, and Hoffer, 1986).

Table 3.1 Potassium-Evoked Glu Kinetics

Average peak amplitudes in both the striatum and frontal cortex significantly differed ($p<0.0001$) between responses to 70 and 120 mM potassium solutions. Typical Glu responses rose to peak amplitude in 1-2 seconds and lasted approximately 10-20 seconds. Reported values for peak amplitude, T_R, and T_{Total} represent the mean ± SEM.

	Striatum		**Frontal Cortex**	
	70 mM KCl	**120 mM KCl**	**70 mM KCl**	**120 mM KCl**
Number of rats	4	3	4	3
Number of responses	160	80	140	90
Peak amplitude (μM Glu)	5.7 ± 0.3	13.3 ± 0.9	8.4 ± 0.5	15.9 ± 0.9
Rise time (T_R (sec))	1.6 ± 0.1	2.8 ± 0.2	1.7 ± 0.1	2.0 ± 0.1
Signal Duration (T_{Total} (sec))	9.7 ± 0.3	13.0 ± 0.3	9.6 ± 0.3	13.4 ± 0.3

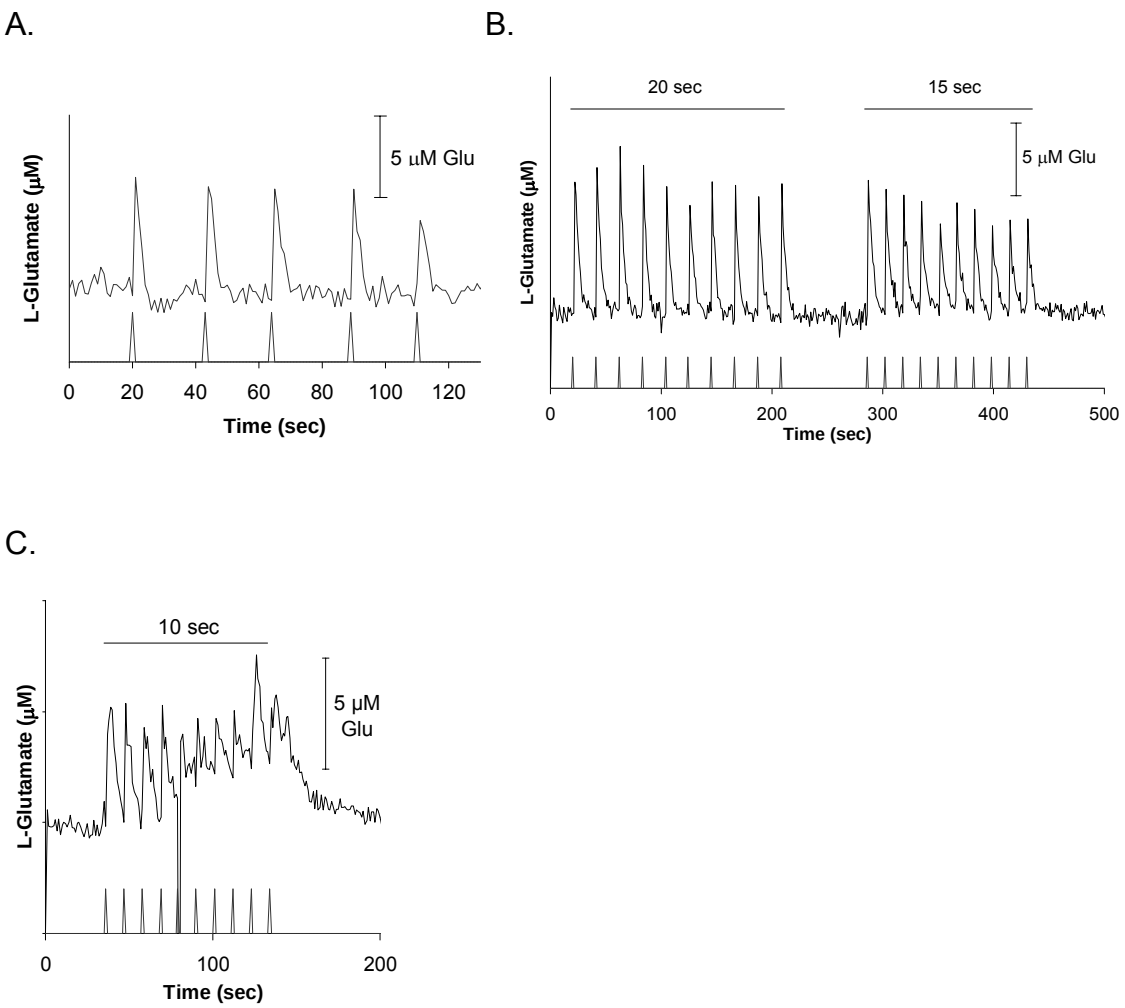

Figure 3.8 The Speed and Reproducibility of Potassium-Evoked Glu Signals

A) The 70 mM potassium ejections (100 nl, black arrows, 20 second ejection intervals, striatum) evoked rapid Glu releases. Following each release, the robust Glu transport system quickly cleared the extracellular space back to basal Glu levels. B) and C) Responses to local 120 mM potassium applications (75 nl each, black arrows, frontal cortex) provide evidence for tremendous reserve and/or rapid replenishment within the Glu neurotransmitter pool in the rat brain. Multiple serial stimulations with decreasing ejection intervals produced signals that were readily reproducible. Each application stimulated Glu release and uptake events that showed a high degree of similarity within the series but remained distinct with as little as 15 seconds between applications. Glu began to accumulate and distinct signals were lost at 10 second stimulation intervals.

Further Confirmation that Glu is the Source of the Potassium-Evoked Glu Signals

To further address the identity of our potassium-evoked signals, we designed experiments to study Glu in a self-referencing recording mode (see Burmeister and Gerhardt, 2001). Enzyme-free sites can detect all of the molecules that enzyme-coated sites can detect except Glu. Qualitatively, these sites act as “sentinels”, alerting us to the presence of interferences. When there are no signal changes recorded on enzyme-free channels, we have very high confidence that detected signals on enzyme-coated sites result purely from the presence of extracellular Glu. Figure 3.9 shows a Glu recording in the anesthetized rat striatum at +0.7 V and +0.2 V (both vs. Ag/AgCl reference). At the higher potential, an enzyme-coated site (+GluOx) recorded potassium-evoked Glu signals (70 mM KCl, 125 nl) while the adjacent enzyme-free site (-GluOx) showed no change in signal. At the lower potential, we repeated the stimulations but observed no responses on either channel. The Glu reporter molecule H_2O_2 oxidizes efficiently at an applied potential of +0.7 V but poorly at +0.2 V. By contrast, many interferents, such as DA, can produce a detectable signal at the lower potential (Pomerleau et al., 2003). Taken together, the potassium-evoked Glu releases that we recorded were both enzyme-dependent and voltage-dependent, supporting that the major source of the potassium-evoked signals is Glu.

Discussion

Using enzyme-coated multisite Pt-based microelectrode arrays to study *in vivo* Glu regulation in the anesthetized rat brain, we have found that Glu levels are tightly regulated in the mammalian CNS, making the dynamics of Glu release and uptake very rapid. Basal Glu is regulated by active release and uptake mechanisms, including TTX-dependent vesicular release. A self-referencing recording mode can be used to further verify the identity of our signal. We also

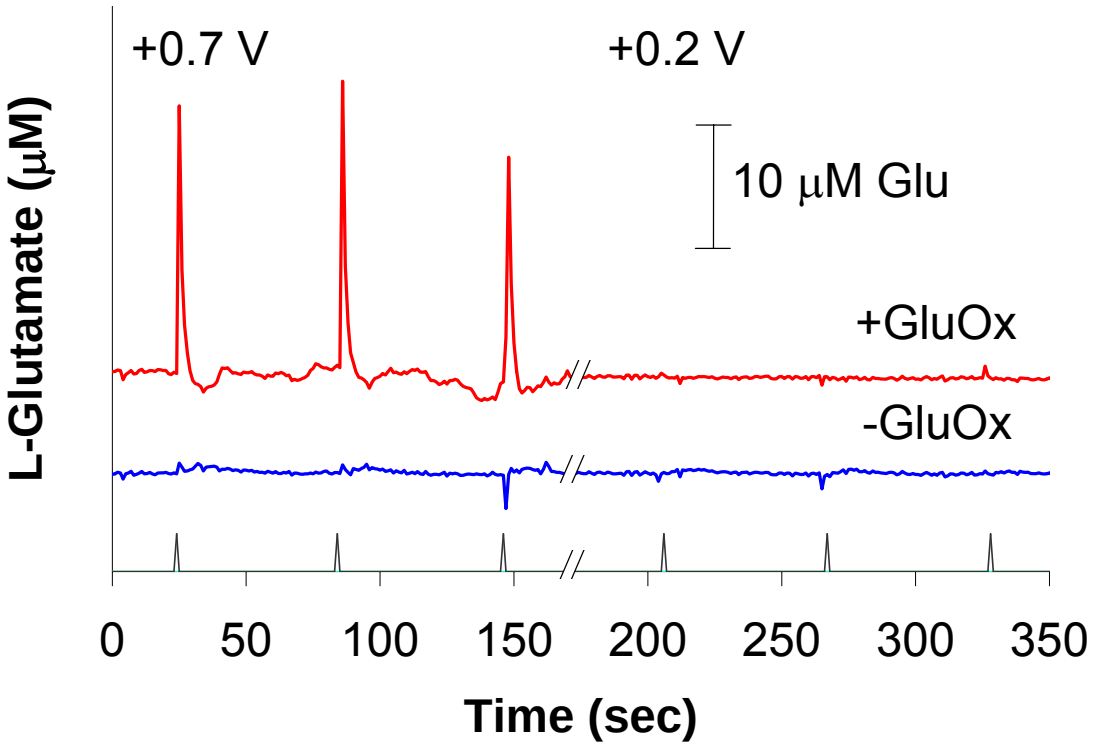

Figure 3.9 Selectivity of Glu Measures

The upper trace shows the signals recorded from an enzyme-coated recording site (+GluOx). The lower trace represents a simultaneous recording on an adjacent enzyme-free recording site (-GluOx). At an applied potential at which H_2O_2 will readily oxidize on platinum (+0.7 V versus Ag/AgCl reference electrode), 70 mM potassium ejections (black arrows) evoked signals detected only on the enzyme-coated channel. This indicates that our signal is enzyme-derived. To further test the theory that the enzyme-derived Glu reporter molecule H_2O_2 is responsible for our signal, we lowered the applied voltage to +0.2 V and repeated the stimulations. At +0.2 V, H_2O_2 oxidizes very poorly on platinum, unlike other electroactive species such as DA. At +0.2 V, we detected no evoked signal on any channel.

used this recording mode to determine absolute basal Glu levels, which were approximately 2 μM in the rat striatum and frontal cortex. These levels did not significantly differ from TTX-dependent Glu concentrations, supporting the hypothesis that basal Glu likely originates from neuronal vesicular release in two regions of the urethane-anesthetized rat brain. Following short burst local potassium stimulations, most Glu signals rose to peak amplitude in 1-2 seconds and lasted approximately 10-20 seconds, creating a characteristic spike pattern of evoked Glu release and uptake kinetics. Both neuronal vesicular Glu release and the Glu uptake system were robust, as potassium-evoked Glu signals were readily reproducible at stimulation intervals as short as 15 seconds.

In the present studies, we used multiple approaches to study basal Glu including examining drug effects on underlying release and uptake mechanisms and implementing new analytical approaches and technological refinements to measure basal Glu levels. Basal measures of Glu may reflect an extracellular steady-state, controlled by active Glu release and uptake mechanisms (Herrera-Marschitz et al., 1996, Lada, Vickroy, and Kennedy, 1998). Known release mechanisms include neuronal vesicular release, excitatory amino acid transporter (EAAT) uptake reversal, and metabolic Glu exchange for other molecules (e.g. cystine) (Fillenz, 1995, Anderson and Swanson, 2000, Baker et al., 2002). In fact, the relationship between basal Glu and the Glu-cystine antiporter has been studied in the rat striatum by Baker et al. (2002). They found that blocking neuronal release had a relatively small effect (0-30% decrease) on microdialysis measures of extracellular Glu compared to inhibition of the Glu-cystine antiporter (60% decrease). Independent TTX and TBOA applications allowed us to inhibit voltage-gated sodium channel-dependent vesicular Glu release and glial and neuronal Glu uptake to reveal the significance of these processes in maintaining steady-state basal Glu levels. We observed a significant but transient increase in our signal following TBOA, supporting that there are steady-state Glu release mechanisms that require active Glu uptake to keep basal Glu levels well-controlled. TBOA was chosen for its potency and non-transportable properties. TBOA inhibits EAAT's by blocking the transporters

without inducing transport currents or heteroexchange for Glu, unlike competitive transporter substrates such as D,L-*threo*-β-hydroxyaspartate (THA) or L-*trans*-2,4-pyrrolidine dicarboxylate (PDC) (Shimamoto et al., 1998, Shigeri et al., 2001). The transient nature of these signal changes may be explained by the fact that local TBOA application leaves a large number of EAAT's unaffected at the periphery of the relatively small drug-affected area. These EAAT's may be clearing Glu as it diffuses along its concentration gradient. Also, because TBOA is a competitive inhibitor, some of the Glu may have been cleared by EAAT's in the recording area if rising levels of extracellular Glu sufficiently increased to dislodge TBOA from the transporters. The TTX-dependent signal decreases that we recorded were significantly greater than the dilution artifacts created by intracranial saline ejections, demonstrating that basal Glu levels are maintained to some extent by action potential-dependent vesicular release. We extended our saline-TTX comparison to quantify how much of the signal change observed following TTX was drug-dependent by subtracting the effects of dilution and arrived at approximately 2 μM Glu in both the striatum and frontal cortex.

However, the prior approach does not necessarily reveal the overall basal Glu levels, and the question of what percentage of total basal Glu is TTX-dependent remained. We configured our microelectrode arrays in a self-referencing recording mode and took two additional approaches based on constant potential and varied potential paired channel recordings to measure total basal Glu. We observed no significant differences in brain region-specific Glu measures between the methods; the average basal Glu was ~2 μM Glu in both the striatum and frontal cortex. Comparing this to our TTX studies, we discovered that basal Glu levels in two regions of the urethane-anesthetized rat brain are fully TTX-dependent and likely arise from neuronal vesicular release. Interestingly, all three subtraction methods that we used to quantify measures of total or neuronally-derived basal Glu yielded very similar results. Basal Glu in the chloral hydrate-anesthetized rat brain has previously been studied using microsensors with electrochemical detection (Kulagina, Shankar, and Michael, 1999). This study used similar investigational strategies including comparing

enzyme-coated and enzyme-free adjacent electrodes and local TTX applications. Both their measures of resting (29.0 ± 9.0 μM Glu) and TTX-dependent Glu levels were larger than our measures possibly due to differences in anesthetic drugs or their recording methods; however, they observed significant signal decreases following TTX applications (100 μM, 200 nl, resulting in a 25-85% decrease vs. original baseline signals), which were similar to our results. Alternatively, published studies support that less than 50% of basal Glu measured by microdialysis is TTX-dependent (Herrera-Marschitz et al., 1996, Timmerman and Westerink, 1997, Baker et al., 2002). The differences that we observed in our assessments of the magnitude and TTX-dependency of basal Glu levels compared to prior electrochemical and microdialysis studies may stem from altered basal Glu regulation related to the anesthetic drug urethane. There are reports of decreased Glu release (Hudspith, 1997) and increased Glu uptake (Danbolt, 2001) due to other anesthetics such as halothane and isoflurane. Highly relevant ongoing Glu recordings in our lab in the awake, freely-moving rat (unpublished data) have started to reveal differences in basal Glu regulation, which support a significant effect of urethane anesthesia on basal Glu measures. We may discover with further investigation that basal Glu levels are much higher in the awake rat brain than those measured in the urethane-anesthetized rat brain, that other anesthetics alter basal Glu regulation to different degrees, and that the fraction of basal Glu that is TTX-dependent differs under awake or alternatively anesthetized conditions.

Previously reported *in vivo* measures have supported the hypothesis that potassium-evoked Glu has fast kinetics of release and uptake (Hu et al., 1994, Burmeister et al., 2002, Burmeister and Gerhardt, 2003). Our experiences with evoked Glu dynamics have consistently resembled the fast release and uptake parameters observed by Hu et al. (1994) who used similar enzyme-based amperometric recording techniques that were highly selective for Glu. Their studies demonstrated Glu responses to potassium stimulations (100 mM KCl, 1000 nl) that rose to peak amplitude in a few seconds and lasted roughly 1 minute, which were reproducible given a 20 minute rest interval. They also

demonstrated fast responses to Glu ejections (1 mM, 200-1000 nl) that peaked in a few seconds and returned to baseline in ~20 seconds, which is consistent with some of our previous observations using Glu selective microelectrode arrays (Burmeister and Gerhardt, 2001). In this chapter, we expanded our studies of potassium-evoked Glu kinetics using two different concentrations of potassium solutions and further investigated the reproducibility of potassium-evoked Glu release. There were potassium concentration-dependent effects on the peak amplitudes, rise times, and total signal times. Interestingly, the rise time data sets did not appear to have normal Gaussian distributions. Instead, at our current sampling rate (1 Hz), the data appeared to follow a Poisson distribution, with over half of the recorded rise times at 1 second (70 mM KCl in both brain regions, 120 mM KCl in the frontal cortex) or within 2 seconds (120 mM KCl in the striatum). These observations emphasize not only that evoked Glu release is rapid, but that even with second-by-second monitoring, we still do not have an accurate measure of the speed of all of our potassium-evoked Glu signals. Overall, the 70 mM potassium solution evoked Glu signals that were slightly smaller and faster than the 120 mM potassium-evoked Glu signals. Potassium-evoked Glu signals stimulated at 20 second intervals displayed a high level of reproducibility. In fact, we were able to stimulate highly reproducible Glu signals at intervals as short as 15 seconds. Most evoked Glu signals lasted approximately 10-20 seconds, so that if we reduced the time interval to 10 seconds, we could stimulate a Glu signal and then evoke additional Glu release before the first Glu signal was cleared (Figure 3.8C). This is an important difference compared to potassium-evoked Glu measures reported by Hu et al. (1994). Our data do not support the hypothesis that there is a lengthy refractory period for evoked Glu release, which was the explanation offered by the authors for the 20 minute rest interval that they observed between reproducible potassium-evoked Glu signals. Though the potassium concentration was similar, their volumes of potassium were higher (1000 nl vs. 50-275 nl) which may explain their larger average signal amplitudes (60.5 ± 9.1 μM Glu), but this does not necessarily explain the lengthy rest period. They were also recording potassium-evoked Glu release in the hippocampus of

urethane-anesthetized rats, while our recordings were reported for the striatum and frontal cortex. However, we have observed rapid reproducibility of potassium-evoked signals in the rat hippocampus (unpublished data), so that the difference is likely not brain region-specific and may relate to their electrode design or other differences in experimental variables. High levels of extracellular potassium and Glu have both been reported to initiate spreading depression in cortical areas (Somjen, 2001), which might explain their findings. The reproducibility of our potassium-based methods for measuring evoked Glu release demonstrate that spreading depression likely does not occur in the brains of the animals that we record. Overall, we have shown that evoked Glu release and uptake are very fast, potassium concentration-dependent, and reproducible. Our results highlight how our microelectrode-based sampling and detection technology with superior spatial and temporal (second-by-second) resolution is well-suited to study Glu kinetics.

We have previously demonstrated that our enzyme-based microelectrode recording technique can reliably measure Glu (Burmeister et al., 2000, Burmeister et al., 2001). However, it is necessary to critically evaluate underlying basal and evoked signals *in vivo* because other electroactive species might interfere with our recordings (Gerhardt and Burmeister, 2001, Robinson et al., 2003). Generally, the major interferent for voltammetric recordings at lower potentials in the extracellular space of the mammalian CNS is AA (Hu et al., 1994, Fillenz, 1995, Kulagina, Shankar, and Michael, 1999, Cui et al., 2000, Gerhardt and Burmeister, 2000). To date, we have successfully used Nafion™ coated on the recording sites to repel anionic interferents such as AA and DOPAC and virtually eliminate their contribution to the overall signal. Furthermore, GluOx is critical to measuring Glu and provides additional specificity. In many brain areas, these coatings allow us to use constant potential amperometry at +0.7 V (vs. Ag/AgCl reference) to measure Glu with confidence in the identity of our signal. However, high potassium stimulation in some brain areas can cause the release of interfering electroactive species. The

demonstrated enzyme- and voltage-dependence of our potassium-evoked measures further support that the major source of our signal is Glu.

Measuring basal and potassium-evoked release of Glu is a beginning to understanding tonic and phasic release of Glu in the mammalian CNS. Tonic Glu is the steady-state extracellular Glu levels thought to be maintained at a low concentration range by the activities of neurons and glia within a brain region (Herrera-Marschitz et al., 1996, Lada, Vickroy, and Kennedy, 1998, Baker et al., 2002). Tonic Glu may be maintained in part by neuronal vesicular release, even basal level burst firing of neurons; however, the tonic Glu concentration is currently not thought to dramatically change on a second-by-second basis. Compared to tonic Glu release, phasic Glu release is a more entrained phenomenon in which synchronized or temporally overlapping neurotransmitter releases raise extracellular Glu higher than background tonic Glu levels. Phasic Glu release is followed by robust active neurotransmitter uptake, which returns the extracellular concentration to basal levels, and the entire process may change the extracellular Glu concentration very rapidly (Timmerman and Westerink, 1997, Danbolt, 2001). Basal and evoked Glu measures may simulate tonic and phasic Glu characteristics. Studies of both basal and evoked Glu regulation are important for understanding the normal glutamatergic system and the role of Glu in brain disorders. In this chapter, the development of methods to measure basal Glu levels using microelectrode arrays was inspired in part by microdialysis techniques, which have the capabilities to measure unstimulated levels of Glu in microdialysate fractions. A strength of microelectrodes coupled with electrochemical detection over microdialysis, however, is better temporal resolution (800 msec vs. commonly 5-20 minutes for microdialysis), which allowed us to monitor both basal and evoked Glu release on a second-by-second basis. Proponents of microdialysis have recognized the need to improve the temporal resolution of their measures and made considerable progress using on-line separation and detection technologies (i.e. CE-LIF), which have reduced the temporal resolution to 5-12 seconds (Lada, Vickroy, and Kennedy, 1997, Lada, Vickroy, and Kennedy, 1998, Kennedy et al., 2002). Ultimately, the temporal

resolution of microdialysis techniques is limited by sampling extracellular neurochemicals through a microdialysis membrane in a medium that is removed from the brain. This may be an important constraint for correlating both basal and evoked measures with electrophysiological events because such investigations may need second-by-second to subsecond temporal resolution to distinguish some of the roles of Glu.

In summary, the present studies using microelectrode arrays configured to record Glu signals on a second-by-second basis have helped us begin to understand basal and potassium-evoked Glu release in two areas of the anesthetized rat brain, the striatum and frontal cortex. We found that basal Glu is actively regulated by TTX-dependent release mechanisms and EAAT-dependent uptake. Quantifying the TTX-dependent portion of the signal changes revealed that a significant, measurable portion of the overall basal Glu levels were TTX-sensitive. Two self-referencing Glu recording methods (constant and varied applied potential) measured the total average basal Glu at roughly 2 μM in both brain regions. These measures did not significantly differ by method, nor were they significantly different from the average TTX-sensitive measures. These findings support that basal Glu is completely TTX-dependent and is likely due to neuronal vesicular release. The spatial resolution, direct sampling, and low micrololar limit-of-detection of our technology are advantageous for both basal and evoked Glu studies, which may simulate tonic and phasic Glu, respectively. Potassium-evoked Glu release and uptake are robust, transient, potassium concentration-dependent, and highly reproducible at intervals as short as 15 seconds.

Chapter Four: Alterations in L-Glutamate Regulation in the Unilateral 6-Hydroxydopamine (6-OHDA)-Lesioned Rat Brain

Introduction

The studies in this chapter build on our knowledge of normal Glu signaling in the rat brain and extend the applications of our microelectrode-based technology to include studies of Glu in an altered rat brain. Although there are several rat models of diseases in which Glu measures may be altered, our group is most interested in neurodegenerative disorders. Keeping with our dual role as members of both the Center For Sensor Technology (CenSeT) and one of currently eleven Morris K. Udall Centers of Excellence For Parkinson's Disease Research nationwide, we enthusiastically focused on studying Glu neurotransmission in a rat model of PD, the hemiparkinsonian unilateral 6-hydroxydopamine (6-OHDA)-lesioned rat. As previously described in Chapter One, PD has been examined more closely over the last decade as a disease of secondary Glu hyperactivity. Two major glutamatergic pathways associated with the involuntary motor system are strongly implicated, the corticostriatal pathway, which is largely the focus of the studies presented in this chapter, and projections from the subthalamic nucleus, which are also extremely interesting but more suitable for future studies.

The rat corticostriatal pathway emanates diffusely from all areas of the cortex to make synaptic connections bilaterally in the striatum (caudate and putamen) (Calabresi et al., 1996, Mitchell, Cooper, and Griffiths, 1999, Calabresi et al., 2000) (Figure 4.1). The caudate and putamen represent the major input nuclei of the involuntary motor pathways, which contain predominantly (95%) cell bodies of GABAergic medium spiny neurons (MSN) as well as some interneurons (INT, large aspiny neurons, 5%) which transmit several neurotransmitters including acetylcholine (Centonze et al., 1999, Mitchell, Cooper, and Griffiths, 1999). The MSN's project along two distinct pathways: the

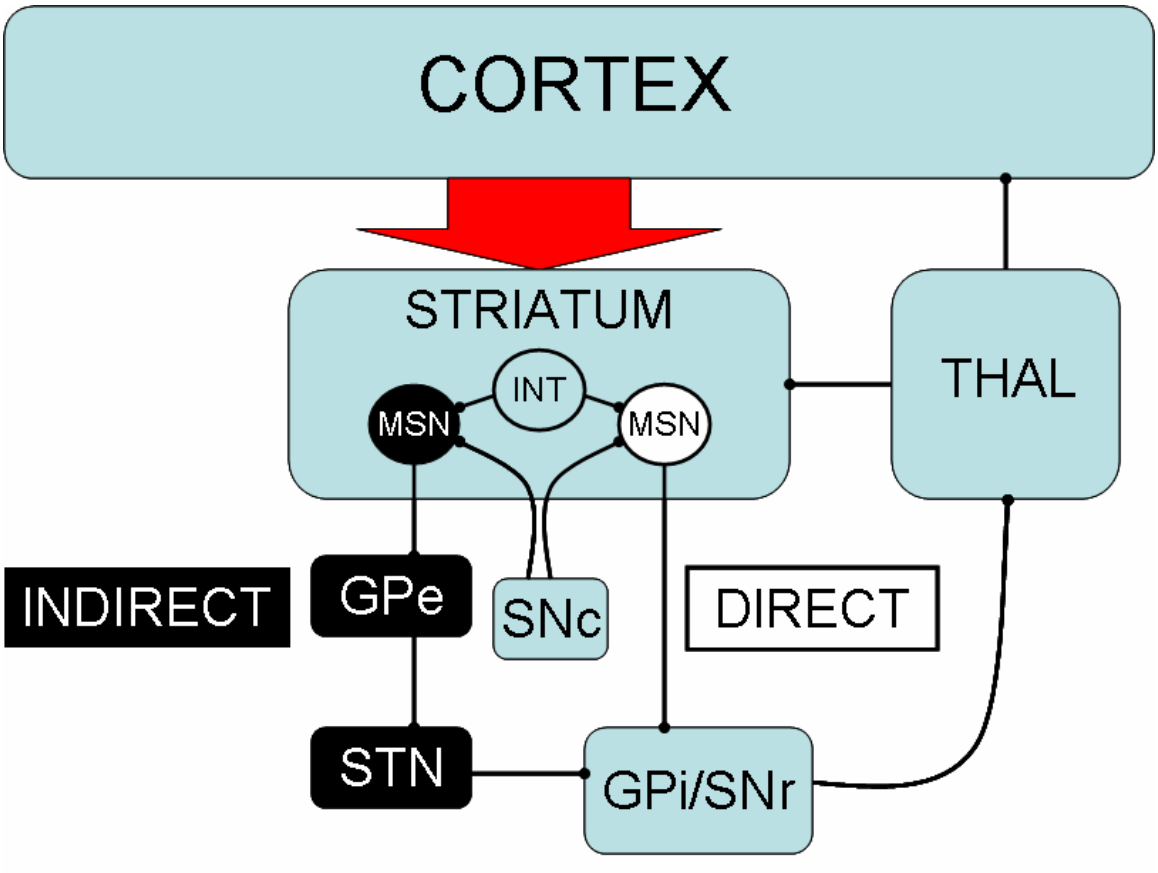

Figure 4.1 The Corticostriatal Pathway and the Basal Ganglia-Thalamocortical Circuitry

Predominantly, Glu descends to the striatum from all areas of the cortex along the corticostriatal pathway (red arrow). The direct and indirect pathways described in the text are also illustrated. See also Figure 1.2 for more details regarding the basal ganglia-thalamocortical pathways.

direct pathway, which facilitates voluntary movement, and the indirect pathway, which inhibits it (Mitchell, Cooper, and Griffiths, 1999, Marino et al., 2002). Glutamatergic projections descending from the cortex are thought to synapse on the heads of the dendritic spines of MSN's. Glu along the corticostriatal pathway provides the major excitatory driving force for the firing patterns of these neurons (Calabresi et al., 1996, Centonze et al., 1999, Calabresi et al., 2000). In the normal rat brain, DA ascends to the striatum from the SNc along the nigrostriatal pathway which is thought to synapse on the dendritic shafts of MSN's, closely apposed to Glu synapses, to modulate cell firing (Figure 4.2). It is also known that both Glu and DA heteroreceptors exist on these presynaptic terminals, so that DA can directly affect presynaptic Glu release events, and vice versa (Calabresi et al., 1996, Bamford et al., 2004).

In the unilateral 6-OHDA-lesioned rat model of PD, the synthetic neurotoxin 6-OHDA is injected into the medial forebrain bundle on one side where it is selectively taken up through the DA transporter into dopaminergic neurons. The 6-OHDA destroys both nerve terminals through axonal disruption and cell bodies through retrograde transport and the production of reactive oxygen species (Hudson et al., 1993, Reader and Dewar, 1999, Schober, 2004). The nigrostriatal pathway on the side of injection may be fully lesioned by this neurotoxin, resulting in unilateral DA denervation in the striatum. As the loss of DA neurotransmission along the nigrostriatal pathway is known to be central to human idiopathic PD, so does this loss of DA neurotransmission in the rat brain produce hemiparkinsonian motor abnormalities. These deficits are revealed in a stably lesioned rat brain by the administration of drugs which act on the DA system such as apomorphine, which is more effective in the supersensitized striatum ipsilateral to lesion and promotes movement in an imbalanced fashion that results in the rat exhibiting contralateral rotations (Perese et al., 1989, Hudson et al., 1993, Deumens, Blokland, and Prickaerts, 2002, Schober, 2004). Rats are considered to be >90% lesioned when they exhibit low dose apomorphine-induced contralateral rotations at a rate of >300/hour (>5/minute) (Hudson et al., 1993).

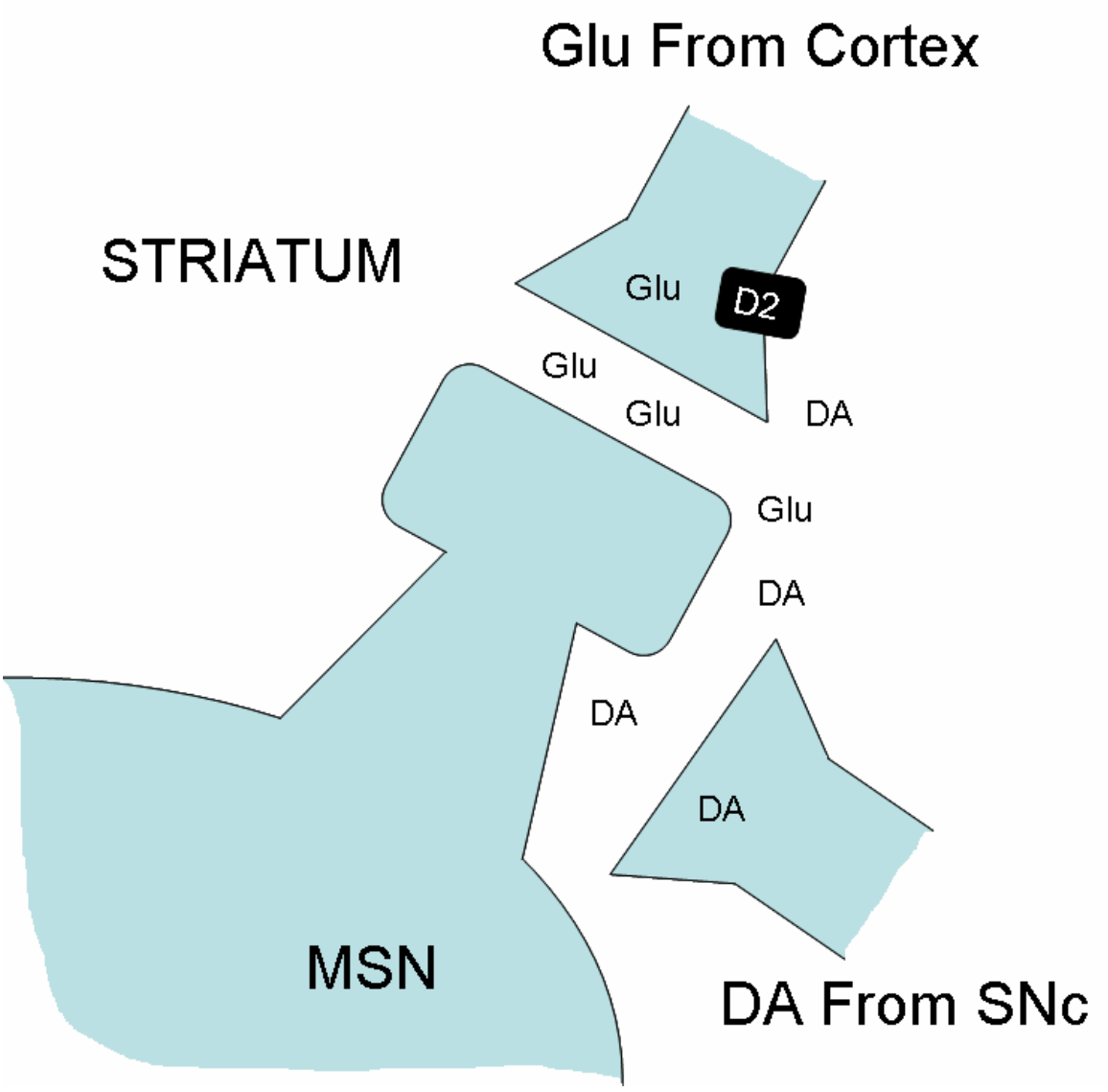

Figure 4.2 Glu-DA Interactions in the Striatum

Glu and DA can influence the firing of striatal projection neurons through direct activation of their receptors on the dendrites of MSN's. Synaptic spillover of these neurotransmitters may also occur, so that both Glu and DA can influence their own or each other's presynaptic release. For example, striatal DA inhibits Glu release through activation of D2-like receptors located on the glutamatergic presynaptic terminals.

The motor deficits in animal models of PD may begin with DA denervation in the striatum, but a large number of neurotransmitter systems are affected including Glu neurotransmission along the corticostriatal pathway (Albin et al., 1989). Such Glu alterations have been reported by several investigators (Tossman, Segovia, and Ungerstedt, 1986, Lindefors and Ungerstedt, 1990, Calabresi et al., 1996, Meshul et al., 1999); however, we had a unique opportunity to examine the dynamics of Glu release and uptake in the 6-OHDA-lesioned rat brain with greater temporal and spatial resolution than prior methods. We focused our studies on potassium-evoked Glu kinetics in the frontal cortex and striatum to collect information about the corticostriatal pathway. We additionally investigated potassium-evoked Glu release and uptake in the nucleus accumbens. Although the nucleus accumbens is cellularly organized almost identically to the striatum, DA is primarily transmitted from a different brain region, the ventral tegmental area (Mitchell, Cooper, and Griffiths, 1999, Lancia et al., 2004). Furthermore, although these structures have overlapping functions (Mitchell, Cooper, and Griffiths, 1999), the nucleus accumbens is primarily a limbic structure whereas the striatum may be more dedicated to movement; thus, there may be interesting regional differences in Glu measures. Potassium-evoked Glu signals from two groups of rats (unilateral 6-OHDA-lesioned and similarly-aged, non-lesioned rats) were characterized by signal parameters and compared by hemisphere both between groups and within the lesioned group. Our hypotheses were that evoked Glu kinetics would differ between lesioned and non-lesioned rats and that there would be ipsilateral and contralateral differences in Glu kinetics within the 6-OHDA-lesioned group.

Methods

Refer to Chapter Two for full descriptions. In the Animal Preparation For *In Vivo* Electrochemical Recordings section, the Normal Young Fischer 344 Rats and Unilateral 6-Hydroxydopamine-Lesioned Young Fischer 344 Rats subsections are relevant to the studies presented in this chapter.

Stereotaxic Implantation and Glu Recordings

Prior to implantation, a 45 mM potassium solution (45 mM KCl, 104 mM NaCl, 2.5 mM $CaCl_2 \bullet 2H_2O$, pH 7.4) was loaded into the single-barrel micropipette attached to the microelectrode array. The 45 mM potassium solution was tested in pilot animals and reliably evoked highly reproducible Glu signals with very few instances of simultaneously evoked DA release. The fully prepared microelectrode/micropipette assembly was implanted into the striatum (AP +1.0, ML ±2.1, DV -3.5 to -6.0 mm), the nucleus accumbens (AP +1.0, ML ±2.1, DV -6.5 to -7.0 mm), and the frontal cortex (AP +2.7, ML ±1.5, DV -2.0 to -4.0 mm). The striatum and nucleus accumbens were recorded in one pass. The microelectrode was removed from the brain, rinsed with 0.9% (physiological) saline, and stereotaxically implanted in the frontal cortex in a second pass. From the initial depth, the microelectrode was advanced into the brain using a hydraulic microdrive (Narishige MO-8) in 0.5 mm steps. This was repeated for the opposite hemisphere. A fifteen minute equilibration period per implantation was allowed prior to initial potassium stimulation, and a two minute equilibration period was allowed between depths. If spontaneous neurotransmitter release occurred when entering a new depth, additional time was permitted for the signal to return to basal levels before applying potassium. Ejections of 45 mM KCl (~300 nl) were made at one minute intervals at each depth to obtain five Glu responses evoked within the acceptable dose range (250 to 350 nl). Evoked Glu signals were recorded on a second-by-second basis by the FAST-16 recording system. At the end of the recording sessions of lesioned rats, the microelectrode

was removed from the brain and rinsed as before. Then, the 45 mM potassium solution was removed from the micropipette and replaced with a 70 mM potassium solution (70 mM KCl, 79 mM NaCl, 2.5 mM $CaCl_2 \bullet 2H_2O$, pH 7.4). The microelectrode/micropipette assembly was implanted in the striatum (AP +1.0, ML ±2.1, DV -5.0). Following equilibration, ejections of 70 mM KCl (~1800 nl) were made, and the resulting Glu and/or DA signals were recorded by the FAST-16 recording system.

Data Analysis

Each potassium-evoked Glu signal was analyzed and characterized by the following parameters: amplitude (μM Glu), uptake rate (μM Glu/sec), and T_{80} (sec). Refer to Chapter Two for a full description of signal parameters. Average signal parameters were compared between hemisphere-matched signals recorded in the 6-OHDA-lesioned animals and age-matched, non-lesioned control animals. They were also compared between signals recorded ipsilateral to lesion and contralateral to lesion within the unilateral 6-OHDA-lesioned group. Statistical comparisons were made using a one-way ANOVA with Bonferroni multiple-comparisons post-hoc test (α=0.05, α^*=0.0083). Values for signal parameters identified as outliers (values greater than 3 standard deviations from the mean) were excluded from analysis. Signals from the first brain area recorded per hemisphere (AP +1.0 ML ±2.1, DV -3.5, slightly superficial to the striatum) were primarily recorded to fine tune our pressure ejection system to deliver volumes of potassium solutions within the accepted dose range. As such, these signals were not considered in the data analysis.

Results

Contralateral DA Release

Unilateral 6-OHDA-lesioned rats were included in this study only if they met established criteria for a full (>90%) lesion of the nigrostriatal pathway on the side of injection (apomorphine-induced contralateral rotations ≥300 turns/hour). To verify this indirect measure of DA depletion, we ejected an extremely high dose of potassium (70 mM, ~1800 nl) bilaterally in the striatum of lesioned rats at the end of the recording sessions to depolarize all of the nerve terminals and directly measure some of the released neurotransmitters. As configured for the present studies, our microelectrode arrays are selective for Glu over anionic interferents such as AA and DOPAC, but display poor selectivity for Glu over the cation DA, which can also be detected (See Figure 3.1). DA is transmitted along the non-myelinated nigrostriatal pathway (Cooper, Bloom, and Roth, 1996), which requires much higher stimulation than myelinated (e.g. glutamatergic) pathways to evoke neurotransmitter release (unpublished data). Figure 4.3 shows that at a level of potassium stimulation approximately 10 times the typical amount used in these studies, we were able to stimulate and detect the release of both Glu and DA on the contralateral side (characteristic spike-dome signal shape). Furthermore, enzyme-free sentinel sites, which are not configured to detect Glu, recorded the DA release only on the contralateral side. Finally, Glu but not DA kinetics were recorded in the ipsilateral striatum (characteristic spike signal shape). Taken together, these results support that there was a full lesion on the ipsilateral side and functional DA terminals on the contralateral side.

Potassium-Evoked Glu Signals in the Striatum

Glu signaling in the striatum originates predominantly from cortical regions along the corticostriatal pathway which provides the primary excitatory influence on MSN cell firing behavior. We bilaterally recorded potassium-evoked (45 mM,

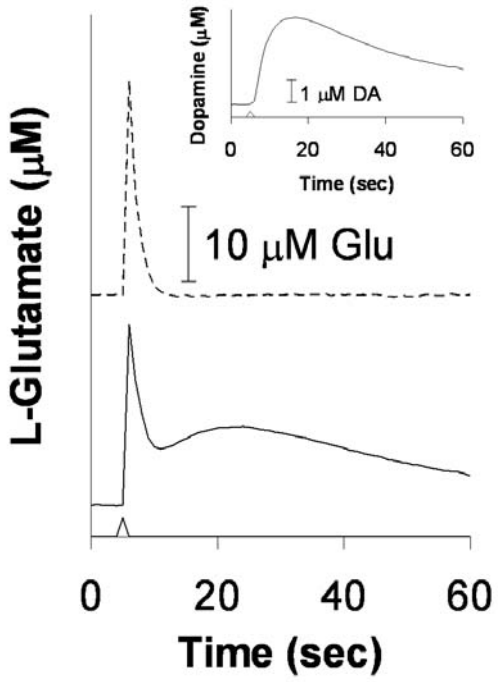

Figure 4.3 Contralateral DA Release

We used an extremely high dose of potassium (70 mM, ~1800 nl, black arrow) to evoke neurotransmitter release from both myelinated (e.g. glutamatergic) and non-myelinated (e.g. dopaminergic) projections. The upper trace (dashed line) shows a typical response on the ipsilateral side, a signal with rapid (spike) kinetics that are characteristic of Glu. The lower trace (solid line) shows a typical biphasic (spike-dome) response to the same stimulation on the contralateral side. The shape of this signal demonstrates simultaneous detection of Glu and DA release and uptake. Inset: A simultaneous recording from an enzyme-free (sentinel/referencing) site shows only the DA kinetics on the contralateral side.

~300 nl) Glu signals in the striatum (5 signals/Glu recording site/depth for 5 depths) of unilateral 6-OHDA-lesioned and non-lesioned rats within the same age range. The recorded signals were analyzed by average signal parameters that provide information about Glu release and uptake events and mechanisms (Table 4.1). Figure 4.4 shows representative traces of potassium-evoked Glu signals in the striatum of both groups of rats. Average Glu signal amplitudes (μM Glu) and uptake rates (μM Glu/sec) were significantly increased bilaterally in lesioned rats compared to hemisphere-matched, non-lesioned rats. Average T_{80}'s (sec) were slightly but significantly faster on the ipsilateral side and did not differ on the contralateral side compared to matched hemispheres in non-lesioned rats. Within the lesioned rat group, there were no significant differences between hemispheres in any of the reported signal parameters (Figure 4.5).

Potassium-Evoked Glu Signals in the Frontal Cortex

Glu terminals in the frontal cortex originate bilaterally from the thalamus and cortex (corticocortical pathways). We bilaterally recorded potassium-evoked (45 mM, ~300 nl) Glu signals in the frontal cortex (5 signals/Glu recording site/depth for 5 depths) of unilateral 6-OHDA-lesioned and non-lesioned rats (5-9 months old). Reported values for average signal parameters are included in Table 4.1. Representative traces of potassium-evoked Glu signals for both groups of rats are shown in Figure 4.6. Average amplitudes, uptake rates, and T_{80}'s of Glu signals from lesioned animals were significantly increased bilaterally compared to matched hemispheres from non-lesioned rats. Within the lesioned group, there were no significant differences between hemispheres for any of the reported signal parameters (Figure 4.7).

Potassium-Evoked Glu Signals in the Nucleus Accumbens

The nucleus accumbens is organized similarly to the striatum and receives Glu projections from similar areas. We bilaterally recorded potassium-evoked (45

Table 4.1 Potassium-Evoked Glu Signal Parameters

All Glu signal parameters are reported as mean ± SEM (*p<0.05, **p<0.01, ***p<0.001, vs. matched hemisphere in non-lesioned rat). The numbers of signals analyzed are indicated in parentheses below each average value. Amplitude, uptake rate, and T_{80} are expressed in μM Glu, μM Glu/sec, and sec, respectively. Within the lesioned group, there were no significant differences in average signal parameters between hemispheres ipsilateral and contralateral to lesion with the following exceptions. In the nucleus accumbens, the average amplitude ($^{\dagger}p<0.05$) and uptake rate ($^{\ddagger}p<0.001$) were increased on the ipsilateral side.

	Right Side/Ipsilateral		**Left Side/Contralateral**	
	Non-lesioned Group	**Lesioned Group**	**Non-lesioned Group**	**Lesioned Group**
	Striatum			
Amplitude	2.8 ± 0.1 (199)	5.4 ± 0.3*** (251)	3.2 ± 0.1 (172)	5.9 ± 0.3*** (247)
Uptake Rate	0.4 ± 0.0 (193)	2.0 ± 0.1*** (251)	0.7 ± 0.1 (169)	2.1 ± 0.1*** (247)
T_{80}	5.9 ± 0.2 (194)	4.6 ± 0.1*** (249)	4.9 ± 0.2 (194)	4.8 ± 0.1 (248)
Frontal Cortex				
Amplitude	2.8 ± 0.2 (198)	4.9 ± 0.3*** (252)	3.8 ± 0.3 (175)	4.9 ± 0.3* (245)
Uptake Rate	0.8 ± 0.1 (187)	1.6 ± 0.1*** (244)	1.3 ± 0.1 (173)	1.9 ± 0.2** (243)
T_{80}	4.1 ± 0.1 (202)	5.3 ± 0.1*** (245)	3.9 ± 0.1 (202)	5.2 ± 0.1*** (243)
Nucleus Accumbens				
Amplitude	2.2 ± 0.2 (77)	5.0 ± 0.5***,† (98)	4.7 ± 0.4 (69)	3.6 ± 0.3 (98)
Uptake Rate	0.4 ± 0.1 (75)	1.7 ± 0.2***,‡ (98)	1.5 ± 0.2 (67)	0.9 ± 0.1* (97)
T_{80}	11.3 ± 1.4 (74)	5.3 ± 0.2*** (98)	4.0 ± 0.1 (80)	5.2 ± 0.1 (100)
All Brain Regions				
Number of rats	4	4	4	4

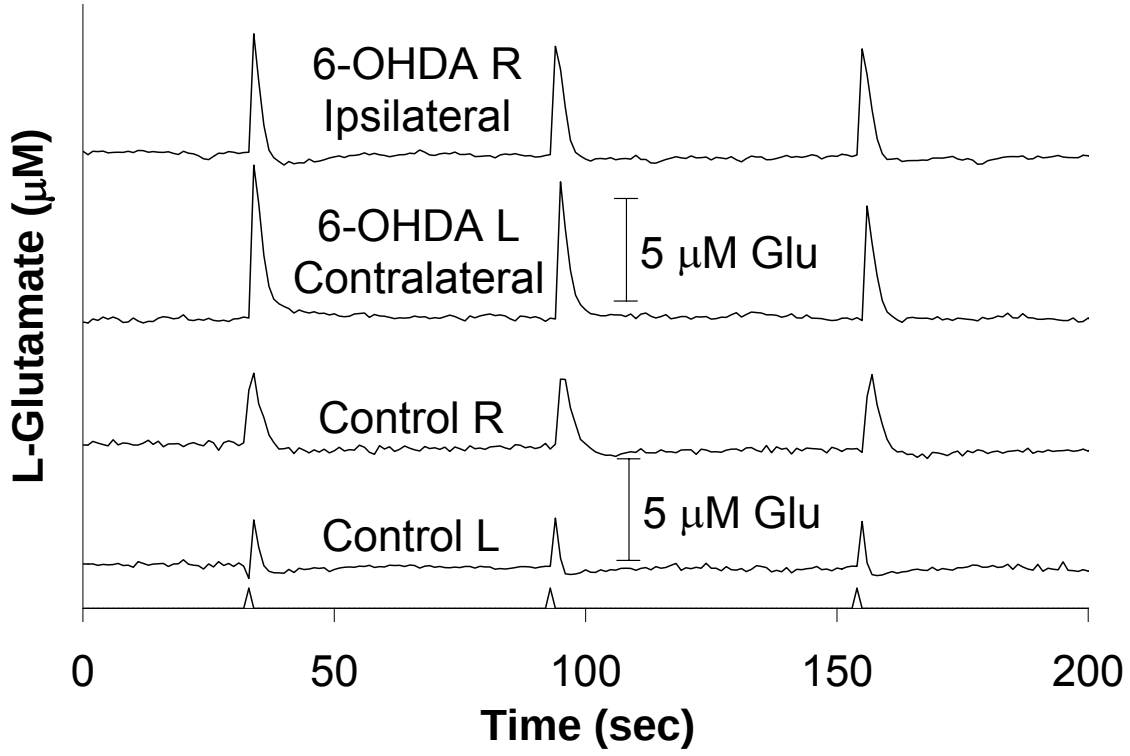

Figure 4.4 Representative Potassium-Evoked Glu Signals in the 6-OHDA-lesioned and Non-lesioned Rat Striatum

Potassium-evoked Glu signals (45 mM KCl, ~300 nl, black arrows) in the striatum of lesioned animals were significantly larger bilaterally compared to non-lesioned rats. Within the unilaterally lesioned rat group, Glu signals in the striatum were similar bilaterally despite the extensive loss of DA transmission only on the ipsilateral side (see Figure 4.3).

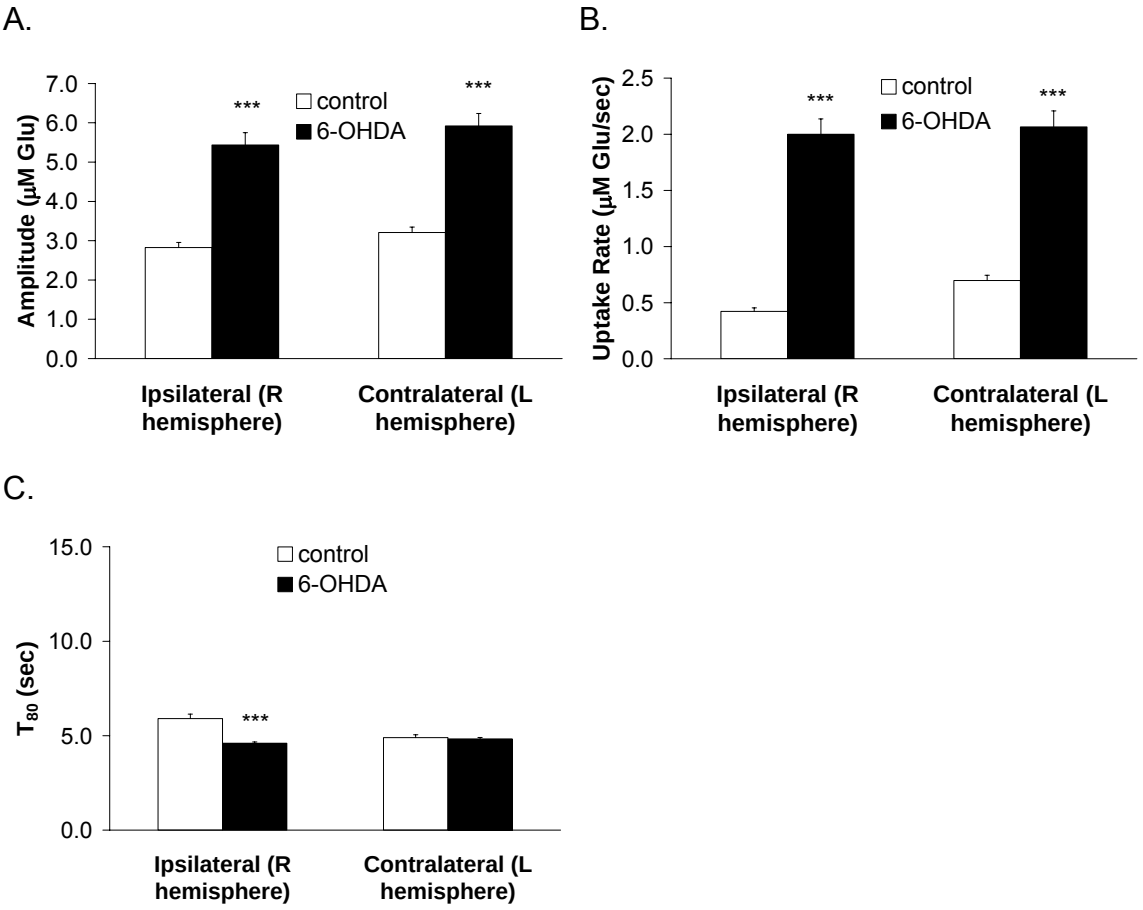

Figure 4.5 Average Potassium-Evoked Glu Kinetics in the Striatum of Unilateral Lesioned and Non-lesioned Rats

The average A) peak amplitudes and B) uptake rates of potassium-evoked Glu signals were significantly longer in the striatal hemispheres of lesioned rats bilaterally (vs. non-lesioned matched hemispheres) but did not differ between hemispheres within the unilaterally lesioned group. C) The average elapsed time from signal peak until 80% signal decay (T_{80}) showed a small but significant decrease in 6-OHDA-lesioned rats on the ipsilateral side (compared to non-lesioned matched hemispheres) but did not differ within the lesioned group. The average T_{80} did not differ between lesioned and non-lesioned rats on the contralateral (left) side.

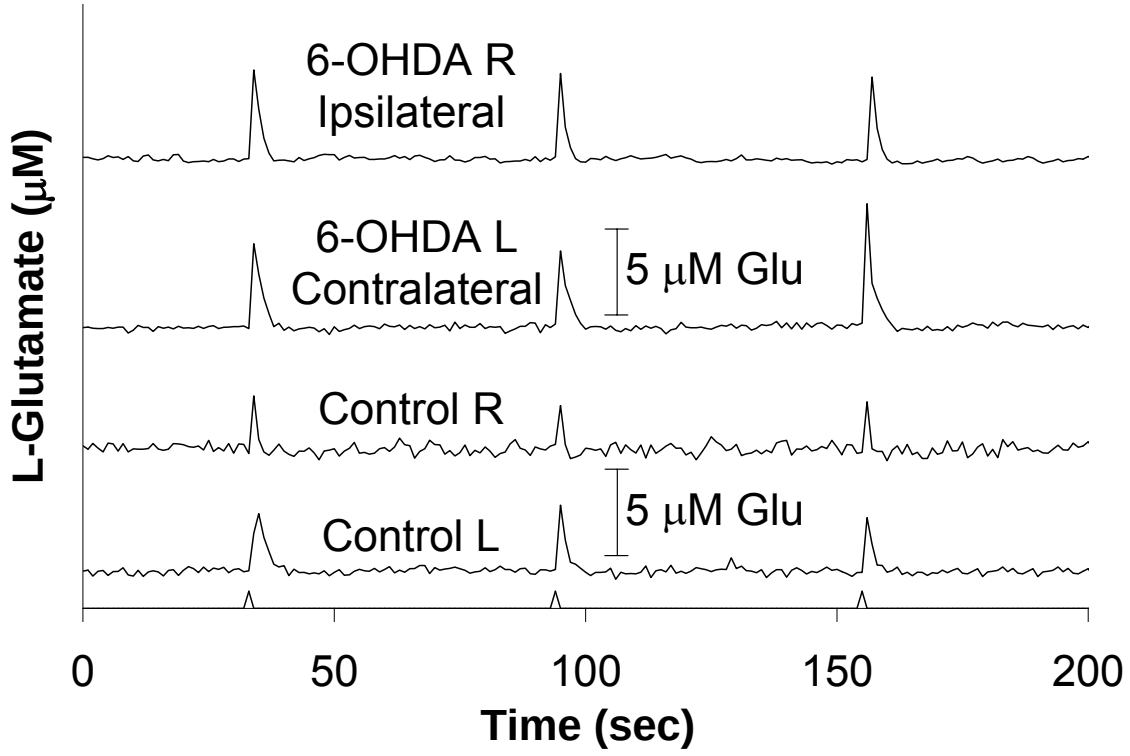

Figure 4.6 Representative Potassium-Evoked Glu Signals in the 6-OHDA-lesioned and Non-lesioned Rat Frontal Cortex

Potassium-evoked Glu signals (45 mM KCl, ~300 nl, black arrows) in the frontal cortex of lesioned animals were significantly larger bilaterally compared to non-lesioned rats. Once again, within the lesioned group, Glu signals in the frontal cortex were similar bilaterally.

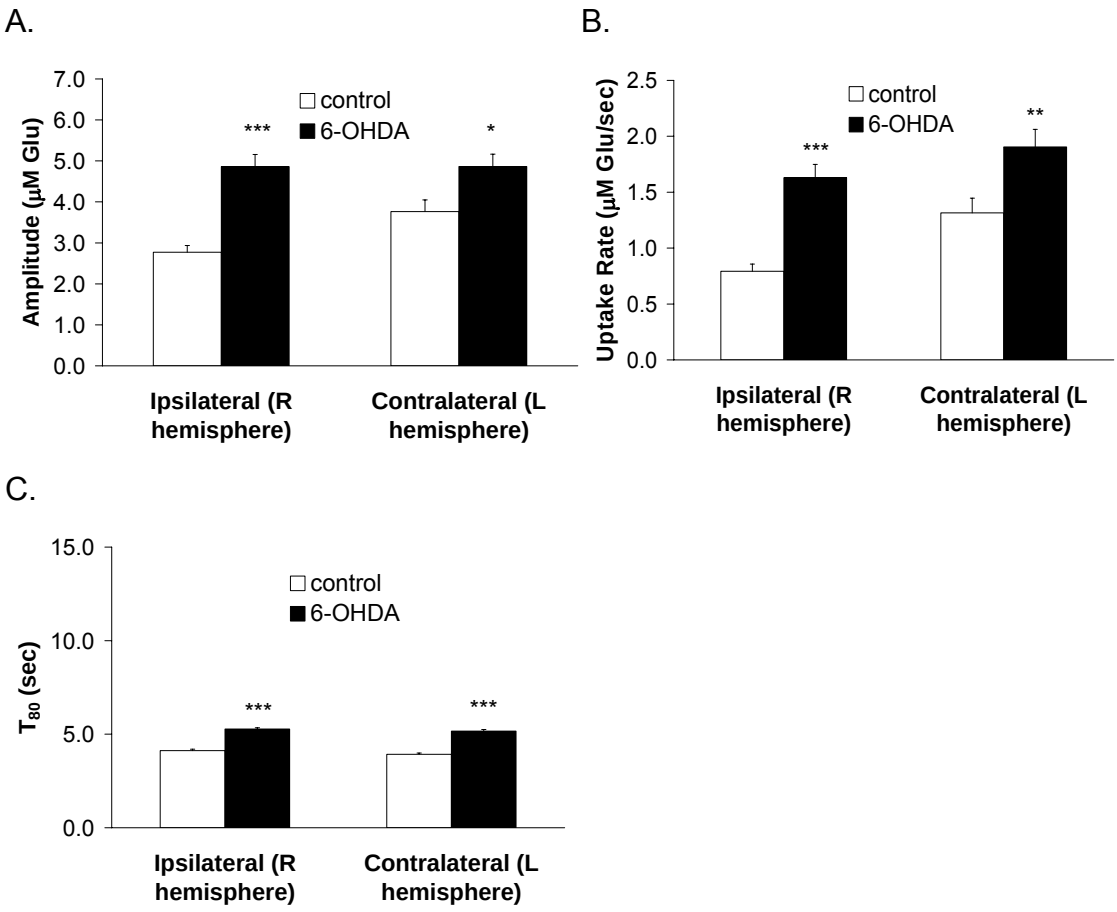

Figure 4.7 Average Potassium-Evoked Glu Kinetics in the Frontal Cortex of Unilateral Lesioned and Non-lesioned Rats

The average A) peak amplitudes, B) uptake rates, and C) T_{80}'s of potassium-evoked Glu signals were significantly higher in the cortical hemispheres of lesioned rats bilaterally (vs. non-lesioned matched hemispheres) but did not differ between hemispheres within the unilateral lesioned group.

mM, ~300 nl) Glu signals in the nucleus accumbens (5 signals/Glu recording site/depth for 2 depths) of lesioned and non-lesioned rats. Reported values for average signal parameters are shown in Table 4.1. Representative traces of potassium-evoked Glu signals for both groups of rats are shown in Figure 4.8. Within the right (ipsilateral) nucleus accumbens of both lesioned and non-lesioned rats, the previously reported trends were maintained. Average amplitude and uptake rate on the ipsilateral side of 6-OHDA-lesioned rats were significantly increased compared to the right side of non-lesioned rats. In contrast, the average T_{80} on the right side was significantly decreased in lesioned vs. non-lesioned rats. Considering the left (contralateral) nucleus accumbens between lesioned and non-lesioned rats, the average amplitude and T_{80} did not siginificantly differ, but the uptake rate was significantly slower. Looking specifically within the lesioned group, the average amplitude and uptake rate were increased on the ipsilateral side, while the average T_{80} did not differ. Within the nucleus accumbens especially in these studies, there is evidence for hemispheric differences within the normal non-lesioned rat group. Note that the average amplitude for Glu signals was significantly increased on the left side, and the average T_{80} showed a roughly 2 to 3-fold increase on the right side (non-lesioned right vs. left side) (Figure 4.9).

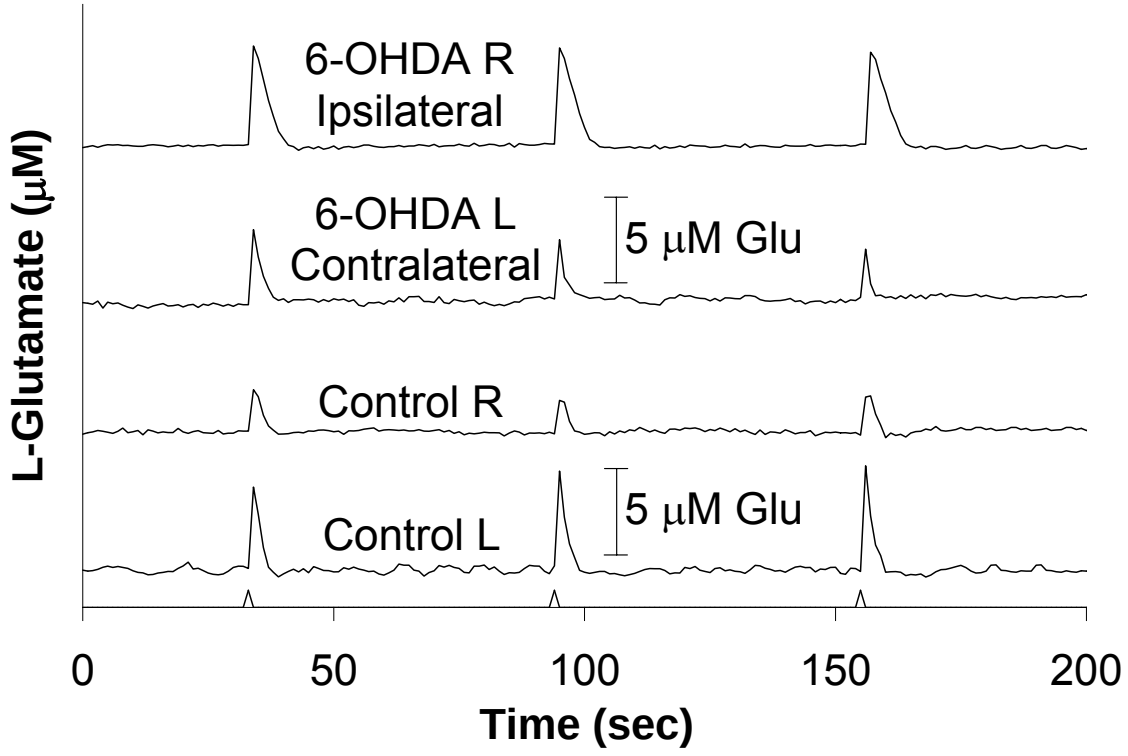

Figure 4.8 Representative Potassium-Evoked Glu Signals in the 6-OHDA-lesioned and Non-lesioned Rat Nucleus Accumbens

Potassium-evoked Glu signals (45 mM KCl, ~300 nl, black arrows) in the nucleus accumbens of lesioned animals did not completely follow the trends seen in the other brain areas. As previously observed, evoked Glu signals on the side ipsilateral to lesion were significantly larger when compared to matched (right-sided) non-lesioned rat hemispheres. In contrast, evoked Glu signals on the side contralateral to lesion were significantly decreased compared to signals from both the ipsilateral hemispheres within the lesioned group and the matched (left-sided) non-lesioned rat hemispheres. In addition, normal potassium-evoked Glu signals were significantly larger on the left side within the non-lesioned rat group.

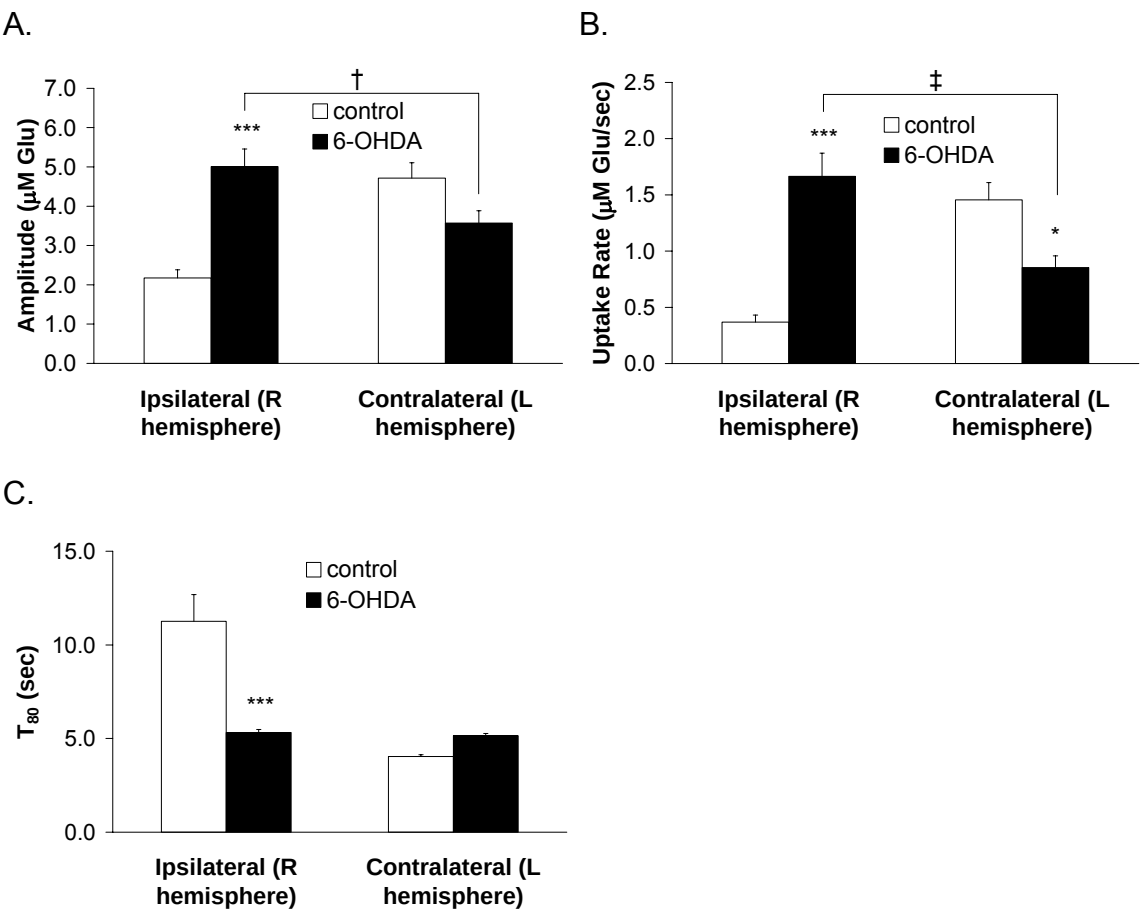

Figure 4.9 Average Potassium-Evoked Glu Kinetics in the Nucleus Accumbens of Unilateral Lesioned and Non-lesioned Rats

A) and B) In the nucleus accumbens on the right (ipsilateral) side, the average peak amplitude and uptake rate of potassium-evoked Glu signals were significantly higher in lesioned rats (vs. non-lesioned). These measures were also significantly higher compared to the contralateral side within the lesioned group ($^{\dagger}p<0.05$, $^{\ddagger}p<0.001$). The average contralateral amplitude and uptake rate tended to be decreased in lesioned rats (vs. hemisphere-matched, non-lesioned rats). C) The average T_{80} showed a significant decrease on the ipsilateral side (compared to non-lesioned matched hemisphere) but did not differ within the lesioned group. Significant hemispheric differences (R vs. L) of evoked Glu signaling in the non-lesioned (normal) rat nucleus accumbens are apparent.

Discussion

The present studies were conducted in Fischer 344 rats to evaluate alterations in potassium-evoked Glu kinetics resulting from loss of DA neurotransmission to the right striatum. The unilateral 6-OHDA-lesioned rat is a commonly used model of PD, and the hemiparkinsonian effects observed in this model are considered desirable because the non-lesioned (contralateral) hemisphere can serve as an "internal control structure" (Schober, 2004). We also investigated Glu dynamics in the non-lesioned rat brain bilaterally to serve as another control group, especially to determine if there were changes in Glu regulation in brain regions contralateral to lesion that would go undetected otherwise. Based on the current understanding of Glu alterations in the parkinsonian brain, we expected to see significant changes on the ipsilateral side compared to both the contralateral side and the hemisphere-matched right side in non-lesioned rats. We also considered that there might be changes on the contralateral side of lesioned rats compared to the hemisphere-matched left side of non-lesioned rats. Animals were recorded at approximately the same age (5-9 months old) to minimize age-related changes that might affect the results. Work conducted in our lab has shown that Glu regulation in normal rats does not dramatically differ from our age group (~6 months old) until after 18 months old (Nickell et al., 2005).

Interpreting hemispheric comparisons both within and between rat groups hinges largely on the assumption that, within a unilateral lesioned rat, there is little or no DA in the striatum on the ipsilateral side and good DA neurotransmission on the contralateral side. This assumption is commonly tested by administering drugs that act on the DA system and evaluating their effects on locomotion. In response to DA denervation, there is an increased number and surface expression of DA receptors, creating a supersensitivity to DA agonist drugs such as apomorphine (Deumens, Blokland, and Prickaerts, 2002). Thus, the administration of low dose apomorphine to a unilateral 6-OHDA-lesioned rat

will act in an imbalanced fashion (ipsilateral > contralateral striatum) to stimulate movement. The gold standard used to determine the lesion status of a unilateral 6-OHDA-treated rat is an average number of apomorphine-induced contralateral rotations greater than or equal to 300 turns per hour. Post-mortem analyses have confirmed that rats that display this drug-induced response have full (>90%) ipsilateral lesions (Hudson et al., 1993). The unilateral 6-OHDA-lesioned rats used in this study were lesioned and subjected to rotational testing at the Medical University of South Carolina. Only rats which met or exceeded this criterion were shipped to the University of Kentucky for electrochemical recordings.

Our use of the animals was somewhat unique, in that we used technology that was capable not only of recording extracellular Glu kinetics but also of detecting DA (See Figure 3.1). This afforded us the opportunity to further verify the lesion status of the 6-OHDA treated group through direct measurement of evoked DA neurotransmission, which we conducted at the end of the recording sessions for each lesioned rat. Figure 4.3 demonstrates that we were able to use a high dose of potassium (approximately ten times the stimulation typically used in these studies) to stimulate and detect DA only on the contralateral side (solid lines). Glu recording sites simultaneously recorded Glu and DA kinetics (spike-dome) while sentinel sites, which are not configured to detect Glu, only recorded the DA kinetics (inset). Figure 4.3 also shows that on the ipsilateral side, no DA-like kinetics were observed, only spike-like signal kinetics that are consistent with pure Glu release and uptake. These results support the full ipsilateral lesion status of the animals predicted by apomorphine testing with no evoked DA signaling on the side of lesion and good DA release and uptake on the contralateral side. Note that the use of very high potassium stimulation was important to stimulate the non-myelinated DA fibers and to fully test the ipsilateral side, which likely had few, if any, DA terminals.

Although in Figure 4.3, the simultaneous detection of Glu and DA was useful, typically we are interested in studying pure Glu signals, and DA is an undesirable interferent. Fortunately, recording DA interferences is not a problem in brain regions that are not DA-rich, such as the frontal cortex or the DA-

depleted striatum in these studies. In DA-rich areas, Glu uptake is very fast relative to DA uptake, which contributes to the characteristic signal shapes of evoked release and uptake (Glu spike vs. DA dome). Signals which reflect simultaneous release of Glu and large amounts of DA (spike-dome, see Figure 4.3 and Burmeister et al., 2002) or smaller amounts of DA (uncharacteristic prolonged signal decay times) were easily recognized and excluded from Glu signal analysis. Furthermore, potassium-evoked DA signals do not show rapid reproducibility unlike Glu signals; this characteristic can also be used during the course of an experiment to evaluate any suspected DA signals (see Gerhardt, Rose, and Hoffer, 1986).

Efforts to discriminate between pure Glu and unwanted, DA-contaminated Glu signals in DA-rich areas have become rare, however, largely because of two methodological advancements. First, all but one of the microelectrode arrays used in this chapter's studies were configured for self-referencing Glu recordings, and DA kinetics could easily be evaluated on sentinel sites. When Glu signals are detected on Glu recording channels while no signals are recorded on sentinel sites, we feel highly confident in the identity of our signal as Glu (see Figure 3.9). Secondly, DA is transmitted along non-myelinated axons that require higher stimulation than myelinated fibers (e.g. glutamatergic) to cause neurotransmitter release; thus, we are able to avoid eliciting DA release in many experiments simply by lowering the potassium concentration and/or volume. Prior to these studies, preliminary work was done in normal Fischer 344 rats testing the effects of 30 mM, 45 mM, and 70 mM potassium solutions. Whereas 30 mM potassium did not reliably evoke Glu release and 70 mM evoked DA release too often for the experimental design, 45 mM potassium reliably evoked Glu signals with good reproducibility and very few instances of simultaneous DA release. Thus, potassium stimulations used in these studies (45 mM, ~300 nl) were specifically chosen to evoke Glu release without stimulating DA release in areas like the striatum and nucleus accumbens.

Glu signal parameters, described in detail in Chapter Two, provide information about Glu release and uptake systems. Often we consider certain

measures (e.g. rise time, amplitude) to be reflective of Glu release mechanisms while others (e.g. decay times, k_{-1}) give us information about Glu uptake. In fact, this split has some validity for potassium-evoked Glu measures because the two divisions may be primarily influenced by the two respective systems. In reality, the rapid fluctuations in extracellular Glu recorded by our technology are driven by the balance between these systems. Glu concentrations rise when Glu release is greater than uptake, fall when Glu uptake is greater than release, and peak or plateau when release and uptake mechanisms are balanced. Often we must consider what multiple signal parameters are supporting to make conclusions about particular Glu systems.

In the striatum of unilateral 6-OHDA-lesioned rats, we found evidence for bilateral effects from a unilateral lesion, consistent with previous studies of hemiparkinsonian animal models (see Cass et al., 1995). Using the same level of potassium to stimulate all signals in both lesioned and non-lesioned rats in our studies, the average amplitudes of signals were significantly increased in the lesioned animals bilaterally compared by hemisphere to non-lesioned control rats. Higher amplitude is most often thought to reflect an increase in evoked Glu release, but could signify a decrease in Glu transport because the extracellular Glu level is determined by the balance between Glu release and uptake. Considering the average decay time T_{80}, which is primarily a measure of Glu transporter function, striatal Glu signals on average did not extraordinarily differ. Even though the mean difference (~1 second) reached statistical significance on the ipsilateral/right side, this change in transport time may not be physiologically significant. Taken together, the higher amplitudes most likely reflect an increased ability to release Glu on stimulation. Bilaterally increased uptake rates were also observed and may seem to contradict the preceding statements; however, the uptake rate (calculated by multiplying the amplitude by the decay constant k_{-1}) can be increased by either increased release or uptake. More Glu was likely released on stimulation, but it took roughly the same amount of time to be cleared from the extracellular space; thus, in this case, the increased uptake rates are most likely due to increased evoked Glu release, as the EAAT's are not

operating at their V_{max}. Strikingly, there were no statistical differences between any of the measures between hemispheres ipsilateral and contralateral to the lesion within the treated group.

The increased Glu release ipsilateral to lesion can be explained by the DA denervation on that side. In the striatum of normal rats, DA is thought to act on D2-like receptors on presynaptic Glu terminals to inhibit Glu release (Calabresi et al., 1996, Bamford et al., 2004) (Figure 4.2). DA denervation would disinhibit Glu terminals and allow increased evoked Glu release. Increased Glu release contralateral to lesion cannot be explained in this manner because DA neurotransmission remains intact on that side (see Figure 4.3). Two possible explanations for contralateral effects include contralateral changes in DA regulation and bilateral effects stemming from the neuroanatomy of the corticostriatal pathway. First, DA levels have been reported to increase on the contralateral side possibly as a compensatory mechanism following unilateral nigrostriatal lesion (Nieoullon et al., 1977, Cass et al., 1995). Increased DA could cause receptor internalization in presynaptic Glu terminals, desensitizing them to the inhibitory effects of DA. In effect, there might be a functional disinhibition of evoked Glu release. Alternatively, the bilateral projections of the corticostriatal pathway may play a role in creating the contralateral effect. The corticostriatal pathway is not a discrete tract but rather a collection of projections that emanate from all areas of the cortex and synapse in the striatum. Nonetheless, two distinct corticostriatal pathways have recently been reported, a unilateral and a bilateral pathway. The unilateral pathway stems largely from lower layer V pyramidal neurons in the motor cortex, which travel along the corticospinal tract carrying commands of voluntary movement. Collateral striatal afferents peeling off this pathway make up the unilateral corticostriatal pathway. The bilateral corticostriatal pathway begins in layer III and upper layer V of the cortex and sends projections to the cortex and striatum ipsilaterally and across the corpus callosum to these structures contralaterally (Reiner et al., 2003, Lei et al., 2004). In association with the bilateral corticostriatal pathway, changes in Glu signaling in the DA depleted striatum may be able to affect Glu signaling on the opposite

side. In fact, reproducing these experiments in conjunction with corpus callosotomy to further investigate the role of the bilateral corticostriatal pathway would be an especially interesting future study. Of course, other explanations are possible, and these hypotheses require further testing.

Bilateral effects on evoked Glu signaling were also seen in the frontal cortex. As explained for the striatum, the bilaterally increased amplitudes taken together with what may be physiologically insignificant changes in decay times (~1 second mean difference) lead to the conclusion that the increased amplitudes are most likely due to increased Glu release with stimulation. Also, as before, the bilaterally increased uptake rates probably reflect increased evoked Glu release. Once again, there are no significant differences in any of the reported parameters between signals recorded in the ipsilateral and contralateral cortical hemispheres within the lesioned rat group. The direct effects of DA loss likely do not explain these differences because there is no nigrostriatal and limited mesocortical DA signaling in the discrete areas of the frontal cortex that we recorded. However, the loss of DA neurotransmission along one of the nigrostriatal pathways creates alterations in several neurotransmitters within and connected to nuclei of the involuntary motor pathways. Impulse flow diagrams of network changes associated with PD often show decreased tone along the glutamatergic pathways from the thalamus to the cortex and from the cortex to its targets, including the striatum (Wichmann and DeLong, 2003). This might lead one to think that we should be observing decreased Glu release in both the striatum and frontal cortex. However, these diagrams are oversimplifications and do not consider all of the local effects of neurotransmitter alterations, such as receptor-coupled release and uptake modulations. Furthermore, although our data in both the striatum and frontal cortex support the hypothesis that there is increased evoked Glu release, which may simulate phasic Glu behavior, our electrochemical recordings do not give us information about cell firing patterns or frequency. Multiple single-unit recordings of ensembles of striatal neurons in freely moving unilateral 6-OHDA-lesioned rats have shown that basal cell firing of medium spiny-like neurons and large aspiny-like neurons increased on the

lesioned side and on both sides, respectively (Kish et al., 1999). Together, these studies support the hypothesis that there is increased excitation bilaterally to the striatum. Similar electrophysiological studies of the frontal cortex under hemiparkinsonian conditions have not been reported. Increased Glu release in the frontal cortex may be a compensatory mechanism for decreased excitatory influences from the thalamus, predicted by impulse flow diagrams, or other cortical regions (ipsilateral and contralateral thalamocortical and corticocortical pathways) and could explain the bilateral effects. In addition, bilateral changes in cortical Glu regulation might affect cortical targets, such as the striatum, in both hemispheres.

In the nucleus accumbens, we did not observe similar bilateral effects when we compared matched hemispheres from the lesioned and non-lesioned groups, and for the first time, we observed significant differences in signal parameters between ipsilateral and contralateral hemispheres within the lesioned group. In the non-lesioned rat group (R vs. L nucleus accumbens), we found on average smaller amplitudes (<50%) and prolonged T_{80}'s (200-300%) on the right side. The long decay time leads us to conclude that Glu transport is much slower on the right side, which would tend to increase amplitudes if there was robust release; however, the small average amplitude reveals that Glu release is instead decreased. Combined, low release and slow uptake explain the low uptake rate. On the left side of non-lesioned rats, we found evidence for much more robust evoked Glu signaling. A higher average amplitude and faster decay time support comparatively increased release and uptake, and a much faster uptake rate. These findings might support the hypothesis that there are normal hemispheric biases in Glu regulation in the nucleus accumbens. Alternatively, the high variability in signal parameters that we observed across the nucleus accumbens data sets may have resulted from difficulties in microelectrode placement. Unlike larger, more superficial intracranial targets such as the frontal cortex and striatum, the nucleus accumbens is a deeper structure with more complicated neuroanatomy. At the anterior-posterior coordinates of this study, the shell of the nucleus accumbens in the rat is medial and deep to the core of

the nucleus accumbens. Although the trajectory of our coordinates should have placed our microelectrode recording sites only in the core, small deviations from this trajectory or biological variances in neuroanatomy may have altered our recording regions within this structure. Of particular concern is the presence of the anterior commissure (AC) traversing through the core ~0.2 mm medial to our final recording depth. Microelectrode placement in the AC dramatically lowers potassium-evoked DA signaling using carbon fibers (unpublished data), and would likely alter potassium-evoked Glu signaling. Without histological confirmation of the microelectrode tract, it is difficult to conclude that normal hemispheric biases truly exist.

If we assume that our recordings were made in the accumbens core, we can continue discussing the nucleus accumbens data, limiting our comparisons to matched hemispheres between lesioned and non-lesioned rats. It is tempting to posit that decreased DA neurotransmission along the lesioned side disinhibited presynaptic Glu release mechanisms, as explained for the ipsilateral effects in the striatum. This might increase Glu release and stimulate the Glu transporter system to function more efficiently, explaining the observed lowered average T_{80} and increased average uptake rate. Cortical afferents carrying Glu to the nucleus accumbens on the contralateral side largely showed no statistically significant changes in evoked Glu signaling compared to the left nucleus accumbens in non-lesioned rats. However, on average, amplitude tended to be lower and the T_{80} longer; slightly less Glu release and slightly slower Glu uptake combined to significantly decrease the Glu uptake rate. A slight decrease in Glu release might be explained by a compensatory increase in DA signaling to the contralateral side, which did not reach the level to internalize DA receptors on presynaptic Glu terminals. Following unilateral 6-OHDA injection in the medial forebrain bundle, the loss of DA to the ipsilateral nucleus accumbens is often less than the loss to the ipsilateral striatum (Lancia et al., 2004); thus, it is conceivable that contralateral DA compensation might also be less and have different effects. The decreased uptake rate on the contralateral side may be a glutamatergic compensatory mechanism in response to the slight lowering of Glu release.

Overall, evoked Glu signaling in the unilateral 6-OHDA-lesioned rat nucleus accumbens showed a very different pattern of effects compared to the striatum, possibly due to inherent hemispheric differences in Glu regulation and/or differences in the loss of DA neurotransmission to these areas.

The striking bilateral effects seen in the striatum and frontal cortex put the use of the contralateral side as a control in unilateral 6-OHDA-lesioned rats in question, at least for some investigations. It has been recognized for a long time that patients with PD often are more severely affected on one side, and that treatments targeted to the more severely affected side have bilateral efficacy (Spencer et al., 1992, Molina et al., 1994). Bilateral projections exist throughout the involuntary motor nuclei and associated brain regions and may help explain these findings (Glowinski, Bessen, and Cheramy, 1984, Barbeito et al., 1989). The data presented in this chapter, in particular, strongly implicate Glu signaling from the cortex as a region and system that might play a central role in connecting unilateral lesion-induced alterations bilaterally. This also opens up the possibility that cortical Glu may be playing a role in the bilateral effects of unilateral PD treatments.

In summary, we investigated differences in potassium-evoked Glu kinetics (45 mM KCl, ~300 nl) in the striatum, frontal cortex, and nucleus accumbens of unilateral 6-OHDA-lesioned rats by comparing measured changes by hemisphere both within the lesioned group and to similarly aged non-lesioned rats. Contrary to one of our original hypotheses, we did not find significant changes within the lesioned rat group in the striatum or frontal cortex. Instead, we found strikingly matched bilateral effects of a unilateral lesion compared to non-lesioned rats. In these brain regions, Glu release was primarily affected, showing significant increases on the ipsilateral and contralateral sides. Ipsilateral effects in the striatum may be directly related to the loss of DA, while contralateral effects in the striatum and all of the effects in the frontal cortex may be due to parkinsonian changes in neurotransmitter signaling and/or the neuroanatomical bilateral connectivity of the involuntary pathways and associated brain regions. Evoked Glu signaling in the nucleus accumbens

showed a similar effect on the ipsilateral side, while the contralateral side remained largely unchanged compared to hemisphere-matched recordings from non-lesioned rats. There was, however, evidence for hemispheric differences within the non-lesioned rat group, which made interpretation of this data difficult. Glu signaling from the cortex may play a central role in bilateral alterations observed in unilateral animal models of PD.

Chapter Five: Normal L-Glutamate Regulation in the Nonhuman Primate (NHP) Cortex

Introduction

In this chapter, we once again build upon our investigations of normal Glu neurotransmission in the anesthetized rat brain by developing and implementing methods to study normal Glu regulation in the brains of anesthetized nonhuman primates. Inherently, this is an interesting pursuit because much of the basic science that is conducted in lower mammalian species is assumed to be applicable to human conditions; however, important biological species differences may exist which can limit the relevance of experimental findings (Roth, Ingram, and Lane, 2001). Species which are more closely related to humans, such as the rhesus monkeys used in these studies, may be more suitable to model humans and represent a logical step along the pathway toward applying our technology in the clinical setting. As such, these studies are examples of our commitment to conducting translational research at the University of Kentucky. However, nonhuman primate studies are not just a stepping stone to human research but also stand alone as important investigations of basic biological processes in a presumably more relevant, higher mammalian species. As this idea relates to our particular research, we explored aspects of basic neurobiology in these animals by conducting microelectrode arrays studies of Glu regulation in the normal young and aged nonhuman primate cortex.

Glutamate has often been suspected to contribute to alterations in brain function in aging and age-related neurodegenerative conditions. The current leading theories of aging primarily implicate free radical formation, largely generated by mitochondria, and the resulting long term effects on cell function and viability (Harman, 1956, Linnane et al., 1989, Ozawa, 1997, Balaban et al., 2005). In other words, cell aging may reflect the cumulative effects of

metabolically-produced reactive oxygen species (ROS) on cellular macromolecules (Michaelis, 1998). Furthermore, calcium signaling has been shown to be altered with age (Foster and Kumar, 2002). Both changes in calcium signaling and ROS production may begin with alterations in the regulation of Glu neurotransmission; thus, extracellular Glu merits study in the aging brain. Such investigations are encouraged by some groups who have reported an increased susceptibility to Glu-induced excitotoxicity with age (Liu et al., 1996, Brewer, 2000). Yet relatively few studies on the regulation of extracellular Glu in the aging brain have been conducted, and the results have been highly inconsistent with respect to basal Glu levels and Glu clearance capacity (Segovia et al., 2001). These inconsistencies may stem in part from some of the limitations of brain slice methods and microdialysis. These techniques do not have the spatial and temporal resolution to adequately characterize neurotransmitters with fast kinetics of release and uptake, such as Glu, and often do not differentiate between neuronal and glial Glu sources (Nickell et al., 2005). Our technology allows us to investigate basal Glu and evoked Glu dynamics in the intact brain closer to the synapse and faster than previously possible.

Faced with the opportunity to conduct research in rhesus monkeys, we were also presented with new challenges. Significant differences exist between working with acutely-studied rats in the laboratory setting and chronically-investigated monkeys in the veterinary operating room. The tasks of general animal handling, anesthesia, surgery, and recovery fell on collaborating teams of experts, and our role was relegated to experimental and technological specialists. We were concerned primarily with how to design the study and modify our voltammetry-based techniques to transition as easily as possible into this new venue. One of our primary concerns was creating a mobile FAST-16 electrochemical detection system that could easily be moved between settings and closely positioned to the anesthetized monkey in the operating room without compromising the sterile field. We also sought to make the system highly self-contained to move all components as a single unit and require minimal setup or additional equipment. Further concerns were related to modifying our preparation

procedures, providing external nitrogen to our pressure-ejection system, implanting a Ag/AgCl reference electrode, and handling sterility with respect to direct contact between our electrodes and surgically-exposed tissue from chronically-used animals.

Briefly, we designed our studies to investigate normal Glu regulation in the anesthetized monkey cortex in three ways. First, all microelectrode arrays used in these studies were configured for self-referencing Glu recordings. This allowed us to use a constant potential paired channel subtraction approach (described in Chapter Three) to monitor basal Glu. Secondly, we investigated potassium-evoked Glu kinetics. In particular, we wanted to compare signal parameters of nonhuman primate evoked Glu release and uptake to the rapid Glu dynamics we had previously observed in the anesthetized rat brain. Next, we ejected exogenous Glu in the recording area to evaluate the Glu uptake system in a more isolated fashion. Finally, all of these experiments were performed in three monkeys from two different age groups, young and aged, to collect preliminary data regarding age-related changes in Glu regulation in the monkey cortex.

Methods

Refer to Chapter Two for full descriptions of microelectrode array design, electrode preparation and use, drugs and chemicals, and data analysis. Any deviations from those procedures are noted below, and a full description of animal preparation for Glu recordings is also described.

Animals

One young (8 years old) and two aged (25 and 28 years old) female rhesus monkeys (*Macaca mulatta*) obtained from a commercial supplier (Covance, Alice, TX) were used in this study. The animals were maintained on a 12-h light/12-h dark cycle and housed in individual cages measuring 9 square feet each, with an elevated perch, front access doors and side rear access doors.

Each cage is a double over-under design containing two monkeys. Each pair of two housing cages has an activity module in the middle, connected to the housing cage via the side rear doors (Figure 5.1). Their diet consisted of certified primate biscuits in the morning (7:30 AM) supplemented daily in the afternoon (1:30 PM) with fresh fruit or vegetables, and water was available *ad libitum*. All procedures, except the MR imaging, were conducted in the Laboratory Animal Facilities of the University of Kentucky, which are fully accredited by the Association for Assessment and Accreditation of Laboratory Animal Care (AAALAC). Veterinarians skilled in the health care and maintenance of nonhuman primates supervised all animal care, and all protocols were approved by the University of Kentucky's Institutional Animal Care and Use Committee (IACUC). The 28 year-old monkey had congenital malformations of the head, including one ear, which made placement in the stereotaxic head frame difficult. For other health considerations, this animal was euthanized and underwent a necropsy following her Glu recording session.

Anatomical MRI Procedures

After being sedated with ketamine hydrochloride (~20 mg/kg; i.m.) plus atropine sulfate (~0.04 mg/kg; i.m.), the animals were anesthetized with sodium pentobarbital (~10 mg/kg; i.v.) and imaged to provide stereotaxic coordinates for implantation of the microelectrode arrays. At the end of the imaging sessions, the animals were recovered and returned to their housing. All MR images were obtained on a 1.5T clinical imager (Siemens Magnetom Vision) using a standard cross polarized extremity coil. The animal's head was positioned in the extremity coil using an MRI compatible stereotaxic head frame (David Kopf Instruments, Model 1430M). This frame kept the animal's head level and immobilized at the center of the radio frequency coil using ear and mouth bars. An initial set of coordinates (antero-posterior, dorsal-ventral, and midline) was taken using the earbars, toothbar and a zeroing bar targeted to the gum line between the two upper middle incisors to allow replication any time the animal was replaced in the

Figure 5.1 Nonhuman Primate Housing System

Pairs of monkeys are housed together to promote social behavior. A variety of customized animal toys are included in the activity module (middle section with monkey) for environmental enrichment.

stereotaxic apparatus. The coil/frame assembly was then positioned to place the animal's head at magnet isocenter. Following acquisition of scout images to confirm correct positioning, sets of T1-weighted 3D-FLASH images were collected for determination of the brain coordinates (TR/TE = 22/9 ms; FA = 35°; FOV = 96 × 96 × 90 mm; Matrix = 128 × 128 × 90; Nacq = 2; TA = 6 min 48 sec). All images were acquired as coronal slices of the brain. Antero-posterior, lateral and vertical coordinates for stereotaxic surgery were derived from the T1-weighted coronal sections through the brain. The interaural line was identified on the scans by modified earbars containing Vitamin E. This provided a precise reference-point on the MRI and frame, which allowed for antero-posterior measurements. Lateral measurements were determined by measuring the distance from midline (defined by the sagittal sinus and/or third ventricle) to the target site. Vertical measurements were determined from the surface of the brain to the target at the lateral coordinate.

Electrochemical Recording System Preparations

We made several preparations in the weeks to months prior to the first experiment day. First, we assembled the mobile FAST-16 electrochemical detection system (Figure 5.2). Components included a computer (tower, monitor, keyboard, and mouse), a 4-channel FAST-16 setup (potentiostat, headstage (pre-amplifier), custom-made plexiglass headstage stand, and dip-socket connector), and a Picospritzer III pressure-ejection system. These components were secured onto a plastic push-cart, all of the data cables were connected, and the power cords were plugged into a central power strip. Additional equipment and materials necessary for conducting the experiment (some of which are shown in Figure 5.2) included a hydraulic microdrive (Narishige, MO-8), a stereotaxic holder, micropipette loading materials, a glass-bodied Ag/AgCl reference electrode (Bioanalytical Systems, Inc., RE-5b), and a stereomicroscope on a boom stand. Finally, fully prepared microelectrode/ micropipette assemblies were securely rested above a bath with the recording

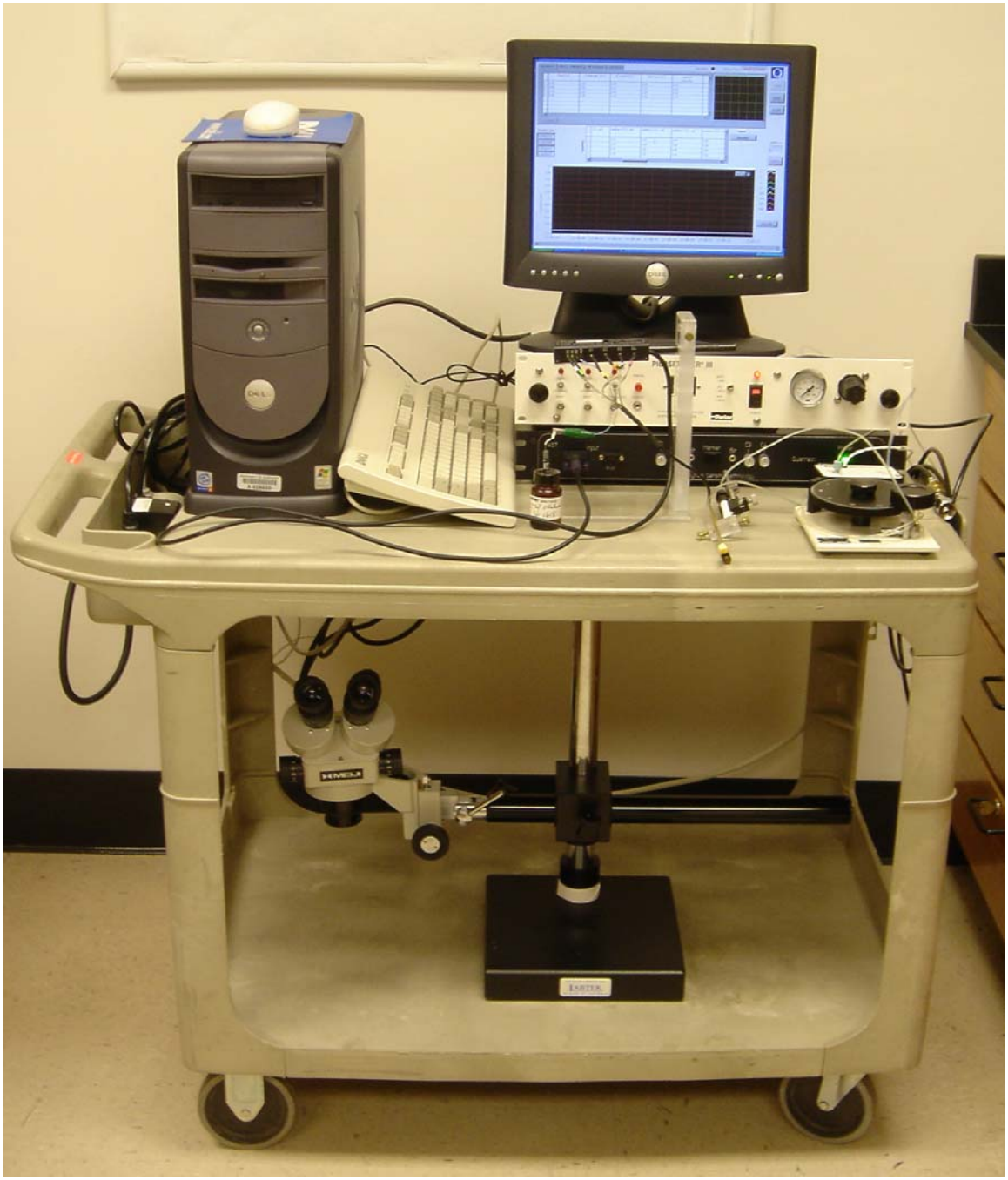

Figure 5.2 Mobile FAST-16 Electrochemical Recording System

sites soaking in PBS. All of the additional components were easily stowed on the push-cart along with the mobile FAST-16. To protect the delicate glass micropipette tips from movement-induced damage, either the microelectrode/ micropipette assemblies were separately hand-carried or the PBS was removed from the bath before transport and refilled when the push-cart was finally positioned in the operating room.

A nitrogen tank was secured in the central tank room for the veterinary surgical suites. It was dedicated to a spigot near the head of the operating table where the mobile FAST-16 was planned to be positioned. A custom-made coupling allowed us to connect our Picospritzer III directly to the spigot on the operating room wall. This setup was tested for gas delivery to the operating room and worked well without any apparent leaks.

Electrode Preparation and Use

Our electrode preparation and use was consistent with most established protocols (see Chapter Two for detailed descriptions); however, certain methodological approaches were refined as follows. Approximately one week prior to scheduled experiment day, we configured four microelectrode arrays to record Glu in self-referencing recording mode. The day before the experiment, single barrel micropipettes were pulled, bumped to an inner diameter of 10-15 µm, and attached to the microelectrode arrays. Also, the mobile FAST-16 was set up and tested. Three and a half hours before the surgical technician team was scheduled to retrieve the rhesus monkey, microelectrode arrays were soaked in PBS for one hour and then calibrated in the laboratory using the mobile FAST-16 system positioned at the benchtop. Based on calibration data, the four microelectrode arrays were ranked by performance. The top two microelectrode arrays were assigned for use with potassium and Glu ejections, respectively. The other two microelectrodes were planned to be used as backups in case of accidental breakage or other unforeseen problems. At this point, the surgical technician team was contacted and told to begin their preparations for

surgery. We purposefully scheduled the experiment day to progress like this, so that we could abort the experiment prior to animal handling in case of any Glu recording system problems. To date, we have recorded from three rhesus monkeys and have never needed to cancel the experiment.

Surgical Procedures

Following sedation with ketamine hydrochloride (~20 mg/kg; i.m.) plus atropine sulfate (~0.04 mg/kg; i.m.), each animal was intubated via the orotracheal method, and intravenous lines were secured. Then, the animal was anesthetized with isoflurane (1-3%) and placed in an MRI-compatible stereotaxic apparatus (David Kopf Instruments, Model 1430M) in a ventral-lateral position. The animal was maintained on a heated blanket and had cardiac and respiratory parameters monitored during the procedure. Coordinates for microelectrode array implantation were determined by MRI prior to the surgery as described above. After being shaved, the scalp area was cleaned with antiseptic. Starting at the incision site and moving circumferentially to the periphery, the shaved area was gently scrubbed with sterile 4 x 4 sponges soaked in chlorhexidine diacetate surgical scrub followed by 70% isopropyl alcohol. This procedure was repeated. After the alcohol dried, Betadine® prep was applied, and the animal was covered with sterile drapes (Figure 5.3). Then, a 5-7 cm incision was made through the scalp, and the skin and muscles were reflected to expose the skull. Small (2 mm diameter) holes were drilled in the skull directly over the targeted areas using a dental drill and a rounded drill bit, and the overlying meninges were removed to expose the surface of the brain. A lateral pocket was made in the fascia at the posterior extent of the incision using blunt dissection. A 70% isopropyl alcohol-cleaned glass-bodied Ag/AgCl reference electrode (Bioanalytical Systems, Inc., RE-5b) was inserted into the pocket. Sterile saline irrigation was used to maintain ionic contact between the reference electrode and the exposed brain. Microelectrode/micropipette assemblies were slowly lowered into each target using a stereotaxic holder as described below. After completion of the recording

Figure 5.3 Recording Glu in the Operating Room

Rhesus monkeys were anesthetized and prepared for electrochemical recordings under sterile field conditions. The mobile FAST-16 was positioned in the room at the head of the operating table. First, a small group of surgeons exposed small areas of cerebral cortex and helped implant the microelectrode/micropipette assembly. Then, a two-person team conducted the experiment, while a separate team of veterinary technicians maintained anesthesia and monitored the monkey's vital signs throughout the procedures.

session, bone wax was placed in the drill holes, and the scalp incision was sutured over the exposed areas per normal procedures. The animal was then given an analgesic (buprenorphine, 0.01 mg/kg, i.m.) and prophylactic antibiotics (combination Penicillin G Benzathine and Penicillin G Procaine, 20,000 U/kg, s.c.). Temperature, heart rate, respiratory rate, and femoral pulse were monitored until the animal recovered from anesthesia. Full recovery was defined as self-sustained balance and posture.

Stereotaxic Implantation and Glu Recordings

Prior to MRI-assisted implantation, a 70 mM potassium solution (70 mM KCl, 79 mM NaCl, 2.5 mM $CaCl_2 \bullet 2H_2O$, pH 7.4) or a 5 mM Glu solution (5 mM Glu in physiological (0.9%) saline, pH 7.4) was loaded into the single-barrel micropipette attached to the microelectrode array. First, a custom-made, pulled stainless steel needle (30 gauge, Popper and Sons, Inc., New Hyde Park, NY, USA) was cleaned externally and rinsed internally with 70% isopropyl alcohol and allowed to air dry. Then, a solution was drawn into a 1 cc syringe, and a sterile syringe filter (0.22 µm pore size, Costar, Corning, NY, USA) and pulled needle were attached. The fully prepared syringe was used to load the sterile-filtered solution into the micropipette. The fully prepared microelectrode/ micropipette assemblies were implanted into the frontal cortex (frontal eye field) and the motor cortex, based individually on coordinates measured from each monkey's MRI. After initially advancing the center of a microelectrode array to the cortical surface (David Kopf Instruments, Model 1760 electrode manipulator), an assembly was sequentially moved through the recording depths (-1.0 mm to -2.0 mm in 0.25-0.50 mm increments) using a microdrive (Narishige, MO-8) (Figure 5.4). In the case of potassium-evoked signals in the frontal cortex, additional depths were recorded (-2.25 mm and -2.5 mm). Potassium-evoked Glu signals were recorded in one hemisphere, while exogenous Glu was ejected and recorded in the opposite hemisphere. For each solution, a separate microelectrode/micropipette assembly was used. For each hemisphere, the

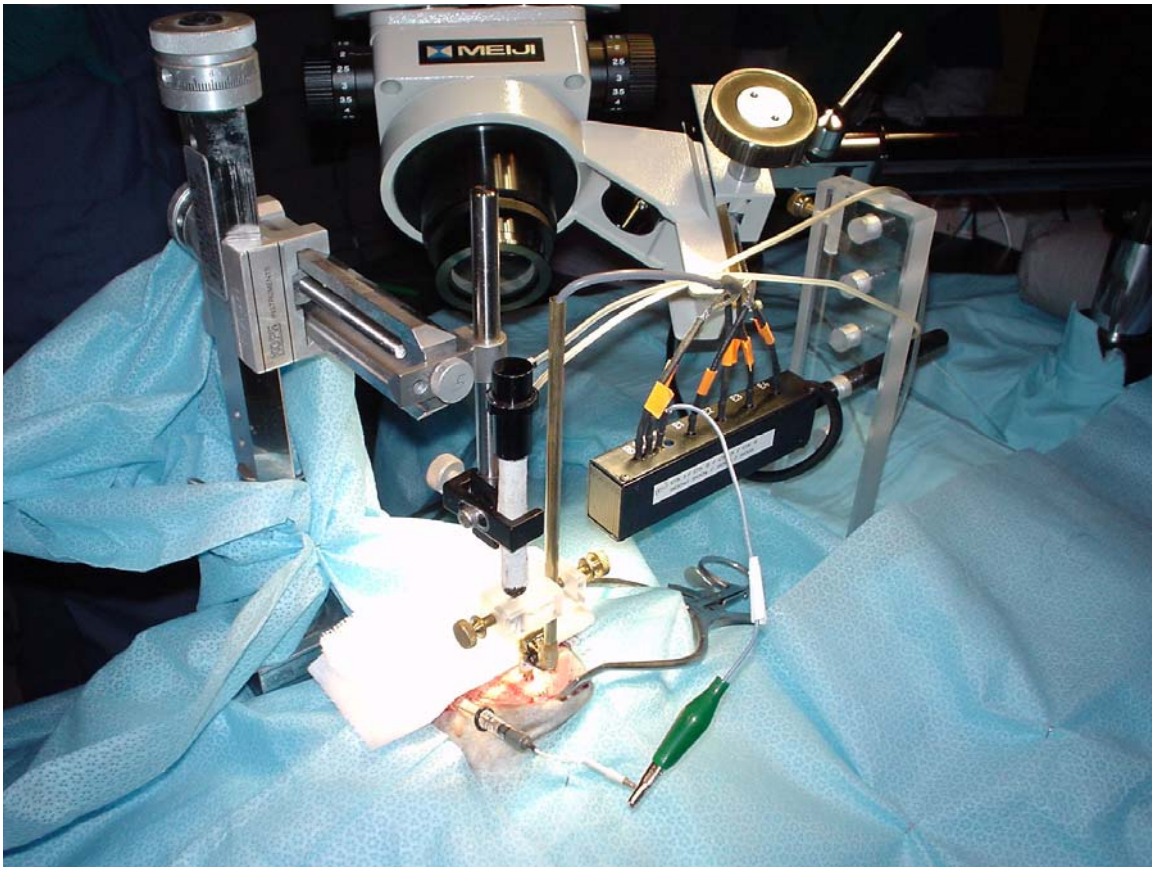

Figure 5.4 The *In Vivo* Glu Recording Setup for Anesthetized Monkey Studies

The microelectrode/micropipette assembly was stereotaxically lowered into cortical regions based on coordinates derived individually from each monkey's MRI. A four-channel headstage (pre-amplifier) plugged into the FAST-16 was placed near the recording area and connected to the microelectrode array using a custom-made connector. A stereomicroscope on a boom stand, focused on the meniscus within the micropipette, was used to monitor the volumes of solutions that were pressure-ejected into the brain.

frontal cortex was recorded in one pass, and then the microelectrode was removed from the brain, rinsed with 0.9% (physiological) saline, and stereotaxically implanted in the motor cortex in a second pass. A fifteen minute equilibration period per implantation was allowed prior to beginning the ejections, and a two to three minute equilibration period was allowed between depths. Basal Glu levels were assessed at each depth in real time, and additional time was allowed to record basal Glu activity when necessary prior to ejections. Ejections of 70 mM KCl or 5 mM Glu were made at one minute intervals at each depth until at least three to five reproducible Glu responses were recorded. For 5 mM Glu ejections, we adjusted our ejection volumes to amplitude-match the signals between monkeys in the ~50-100 μM range for analytical purposes. Volumes were controlled by a pressure-ejection system and monitored using a stereomicroscope fitted with a reticule (see Friedemann and Gerhardt, 1996). Glu signals were recorded (+0.7 V vs. Ag/AgCl reference) on a second-by-second basis by the FAST-16 recording system.

Data Analysis

Average measures from one young monkey were compared to those from one aged monkey. A second aged monkey with congenital head malformations was recorded. On necropsy, we discovered that our recordings were too far anterior. Thus, measures from this animal are not presented with one exception. We observed extraordinary basal Glu activity in an area of this aged monkey's brain that was identified as the frontal cortex during post-mortem examination.

Basal Glu measures were calculated for each depth by a constant applied potential paired channel subtraction approach (described in Chapter Three). Low basal Glu measures require within-array performances that exceed normal recording requirements. Microelectrode array recordings that displayed obvious mismatches in performance were omitted. Briefly, at the end of equilibration, a stable paired channel (enzyme-coated vs. enzyme-free) Glu recording of one minute duration was evaluated. For extraordinary basal Glu activity, longer

comparison times (three to five minutes) were used. Paired channel signal differences were converted into Glu concentrations using an appropriate calibration factor. Average Glu concentrations over these time intervals were calculated for each depth, and the average Glu concentration for each brain region was also determined. Both potassium-evoked and Glu ejection-produced Glu signals were analyzed and characterized by the following parameters: amplitude (μM Glu), rise time (sec), T_{Total} (sec), T_{80} (sec), and uptake rate (μM Glu/sec). Refer to Chapter Two for full descriptions. The average amplitude per nanoliter of ejected solution (amp/nl, μM Glu/nl) was also calculated. Average basal Glu measures and Glu signal parameters were compared between the young and aged monkey using unpaired t-tests (α=0.05). Welch's correction was used when required.

Results

Potassium-Evoked Glu Signals in the Motor Cortex

We recorded fast kinetics of potassium-evoked Glu release and uptake in the motor cortex of both the young and aged monkey. These signals displayed a characteristic spike shape (Figure 5.5) and were very similar in character to the signals that we routinely observed in the normal young rat cortex. Glu signals in the normal young monkey (n=20) rose to peak amplitude in 2.0 ± 0.1 seconds and lasted 16.1 ± 1.0 seconds (mean ± SEM used throughout the Results section). This is comparable to potassium-evoked Glu signals in the young rat cortex, which rose to peak amplitude in 1-2 seconds and lasted 10-20 seconds (see Chapter Three). Glu signals in the normal aged motor cortex (n=30) rose more slowly (3.3 ± 0.1 sec, $p<0.0001$) but lasted approximately the same time (14.4 ± 0.3 sec, N.S.). Likewise, the average time from signal peak to 80% decay (T_{80}) did not significantly differ between the young and aged monkey (10.4 ± 0.6 sec vs. 11.2 ± 0.2 sec, N.S.). The average signal amplitude was significantly

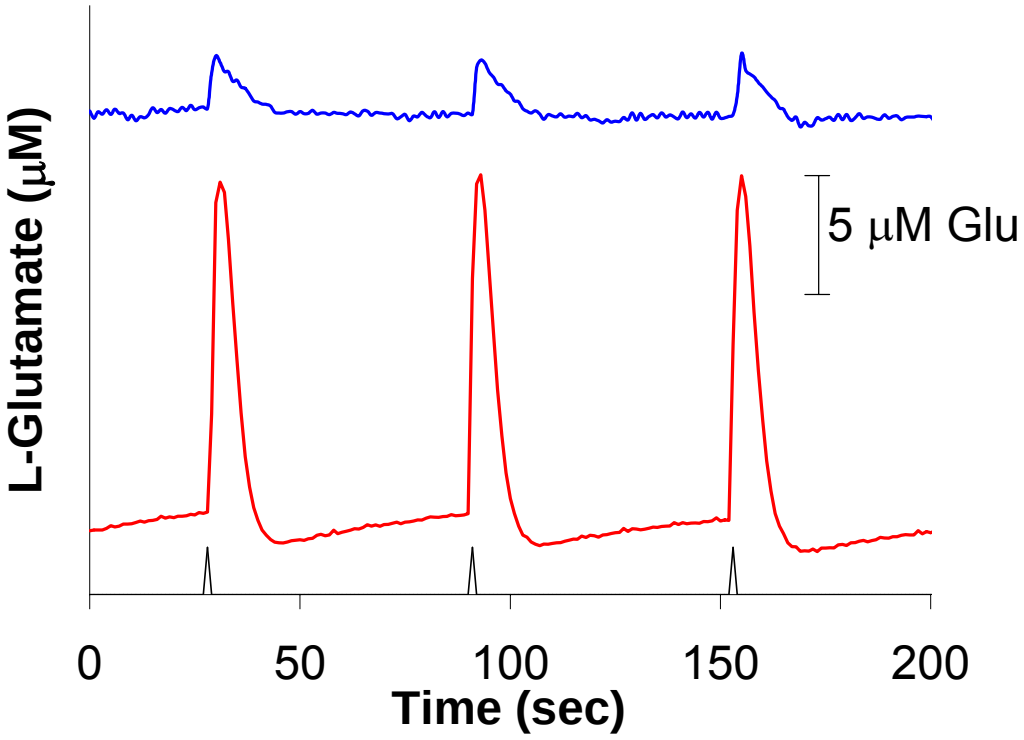

Figure 5.5 Potassium-Evoked Glu Signals in the Motor Cortex

Potassium ejections at one minute intervals (black arrows) in the monkey motor cortex evoked fast Glu release and uptake. Smaller amplitude signals were observed in the motor cortex of the young monkey (top trace (blue), responses to 100 nl potassium volumes) compared to the aged monkey (bottom trace (red), responses to 250 nl potassium volumes).

larger in the aged monkey (3.3 ± 0.4 μM Glu vs. 13.3 ± 0.3 μM Glu, young vs. aged, $p<0.0001$) as was the average uptake rate (0.21 ± 0.04 μM Glu/sec vs. 1.37 ± 0.06 μM Glu/sec, young vs. aged, $p<0.0001$); however, the potassium dose (volume) was also much larger in the aged monkey (100.0 ± 0.0 nl vs. 236.7 ± 17.9 nl, young vs. aged, $p<0.0001$).

Glu Ejections in the Motor Cortex

Glu ejection-produced Glu signals in the motor cortex of young and aged monkeys were well-matched (Figures 5.6 and 5.7). The average amplitude of these signals (young: n=30, aged: n=29) fell into our targeted 50-100 μM range (73.9 ± 2.5 μM Glu vs. 67.1 ± 3.4 μM Glu, young vs. aged, N.S.). The volumes of 5 mM Glu required to achieve these amplitudes dramatically differed (48.3 ± 1.7 nl vs. 531.7 ± 11.6 nl, young vs. aged, $p<0.0001$) as did the resulting amp/nl (1.6 ± 0.1 μM Glu/nl vs. 0.1 ± 0.01 μM Glu/nl, young vs. aged, $p<0.0001$). Average T_{80}'s were significantly longer in the aged monkey (10.5 ± 0.3 sec vs. 14.4 ± 0.3 sec, young vs. aged, $p<0.0001$), and the average uptake rate was significantly slower in the aged monkey (18.5 ± 0.6 μM Glu/sec vs. 7.1 ± 0.6 μM Glu/sec, young vs. aged, $p<0.0001$).

Potassium-Evoked Glu Signals in the Frontal Cortex

Glu signals with fast release and uptake kinetics were also observed in the young monkey frontal cortex but not in the aged monkey. These signals differed from the Glu signals that were recorded in the monkey motor cortex and in the rat cortex primarily with respect to size. Low amplitude Glu signals (1.8 ± 0.2 μM Glu, n=18) in the young monkey frontal cortex were recorded at an average potassium dose (152.8 ± 14.7 nl) that typically evokes robust Glu release and uptake. These signals rose to peak amplitude in 2.2 ± 0.1 seconds but lasted only 7.7 ± 1.2 seconds. Overall, most potassium-evoked Glu signals in the monkey frontal cortex were atypical low amplitude, slow release, slow uptake signals (young: n=6, aged: n=40). Figure 5.8 demonstrates that this population of

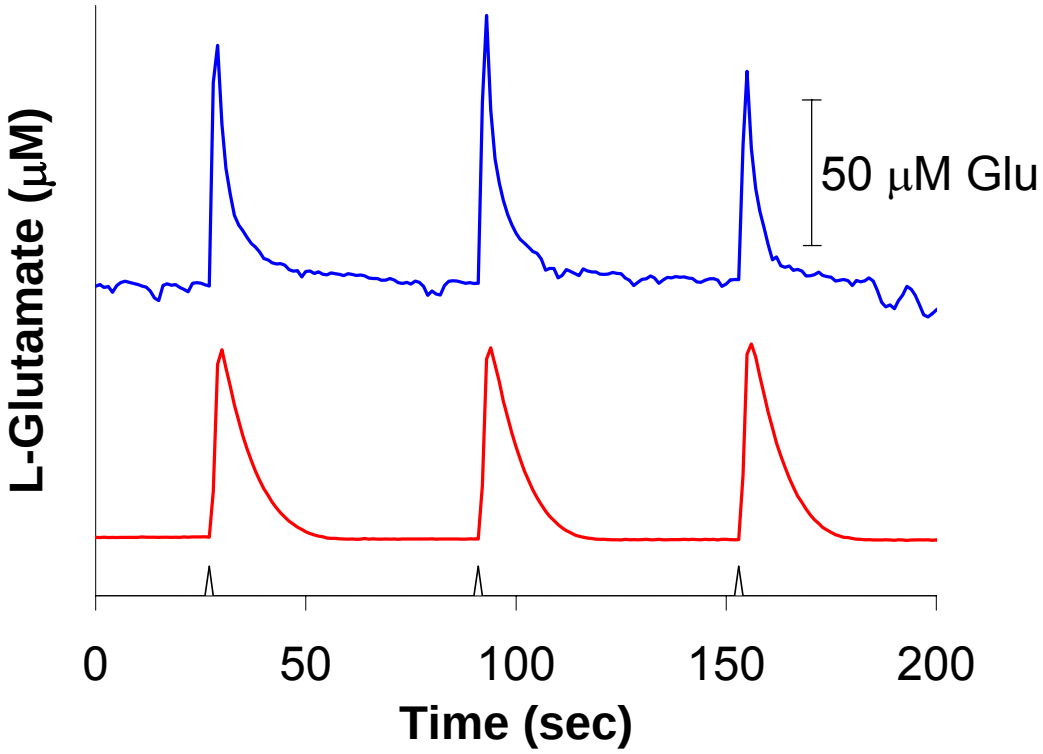

Figure 5.6 Glu Ejections in the Motor Cortex

Ejections of 5 mM Glu (black arrows) were volume-adjusted to produce Glu signals of similar amplitudes for comparison. The top trace (blue) shows recorded ejections of 50 nl of Glu in the young monkey motor cortex while the bottom trace (red) shows Glu ejections in the same brain region of the aged monkey. Much larger volumes of Glu solution (550, 525, 550 nl) were needed in the aged animal to achieve amplitudes between 50 and 100 μM. Increased time for signal decay and decreased uptake rate are also apparent in the aged animal.

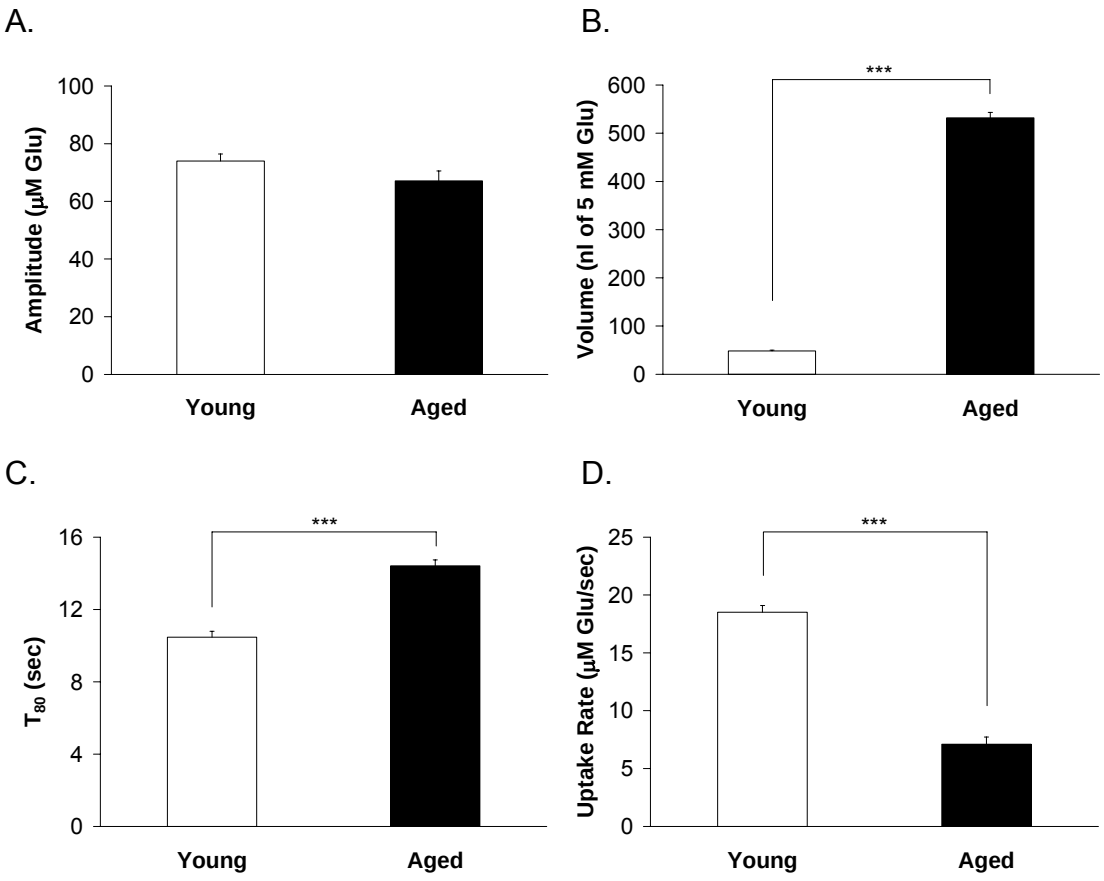

Figure 5.7 Measures of Glu Ejections in the Motor Cortex

A) Glu ejection-produced Glu signals in the motor cortex were amplitude-matched for comparison. B) Volumes of 5 mM Glu approximately ten times those used in the young monkey were required to achieve the same amplitudes ($p<0.0001$). C) The time from peak amplitude until 80% Glu signal decay was significantly increased in the aged monkey ($p<0.0001$). D) At similar average amplitudes, the average uptake rate was significantly decreased in the aged monkey ($p<0.0001$).

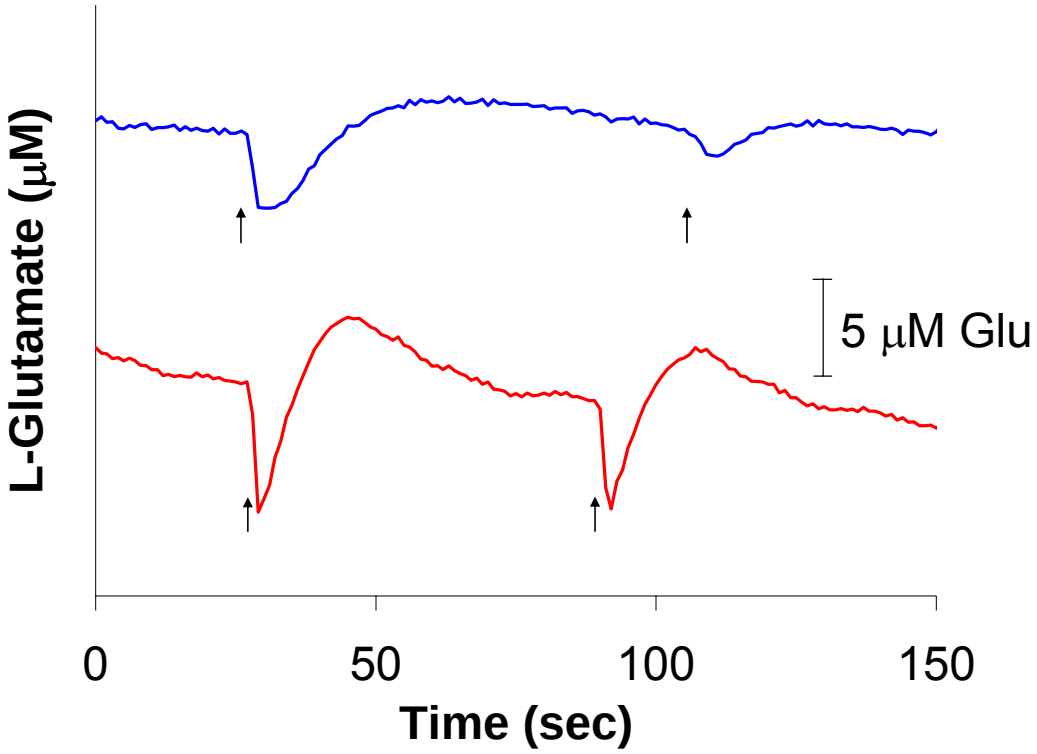

Figure 5.8 Potassium-Evoked Glu Signals in the Frontal Cortex

We observed unusually slow potassium-evoked Glu signaling in the frontal cortex. These signals were seen at one depth in the young animal (top trace (blue), 175 and 50 nl ejections marked with arrows). Slow evoked Glu signals were seen at all depths in the aged animal (bottom trace (red), 250 nl ejections marked by arrows).

Glu signals achieved average amplitudes of 1.5 ± 0.6 μM Glu and 1.3 ± 0.2 μM Glu (young vs. aged, N.S.), rose to peak amplitude very slowly (39.0 ± 6.5 sec vs. 22.8 ± 1.7 sec, young vs. aged, $p<0.01$), and decayed very slowly (young vs. aged, average T_{80}: 99.3 ± 13.7 sec vs. 37.8 ± 2.1 sec, $p<0.05$; average uptake rate: 0.0038 ± 0.0008 μM Glu/sec vs. 0.0098 ± 0.0028 μM Glu/sec, $p<0.05$). The volumes of potassium used to stimulate these signals did not significantly differ between the differently aged monkeys.

Glu Ejections in the Frontal Cortex

We adjusted volumes of Glu ejections in the frontal cortex to produce Glu signals (young: n=30, aged: n=30) that were amplitude-matched (107.8 ± 7.4 μM Glu vs. 109.3 ± 6.3 μM Glu, young vs. aged, N.S.) (Figures 5.9 and 5.10). On average these signals were very similar in the young and aged monkeys (rise times: 2.7 ± 0.2 vs. 2.2 ± 0.1, $p<0.05$, T_{80}'s: 9.9 ± 0.5 vs. 11.3 ± 0.5, N.S.). Average uptake rates were also nearly identical (19.8 ± 2.2 μM Glu/sec vs. 20.6 ± 1.6 μM Glu/sec, young vs. aged, N.S.). However, as we had previously observed in the motor cortex, the aged monkey required much larger volumes of 5 mM Glu to achieve the same amplitudes (46.7 ± 2.3 nl vs. 413.3 ± 37.9 nl, young vs. aged, $p<0.0001$), and the amp/nl significantly differed (2.4 ± 0.2 μM Glu/nl vs. 0.3 ± 0.04 μM Glu/nl, young vs. aged, $p<0.0001$).

Basal Glu Measures

Basal Glu measures were made at three depths in the motor cortex (n=6 for each monkey) and five depths in the frontal cortex (n=10 for each monkey) in both the young and aged monkey. Average basal Glu measures in the young monkey tended to be larger than those in the aged monkey in the motor cortex (5.3 ± 1.8 μM Glu vs. 0.7 ± 0.2 μM Glu, N.S.) and were significantly larger in the frontal cortex (10.3 ± 3.3 μM Glu vs. 2.7 ± 0.5 μM Glu, $p<0.05$). Significantly larger average basal Glu measures in the young monkey's frontal cortex resulted in part due to extraordinarily large basal Glu measures (Figure 5.11) at two

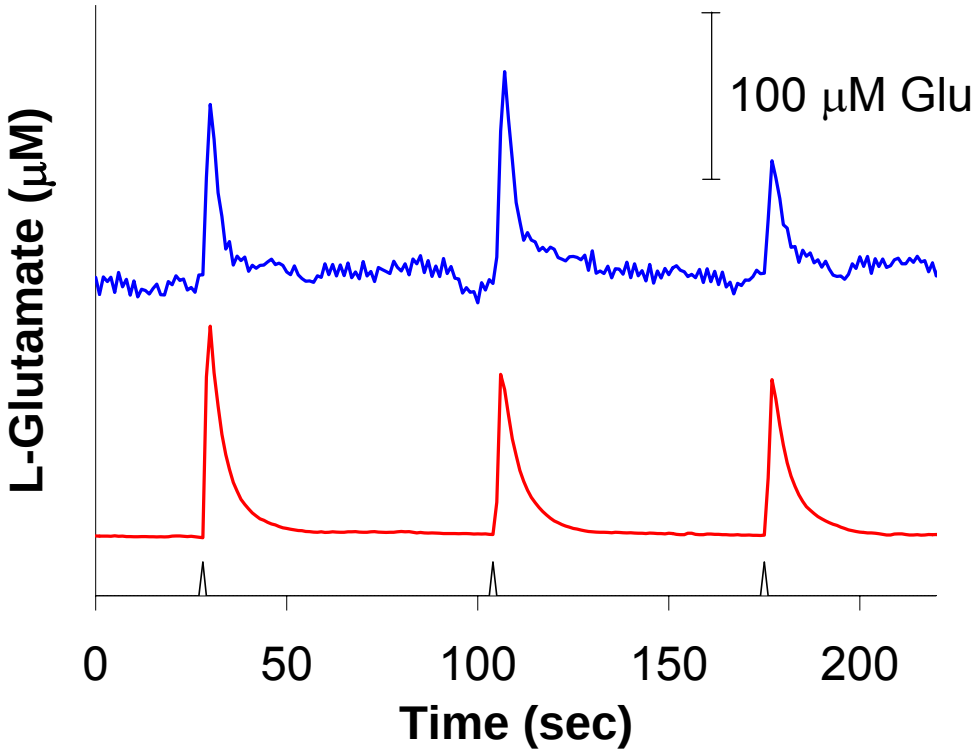

Figure 5.9 Glu Ejections in the Frontal Cortex

Adjusted volumes of 5 mM Glu were ejected in the monkey frontal cortex (black arrows) to produce similar Glu signals for comparison. Glu signals in the aged animal (bottom trace (red), 550, 525, 525) required larger volumes than the young animal (top trace (blue), 50, 50, 25 nl). Note that the signals have very similar release and uptake characteristics.

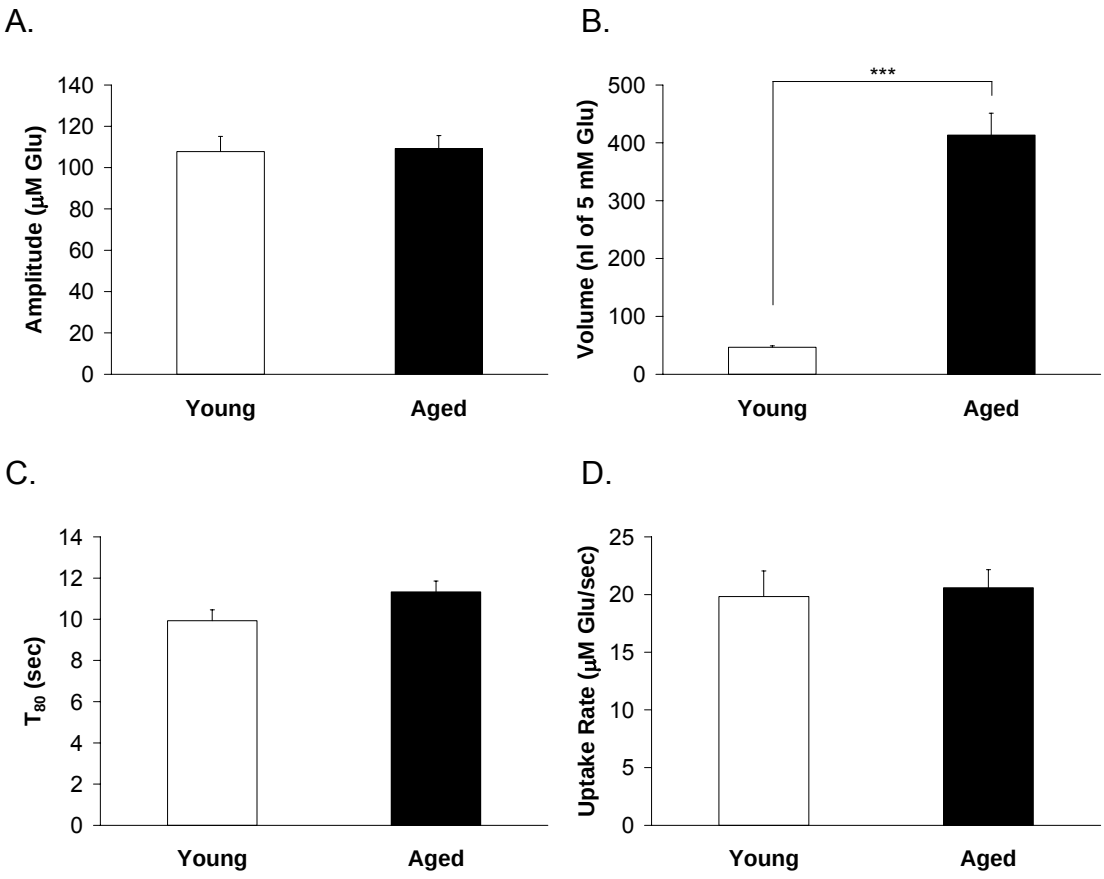

Figure 5.10 Measures of Glu Ejections in the Frontal Cortex

A) Glu ejections in the monkey frontal cortex produced Glu signals that were amplitude-matched. B) The aged animal required nearly ten times the volume of 5 mM Glu to achieve similar amplitudes ($p<0.0001$). C) and D) Measures of Glu uptake did not significantly differ.

A.

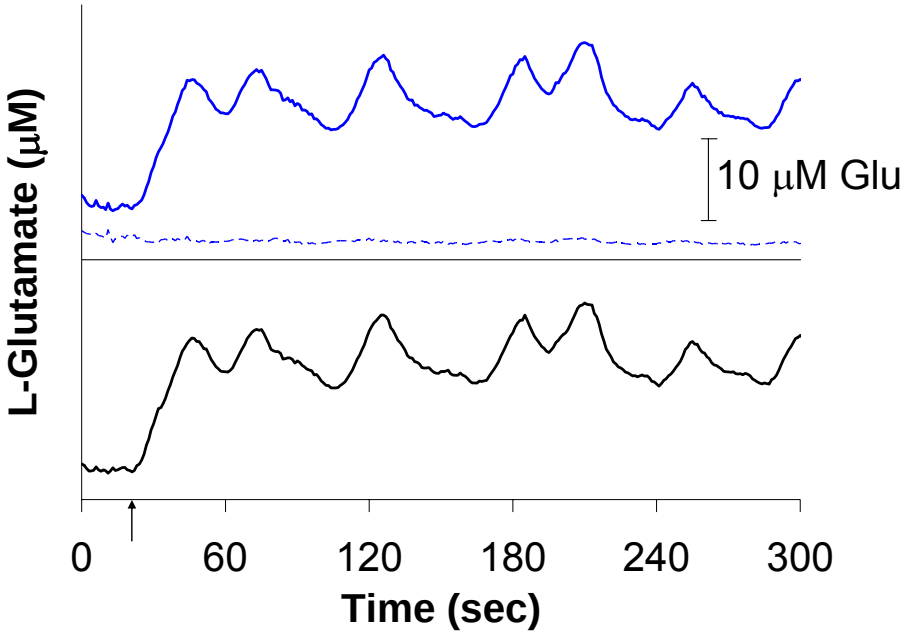

B.

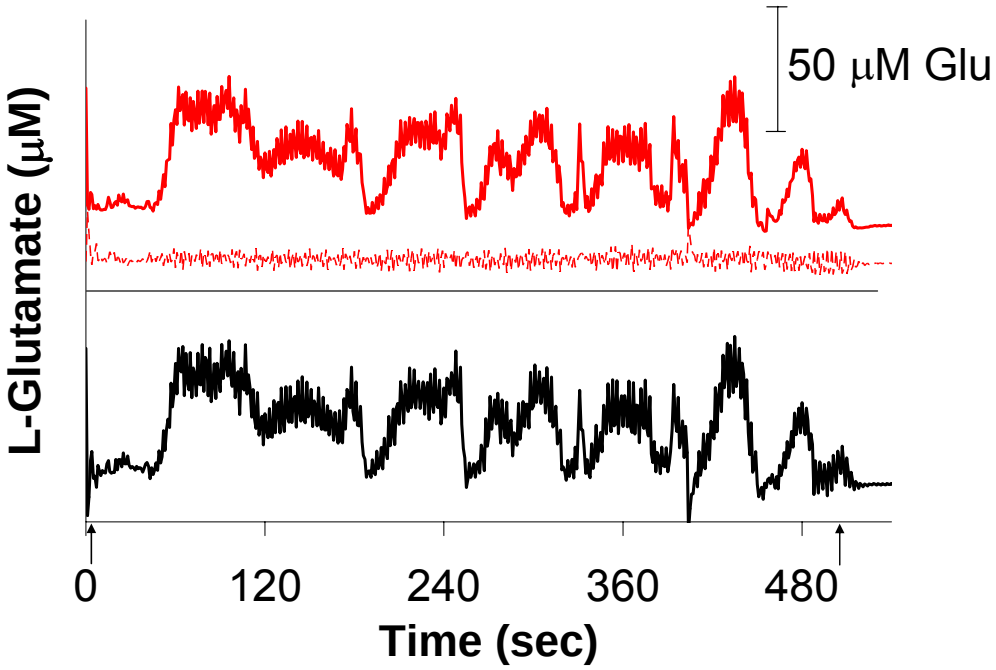

Figure 5.11 Novel Basal Glu Activity in the Frontal Cortex

(Figure legend on the following page)

Figure 5.11 (continued)

Microelectrode arrays configured for recording Glu in self-referencing mode were used in these studies. Each graph shows the apparent Glu concentrations from the paired channel traces (enzyme-coated (top-most trace, colored solid line) and enzyme-free (middle trace, colored dashed line)) which were subtracted to quantify basal Glu levels (bottom trace, solid black line). Black arrows indicate lowering the microelectrode array to a new depth. A) Upon lowering to -2.25 mm (DV) in a young monkey's frontal cortex, we passively recorded a robust rise in basal Glu levels which leveled and oscillated around an average measure of 13.4 μM Glu over 3 minutes and 20 seconds. This activity disappeared when the microelectrode array was lowered to the next depth (not shown). B) When we lowered to a depth of -1.25 mm (DV) in an aged monkey's frontal cortex, we passively recorded a dramatic increase in basal Glu levels which irregularly oscillated around an average measure of 44.4 μM Glu over 5 minutes. Once again, this activity was not observed at the next depth.

depths in this animal. Figure 5.11A shows an example of such measurements from the frontal cortex of the young monkey. As stated previously, Glu signals in a second aged animal were recorded. In this animal, we observed extraordinary basal Glu activity at two depths in a brain region that was visually confirmed to be the frontal cortex on post-mortem examination. Figure 5.11B shows an example of this novel basal Glu finding from an aged monkey. We observed dynamic basal Glu activity with oscillatory behavior in the frontal cortex of both a young and an aged rhesus macaque. Such activity has never been observed in the rat brain.

Discussion

We successfully achieved our goal of applying our Glu detection technology in a higher mammalian species in an operating room setting. This would not have been possible without a professional team effort and careful planning based on the collective expertise of all involved. The rhesus monkey handling team, surgery team, and veterinary technicians were experienced and prepared to fulfill their responsibilities, so that the primary obstacles fell on the Glu recording team. Our main challenges were developing a mobile recording and experimental setup and modifying our methodologies so that both would be compatible with operating room conditions. Creating the mobile FAST-16 was simplified by the compact design and limited number of hardware elements required to conduct electrochemical recordings. A dry run was made from our laboratory to the veterinary operating room and back to assess the security of the components and the effects of movement vibrations on our connections. At the end of this run, the FAST-16 system was tested and performed without error. Once in the OR, all the mobile setup needed was electrical power and a nitrogen supply for our pressure-ejection system. Fortunately, modern operating rooms have central vacuum and gas supplies with wall spigots in the individual surgical suites. We simply had to transport a nitrogen tank to the central tank room one

time in advance and develop a custom-made coupling to gain control over our supply of pressurized nitrogen for all experiments. This was an important challenge to overcome because transporting a nitrogen tank to the surgical suite and securing it in the room for each experiment would be a laborious, time-consuming, and possibly dangerous task.

In addition to these advanced preparations, we also modified our methods to progress in a timely and logical fashion and adapted them for chronic animal use in a sterile OR setting. Potentially time-intensive elements such as micropipette attachments were performed the day before an experiment, and calibrations were started hours before the scheduled OR time to ensure that we had good functioning Glu recording devices prior to animal retrieval. We increased the number of prepared microelectrode arrays per experiment from two to four also for this reason and to have backups in case of accidental damage or other unforeseen problems. We also modified our Ag/AgCl reference electrode implantation protocol for the safety of the rhesus monkey because prolonged exposure to bare wire Ag/AgCl reference electrodes can damage brain tissue. The use of bare wire Ag/AgCl reference electrodes is highly acceptable for acute animal studies, but might be inappropriate for chronic animal use, especially when we have a good previously-tested alternative (see Gerhardt et al., 1995, Cass et al., 1995). We were able to implant the glass-bodied reference electrode under a saline-irrigated skin flap because the Ag/AgCl reference electrode works as long as it remains in ionic contact with the brain. The sterilely gowned and gloved surgery team handled the reference electrode by holding the non-sterile end with sterile gauze and rinsing the implanted portion with 70% isopropyl alcohol which was allowed to dry before making contact with the exposed monkey tissue. Sterilizing the implanted microelectrode arrays remains a challenge because both commonly-used heat and gas sterilization techniques disrupt the layered coatings that make the recording sites selective for Glu. It is common practice to use small, clean but non-sterile, implantable devices, such as microdialysis probes and carbon-fiber microelectrodes, in animal research including chronic nonhuman primate studies. Standard veterinary protocols

already include prophylactic antibiotics following surgery in a chronically-used large animal. Neither of the recovered monkeys developed a post-experimental brain infection or any other poor outcome, so we feel confident that our techniques are safe. Nonetheless, we continue to research ways to sterilize our microelectrode arrays without compromising performance.

We applied this technology to a pilot study of normal Glu neurotransmission in the cerebral cortex of young and aged rhesus monkeys in a sterile field operating room setting. Most importantly, we were able to assemble collaborative teams of experts and modify our methods successfully to conduct Glu recordings in the intact brain of monkeys in a safe and efficient manner. This was our primary goal and achieving it creates opportunities for many important future studies using this technology in nonhuman primates and/or the operating room setting. We observed Glu signaling that was both very familiar and very different from our experiences with Glu regulation in the rat brain. These facts validate our research in lower mammals while also highlighting the need to advance this technology into higher mammals to improve our studies' relevance to human conditions. All Glu measures were compared between one young and one aged animal. The low number of animals per age group and the lack of a middle-aged group limit the contributions of this study to aging research. Nonetheless, we were able to detect significant differences in Glu regulation in two cortical areas from individual monkeys of different ages. These results support that alterations in Glu regulation likely occur with aging, as has previously been reported in recent rat studies (Nickell et al., 2005); thus, a larger study is merited.

If the monkeys used in this study prove to be representative of their age groups, significant age-related alterations occur in Glu release and uptake mechanisms which affect evoked and basal Glu regulation. Within the motor cortex, we observed some of the most familiar evoked Glu signaling to our experiences with potassium-evoked Glu regulation from the young rat cortex. In particular, average potassium-evoked Glu signals in the young monkey motor cortex rose to peak amplitude in ~2 seconds and lasted ~16 seconds. This

compares well with our 70 mM potassium-evoked signaling from the rat brain which rose to peak amplitude in 1-2 seconds and lasted 10-20 seconds (see Chapter Three). The same stimulations in the aged monkey motor cortex produced signals that closely matched these times. Larger signal amplitudes in the aged monkey represent the primary difference between the two animals. Higher amplitudes without significant differences in Glu transporter function (i.e. non-significant difference in T_{80}'s) drove the significant increases that we observed in the uptake rate. The measures support that we were observing a difference in Glu release while uptake was unchanged at the low Glu release levels. We cannot, however, attribute this change solely to differences in age because the potassium doses were also significantly higher in the aged monkey motor cortex. We have previously observed a limited dose-response to increasing potassium volumes in the young (see Burmeister et al., 2002) and aged rat brain (unpublished data); thus, the higher amplitudes in the aged animal may simply be due to higher depolarizing stimulations.

While we could not detect significant differences in the Glu uptake system by studying low volume 70 mM potassium-evoked Glu signals, highly significant uptake changes were evidenced by the recordings of 5 mM Glu ejections. We adjusted the ejected volumes to match Glu signal amplitudes in a targeted range to better compare signal parameters, especially measures of the Glu uptake system (e.g. T_{80} and uptake rate). While uptake rate can reflect changes in Glu release or uptake (see above, Chapter Two Data Analysis, and Chapter Four Discussion), it is mainly reflective of the Glu uptake system when signals have the same amplitudes. The higher volumes of 5 mM Glu that were needed to produce target amplitudes in the aged monkey can be explained in at least two ways. First, there may be increased uptake in the aged monkey because more of the ejected Glu was being cleared from the extracellular space in the 50-100 μm distance between the micropipette tip and the microelectrode array recording sites. Second, there may be an age-related change in the excitability of Glu fibers (i.e. a change in the level of exogenous Glu-induced endogenous Glu release). Further analysis of our signals shows that Glu uptake-related signal parameters

in the aged monkey (longer T_{80} and decreased uptake rate) support a decrease in Glu uptake. Recently, a series of studies in young (6 month old), late middle-aged (18 month old), and aged (24 month old) rats have expanded our understanding of age-related changes in the mammalian Glu system. Consistent with our pilot work in monkeys, Nickell et al. (2005) showed that, in the aged rat brain, greater volumes of 5 mM Glu were required to produce amplitude-matched signals, and there was a decrease in the average uptake rate compared to younger rats. Additional Western blots analyses were completed to examine the amount and surface expression of rat Glu transporters (GLAST and GLT-1 (glial) and EAAC1 (neuronal)), which revealed that there were no age-related changes in total protein levels; however, the surface expression of GLAST was significantly decreased in the late middle-aged and aged rats. Thus, although gliosis (an increased number of glial cells, such as astrocytes that account for most of Glu uptake) has been reported in the aged mammalian brain (Unger, 1998), data in rats support an age-related decrease in the number of Glu transporters available for Glu uptake. This may explain the decreased uptake rate seen in both the aged rat and monkey. Furthermore, there is no supporting evidence to conclude that increased uptake accounted for the increased volumes of 5 mM Glu needed to produce amplitude-matched signals in either the aged rat or monkey brain. Instead, this may reflect an age-related decrease in the excitability of Glu terminals.

We also recorded potassium-evoked Glu signals in the monkey frontal cortex, yet many of the characteristics of these signals differed from the typical evoked Glu kinetics that we observed in the motor cortex. First, we evoked both fast and relatively slow Glu signals in the young monkey, while only slower Glu signals were seen in the aged monkey. The fast Glu signaling differed from our typical signals primarily with respect to amplitude. It is interesting to consider that we also recorded extraordinarily high basal Glu activity in this brain region, which may have been tonically activating presynaptic metabotropic Glu autoreceptors that inhibit Glu release. This may explain the reduction in amplitude and decreased signal times. That we did not see fast Glu signaling at all in the aged

monkey may have been due to the age difference; however, this animal was being maintained at a higher level of anesthesia (3% isoflurane, an induction level) than the young monkey during these recordings. Isoflurane has been reported to decrease Glu release and increase Glu uptake in mammals (Hudspith, 1997, Danbolt, 2001), and the higher dose in the aged animal makes definitive conclusions difficult. The anesthesia was lowered to a more typical maintenance level (2%) before additional Glu recordings were made. In both the young and aged monkey frontal cortex, we also observed unusual Glu signals which showed reproducible slow release and uptake characteristics. Once again, the higher basal Glu activity may explain the lowered Glu release but does not explain the decreased uptake. At least two possibilities can explain the decreased Glu uptake at these low levels of Glu release. First, the frontal cortex may be a more susceptible region to the effects of isoflurane on Glu regulation, which may have also contributed to decreased Glu release, and secondly, we may be observing novel normal Glu regulation. The complementary Glu ejections in the frontal cortex do not support that this region has diminished Glu transporter function. In fact, the Glu uptake rate was roughly equivalent or even higher than that seen following Glu ejections in the motor cortex. If this region is predisposed to higher, often oscillatory, basal Glu levels, an increase in extracellular Glu concentration of ~1-2 μM (average potassium-evoked Glu signal amplitudes seen in the frontal cortex) may not always elicit the fast uptake responses that we have previously characterized and may represent a new kind of Glu signaling in the brain. Interestingly, low level evoked Glu release and uptake was faster (faster rise times and T_{80}'s) in the aged monkey frontal cortex.

Once more, when we challenged the Glu uptake system with much higher levels of exogenous Glu ejections, Glu uptake was robust and revealed a difference in Glu uptake between the young and aged animals. In nearly every measure, these Glu signals were very closely matched. The most striking difference was that average volumes of nearly ten times as much 5 mM Glu were needed to achieve the target amplitudes in the aged monkey, which may again be explained by an age-related change in glutamatergic excitability (decreased

Glu-induced Glu release in the aged monkey). Unlike in the motor cortex, the average uptake rates and T_{80}'s were not different, so that the Glu uptake system appears to remain functionally unchanged with age in the frontal cortex.

Average basal Glu measures were larger in both cortical regions of the young monkey compared to the aged monkey. The young monkey measures showed a statistically significant mean increase in the frontal cortex but only tended to be larger in the motor cortex despite a large mean difference ($p=0.052$). Basal Glu signals were recorded in a second aged monkey in two brain regions. Extremely high basal Glu measures (43.4 ± 14.9 μM Glu, n=10) were calculated for a brain region that was identified as the frontal cortex on post-mortem examination. These levels were much larger than the average frontal cortical levels from the young monkey and the other aged monkey (10.3 ± 3.3 μM Glu and 2.7 ± 0.5 μM Glu, respectively). Thus, it is difficult to conclude that there is any age-related change in basal Glu levels in this region, as aged monkeys individually showed much lower and much higher basal Glu levels in the frontal cortex than a young monkey. This emphasizes that many of the comparisons discussed for the various Glu measures so far may not be due to age differences but simply biological variability between animals. As previously mentioned, this discussion of age-related differences in Glu regulation assumes that these animals are representatives of their age groups. This assumption can only be tested by conducting a much larger study.

Particularly interesting findings in two of the three monkeys were strikingly increased basal Glu levels at discrete depths within the frontal cortex. Both the temporal behavior and, in the case of the 28 year-old monkey, the magnitudes of the average basal Glu measurements (129.2 μM Glu and 44.4 μM Glu, both over 5 minutes) had never been seen before in any Glu recording from a mammalian brain. As we lowered into these depths, the sentinel recording sites maintained baseline activities, while the Glu recording sites passively displayed high basal Glu levels that tended to oscillate over time. The periodicities of these oscillations were approximately 30 seconds to a minute, time periods much too long to correspond to other biological or mechanical interferences such as heart rate or

ventilation. In fact, the aged monkey traces showed a smaller, superimposed higher-frequency oscillation on both the sentinel and Glu recording channels (see Figure 5.11B). These fluctuations may reflect the pulse pressure created by a typical anesthetized rhesus monkey heart rate, which leads us to hypothesize that, in the case of the aged monkey, we may have been recording basal Glu levels near a cortical blood vessel. In this animal, the average basal Glu level dropped in an almost logarithmic fashion as we lowered the microelectrode array further supporting the hypothesis that we began close to a concentrated source of Glu and moved away from it. In the young animal, however, we saw neither the superimposed frequency nor did the level drop in a predictable fashion. Both depths that showed extraordinary basal Glu activity in the young monkey were inferior and superior to depths that had much lower basal Glu levels. These new and exciting findings would not have been possible without the spatial and temporal resolution that implantable microelectrode arrays provide.

In summary, we achieved our primary goal of safely and efficiently advancing second-by-second microelectrode array Glu recordings into the nonhuman primate brain in the veterinary operating room. This began with careful planning on the parts of several collaborating teams of specialists who helped recognize the challenges of this task. Specifically, we developed a mobile Glu recording setup, made several advanced preparations, and adapted our protocols to maximize the likelihood of executing successful experiments. Accomplishing our primary goal creates many opportunities for future studies in nonhuman primates and/or in the OR setting. These efforts were also part of a pilot study of age-related changes in Glu regulation in the nonhuman primate cerebral cortex. Although we collected data from only three animals in two age groups, we were already able to see differences in Glu regulation in differently aged individual animals. Our Glu recordings in the rhesus monkey cortex displayed both the fast kinetics that we had previously characterized in the rat brain and novel potassium-evoked and basal Glu activities. Larger studies are merited to further explore differences in normal Glu signaling and age-related alterations in Glu regulation in the nonhuman primate brain.

Discussion & Conclusions

Our development of ceramic-based enzyme-coated multisite microelectrode arrays that use electrochemical detection to selectively record Glu levels with high spatial and temporal resolutions (15 x 333 μm, 800 msec) created an exciting new research tool to examine direct Glu measures in the intact mammalian CNS. The premier conclusion that emerged from the initial work using Glu selective microelectrode arrays confirmed that *in vivo* measures of extracellular Glu displayed fast kinetics of release and uptake that required a fast monitoring technology (see Burmeister, Moxon, and Gerhardt, 2000, Burmeister and Gerhardt, 2001, and Burmeister et al., 2002). The second-by-second recording capabilities are a distinct advantage of microelectrode array studies of Glu. In this dissertation, these capabilities were used repeatedly to investigate the dynamics of Glu release and uptake in the mammalian brain. However, we also expanded the use of this technology to study basal Glu regulation including achieving the important task of measuring basal Glu levels. In addition to technological advancements that expanded and improved our Glu recording capabilities, we also advanced the biological applications of microelectrode arrays to complement the initial *in vivo* recordings in the normal rat brain and pushed this technology into a rat model of PD and into young and aged normal rhesus monkeys in the veterinary operating room setting. Ultimately, as our technology and biological applications progress, we would like to conduct Glu recordings in the intact human brain in the clinical setting to advance our scientific understanding of Glu regulation and possibly benefit patient care.

In Chapter Three, we used microelectrode arrays to study basal and potassium-evoked Glu regulation in the normal anesthetized young rat brain. Glu kinetics studies had already been performed in the normal rat CNS using both potassium and Glu ejections; however, the speed and reproducibility of different concentrations of potassium had not been fully investigated, and no work had been carried out to explore basal Glu using microelectrode arrays. Our studies in

the striatum and frontal cortex revealed that TTX lowered while TBOA increased signals across individual Glu recording channels to significantly different levels than physiological saline ejections alone, which lowered the signal slightly due to dilution of the recording area. The TBOA-dependent effects (1-3 μM Glu increase) support the hypothesis that active Glu release and uptake occurs at a basal level. The TTX-dependent effects (~2 μM Glu decrease) support the hypothesis that a significant measurable portion of basal Glu originates from action potential-dependent neuronal release. To determine what fraction of basal Glu was TTX-dependent, we had to further develop our technology to quantify overall basal Glu levels. We developed two methods using the self-referencing capabilities of our microelectrode arrays. The first method measured baseline signal differences between pairs of enzyme-coated and enzyme-free channels at constant applied potential (+0.7 V vs. Ag/AgCl reference). The second was a varied applied potential method that switched the potential between +0.25 V and +0.7 V (both vs. Ag/AgCl reference) and measured the differences in voltage-dependent signal changes between the same paired channels. We applied these techniques in the rat striatum and frontal cortex to find that the overall basal Glu level was ~2 μM Glu in both regions with no significant difference between the methods. Taken with the previous TTX-saline comparisons, our data support that basal Glu is fully TTX-dependent in two regions of the urethane-anesthetized rat brain. Our results compare favorably in concept to another voltammetry-based investigation of basal Glu (Kulagina, Shankar, and Michael, 1999) except the magnitude of our TTX-induced signal changes and overall basal Glu levels are lower. Alternatively, our basal Glu levels are similar to reported microdialysis measures; however, microdialysis studies do not support greater than 50% TTX-dependency of basal Glu levels. These differences may be related to our use of the anesthetic drug urethane, which may be lowering basal Glu levels and altering the TTX-dependent fraction. Investigations in the awake, freely-moving rat in our laboratory to resolve this issue are ongoing. We also investigated 70 mM and 120 mM potassium-evoked Glu signals in the same brain regions and determined the speed of these signals. Overall, the potassium-evoked signals

supported robust Glu release and uptake, rising to peak amplitude in 1-4 seconds and lasting 10-20 seconds. The 70 mM potassium-evoked Glu signals were slightly smaller and faster than 120 mM and were less likely to show any signs of interference from other electroactive molecules such as the neurotransmitter DA. All potassium-evoked signals were routinely reproducible at 20 seconds intervals and remained distinct at intervals as short as 15 seconds. These results are comparable to earlier studies of potassium-evoked Glu release using similar technology (Hu et al., 1994), especially with respect to the fast kinetics of Glu release and uptake. Finally, we responded to one of the most common criticisms of microelectrode-based detection systems, signal identity. To address this issue, we recorded potassium-evoked Glu responses in a self-referencing mode to demonstrate that our evoked signals were both enzyme- and voltage-dependent, further confirming that the major source of our evoked signals is Glu.

In Chapter Four, we built on our previous investigations of normal Glu to advance this technology to study a rat model of PD. In the last decade, PD has been reexamined as a disease of secondary Glu hyperactivity along pathways related to the disease-altered involuntary motor system, namely the glutamatergic corticostriatal and subthalamopallidal pathways. Conducting microelectrode array studies in the brains of unilateral 6-OHDA-lesioned young rats, we focused on the corticostriatal pathway, recording in both the striatum and frontal cortex. We also examined evoked Glu signaling in the nucleus accumbens, a brain area that is cellularly organized almost identically to the striatum but receives DA primarily from a different area of the midbrain. Like many investigators, we used the unilateral lesioned rat model so that we could make comparisons to the contralateral side as a within-animal control. We also recorded non-lesioned rats in the same age range as another control group. Our hypotheses entering the study were that there would be ipsilateral and contralateral differences in evoked Glu kinetics within the 6-OHDA-lesioned group and that evoked Glu kinetics would differ between matched hemispheres of lesioned and non-lesioned rats. Potassium ejections (45 mM KCl, ~300 nl)

were used to stimulate Glu signals in all animals. At the end of the recording sessions, we used roughly ten times higher potassium stimulation in the striatum to record simultaneous Glu and DA release to further confirm the unilateral lesion status of the 6-OHDA-treated animals. In the striatum and frontal cortex, there were no significant differences in any of the reported average signal parameters (amplitude, uptake rate, T_{80}) between hemispheres within the unilaterally lesioned group; however, Glu signal measures were significantly altered in both lesioned hemispheres compared to matched hemispheres in non-lesioned rats. Taken together, we observed a striking bilateral effect of a unilateral lesion on Glu signaling in the striatum and frontal cortex. Closer examination of the signal parameters supported that the primary difference in lesioned rats was increased Glu release on stimulation. In the normal rat striatum, DA release tends to inhibit Glu release through D2-like receptors on the presynaptic Glu nerve terminals. In the DA denervated striatum on the ipsilateral side, the presynaptic Glu terminals may be disinhibited so that they release more Glu when evoked. In the DA innervated striatum on the contralateral side, the same disinhibition cannot occur because DA is present; however, an increased DA compensation on this side, as previously reported (Nieoullon et al., 1977, Cass et al., 1995), might internalize some DA receptors and cause a functional disinhibition of Glu release. Alternatively, a distinct bilateral corticostriatal pathway has been reported (Reiner et al., 2003, Lei et al., 2004), which may play a role in sychronizing events between the ipsilateral and contralateral striatum due to bilateral connectivity through the cortex. In fact, bilaterally increased potassium-evoked Glu release in the frontal cortex was also measured in the unilateral lesioned rat group. These findings may result from the downstream effects of lesioning the nigrostriatal pathway as the cortex is known to be involved in parkinsonian motor abnormalities. Again, the bilateral effects may relate to the high connectivity of the cortex to the striatum and to other cortical areas within both hemispheres. In the nucleus accumbens, we measured significant differences in evoked Glu signaling within the lesioned rat group; however, we also found compelling evidence for normal hemispheric differences within the non-lesioned rat group

that may have reflected greater difficulties in microelectrode array placement in this brain region. Restricting our discussion to hemisphere-matched comparisons between lesioned and non-lesioned rats, the increased evoked Glu release was maintained in the ipsilateral nucleus accumbens; however, there was also a significant increase in Glu uptake. In the contralateral nucleus accumbens, there was no significant effect of lesion on evoked Glu measures except for a slight but significant decrease in Glu uptake. Interestingly, DA depletion to the nucleus accumbens is relatively spared following 6-OHDA treatment (Lancia et al., 2004), which may have contributed to some of the differences that we measured compared to similar brain areas like the striatum. Overall, this work puts the use of the contralateral side in the unilateral 6-OHDA-lesioned rat as a control into question for some measures, as we would not have recognized any difference in evoked Glu kinetics in the striatum and frontal cortex of lesioned animals without another control group. Furthermore, the effects that we measured in both hemispheres in lesioned rats place the cortex and the neurotransmitter Glu as prime candidates for modulating bilateral effects of unilateral treatments, including 6-OHDA-lesions and possibly PD therapies.

In Chapter Five, we returned to investigating normal Glu regulation by advancing our technology to study both young and aged rhesus monkeys. Our primary goal was to modify our technology and methods to safely and efficiently conduct nonhuman primate Glu recordings in the veterinary operating room. We also wanted to compare characteristics of normal Glu regulation between our initial rat work and the higher mammalian species, determine if there were regional changes within the monkey cortex, and collect preliminary data to evaluate whether there were age-related differences in Glu regulation. Accomplishing our primary goal began with extensive planning between the collaborating teams and a number of modifications to our standard Glu recording approach. First, we created the mobile FAST-16, a self-contained electrochemical recording system that could be easily moved between the laboratory and operating room with minimal setup requirements. In advance, we supplied the surgical facilities with pressurized nitrogen and created a custom-

made coupling so that our pressure-ejection system would be compatible with typical OR gas supply lines. We also modified our experimental preparations to conform to the timeline of nonhuman primate surgery and improve our chances for successful Glu recordings. First, we increased the number of microelectrode arrays prepared per animal from two to four. Then, we moved time-intensive steps such as micropipette attachment to the day before surgery. Finally, we calibrated the microelectrode arrays several hours before surgery to evaluate their quality prior to the start of pre-surgical monkey preparation. We did this so that, if necessary, the experiment could be cancelled in a timely manner to avoid inefficient animal use. With these new methods in place, we successfully recorded Glu signals in three rhesus monkeys (8, 25, and 28 YO) with no experiments cancelled. We measured basal Glu levels and studied Glu signals resulting from local ejections of 70 mM potassium and 5 mM Glu solutions. In the motor cortex of all monkeys, we observed the fast kinetics of Glu release and uptake that we had previously characterized in the rat brain. Fast Glu uptake was also seen in the frontal cortex of all monkeys following exogenous Glu challenge; however, potassium-evoked Glu responses were unusual in this brain region. All potassium-evoked signals were low amplitude (<2 μM Glu), and both fast (young monkey) and slow (both young and aged monkey) Glu release and uptake kinetics were recorded. Interestingly, novel basal Glu activity was also observed in this brain region in both a young and an aged monkey, which might contribute to some of the atypical release and uptake characteristics. The average basal Glu levels in the isoflurane-anesthetized monkeys were higher in the frontal cortex than those we have measured in the urethane-anesthetized rat frontal cortex, and both species and anesthetic changes may play a role in these differences. More strikingly, average basal Glu levels at discrete depths were often very high (~10-120 μM Glu) and displayed dynamic oscillatory behavior. These basal Glu magnitudes and activities had never before been recorded in the anesthetized mammalian brain. The primary age-related difference that we observed was related to Glu uptake. In both cortical regions, we had to deliver roughly ten times the volume of 5 mM Glu in the aged monkey to match the

amplitudes we achieved in the young monkey. This may be due to an age-related decrease in the excitability of Glu fibers in the monkey cortex. We also saw an age-related decrease in uptake rate in the motor cortex. The low number of animals per group limits the relevance of these findings to aging research; however, we already have data supporting differences in Glu regulation in young and aged individual monkeys, and a larger study is merited.

Overall, we have made good progress to both advance and refine the technology and expand its biological applications to better study Glu in the mammalian brain. Beginning with the characteration of basal and potassium-evoked Glu regulation in the anesthetized rat brain, we moved the technology forward to study disease-altered Glu regulation in the hemiparkinsonian rat brain and normal Glu neurotransmission in young and aged rhesus monkeys. Based on our experiences to date, we would like to continue pushing our technology forward to record Glu in the intact human brain. This dissertation began by introducing the idea that using implantable microelectrode arrays to advance science and medicine is neither science-fiction nor radical, but potentially a common and valuable tool that might be used by physicians to improve patient care. The appendix documents our first experience with excised human brain tissue and how we might logically proceed to introduce Glu selective microelectrode arrays into clinical applications.

Appendix: Investigating Glu Neurotransmission in the Human Brain

Introduction

Throughout the graduate studies of my combined M.D./Ph.D. training, I have been especially interested in advancing our technology toward clinical applications. Because the initial use of microelectrode arrays to study normal Glu dynamics in the intact rat brain shortly predated the start of my dissertation research, my role in this effort began at the benchside. Though we had published data supporting the rapid nature of extracellular Glu signaling, many aspects of Glu neurotransmission required further investigation. In response, I conducted several additional studies of normal Glu regulation in the rat brain, focusing on both basal and potassium-evoked measures. Building on these studies, we also investigated Glu signaling alterations in the unilateral 6-OHDA-lesioned rat model of PD. Together, these acute investigations provided biological, methodological, and analytical bases for moving our technology into chronically-used nonhuman primates in the veterinary operating room. This effort represented a logical step in the advancement of our technology toward human applications and an important opportunity for us to begin modifying our methods to transition into a clinically-relevant setting. In a parallel fashion, actual human brain tissue recordings have begun at the benchside, and hopefully they will ultimately be applied in the clinical arena to benefit patient care.

Preliminary Human Tissue Study

In collaboration with neurosurgeon Craig van Horne M.D., Ph.D. and his laboratory team at the Harvard Institutes of Medicine (HIM, Boston, MA), we attempted to record Glu from a piece of excised human brain tissue. We began working toward this goal in the Spring of 2003 when I traveled to the Brigham

Hospital and the HIM to deliver, set up, and test his FAST-16 electrochemical detection system. During this trip, I also supplied his laboratory with many of the materials and equipment necessary to conduct independent microelectrode array studies and trained his staff. With these basic requirements satisfied, we allowed time for our partners to become proficient with the technology, and set up additional training for a new member of Dr. van Horne's team here at the University of Kentucky later that year. I spent one more week in Boston during the Spring of 2004, and we recorded signals from a small piece of freshly-excised human brain provided by Dr. van Horne.

Our goal was simply to prove that we could record Glu from a surgically resected piece of human brain tissue. At the same time, we wanted to plan ways to refine our excised human tissue methods to conduct safe and efficient Glu recordings in the future. Several refinements are needed as we faced many challenges from the onset of this first effort. Our equipment was primarily limited to the basic FAST-16 recording setup and a brain slice recording chamber. We did not have timely access to oxygenation, perfusion, or heating systems for the chamber. The resected brain tissue had to be evaluated by the Pathology Department before it was released for further testing. Furthermore, the physical dimensions of the tissue also presented a problem for implantation-based Glu recordings.

To overcome these limitations, we had to adapt new ways to conduct the experiment and stimulate detectable Glu release. Microelectrode arrays configured for recording Glu on all sites were calibrated beforehand. We could not implant a microelectrode array due to the size and shape of the brain tissue. Instead the brain tissue was removed from ice storage and floated in a pool of 0.05 M PBS in the central reservoir of the recording chamber at room temperature. The microelectrode array was lowered into the saline pool at a shallow angle, and recordings were begun. Using microforceps, the brain tissue was gently moved toward the microelectrode until it rested atop all four recording sites (see Figure A.1). To stimulate endogenous Glu release from the tissue, we applied small drops of a 120 mM potassium solution (120 mM

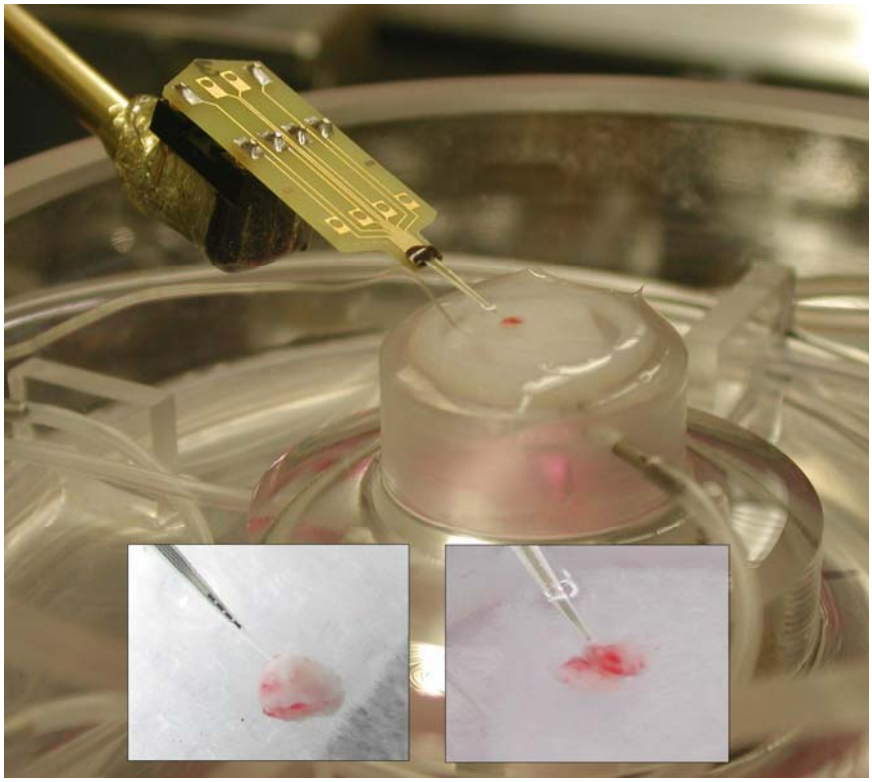

Figure A.1 Recording Setup for Our First Experience with Excised Human Brain Tissue

Our basic setup included the FAST-16 recording system and a brain slice recording chamber. The inset photographs show the relationship of the microelectrode array and tissue before (left) and after (right) positioning the tissue onto the recording sites. The four platinum recording sites are clearly visible in the left inset picture.

KCl, 29 mM NaCl, 2.5 mM $CaCl_2 \bullet 2H_2O$, pH 7.4) directly onto the tissue using a pipettor. Because the microelectrode arrays were not configured for self-referencing Glu recordings, we could not assess steady-state Glu levels.

These simple manipulations gave us the following results. Figures A.2 and A.3 demonstrate that when we moved the tissue onto the Glu recording sites (white arrows), we recorded signal increases on all four channels. Figure A.3 also shows the recorded responses to high potassium applications (black arrows). The initial potassium application created prolonged signal increases on all four channels, while a second application had diminished or virtually no effect on the recorded signals. The final application floated the tissue off of the recording sites, and we observed universal signal decreases.

Unfortunately, at this point, we cannot definitively conclude that we achieved our goal of recording Glu from an excised piece of human brain tissue. This is primarily because we were not able to use microelectrode arrays configured to record Glu in a self-referencing mode for this experiment. Without evidence that our signal changes were not due to interfering neurochemicals, we simply cannot be sure that our results were wholely or partially due to endogenous Glu release. Whereas monitoring interferences is routinely beneficial, it is especially important when attempting to record from a piece of traumatized brain tissue that may be releasing chemicals that do not normally exist in the extracellular fluid at such high concentrations. Nonetheless, the behavior of the signals in response to our manipulations might be consistent with spontaneous (initial tissue contact) and evoked (potassium-driven depolarization) Glu releases, and we are hopeful that with appropriate modifications we will succeed in definitively recording Glu from human brain tissue. Ultimately, this experiment was an important opportunity to identify difficulties associated with excised human tissue recordings so that we can design better future studies.

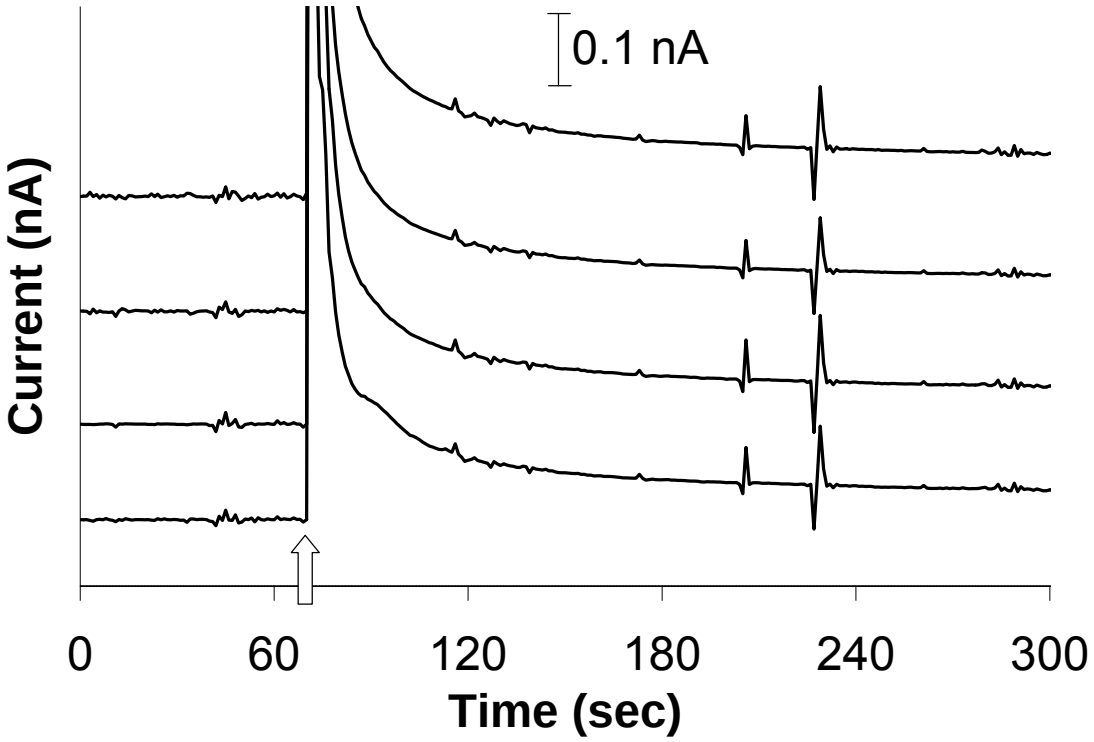

Figure A.2 Initial Contact of the Excised Human Brain Tissue with the Microelectrode Array

Immediately upon contact between the excised human brain tissue and the microelectrode array (white arrow), we observed dramatic signal increases on all four channels. The signals immediately began to approach steady levels, and remained higher than pre-contact levels after several minutes of recording. If these changes in signal are due to Glu detection, a 0.1 nA change in signal is approximately equal to 17.3 μM change in Glu concentration according to the calibration slopes for the microelectrode array used in these recordings. The traces have been offset from one another for clarity.

A.

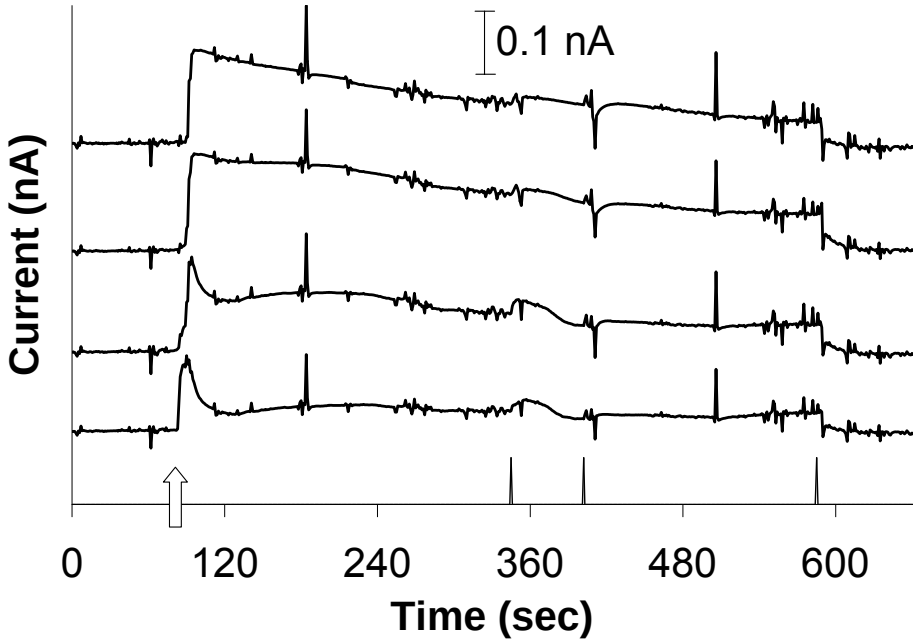

B.

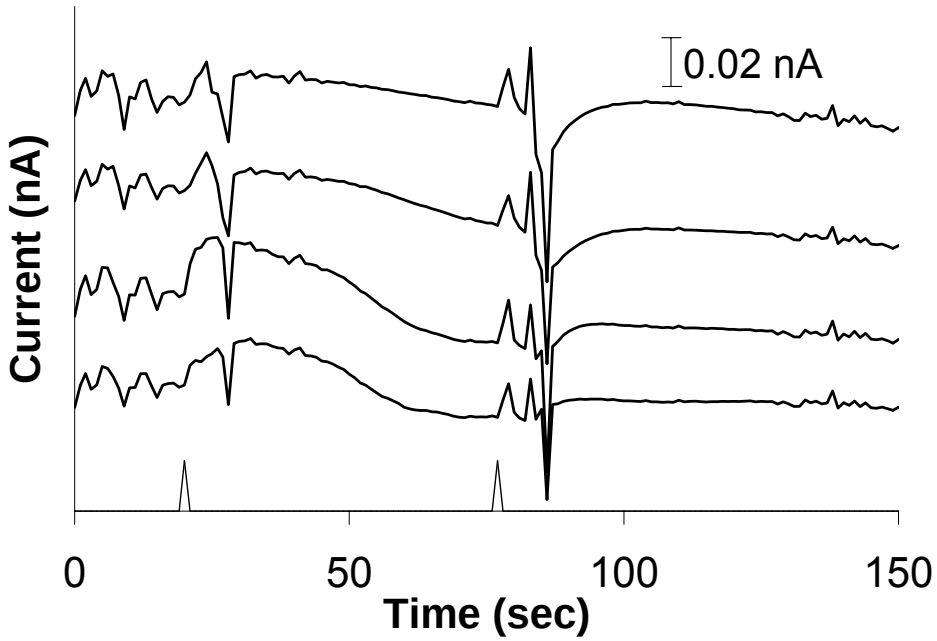

Figure A.3 Potassium-Evoked Signals from Excised Human Brain Tissue

(Figure legend on the following page)

Figure A.3 (continued)

A) As we previously observed, all four channels displayed signal increases upon contact between the tissue and the recording sites (white arrow). Individual differences in response may be due to the fact that each recording site is contacting a different part of the brain tissue's surface. The signals were allowed to equilibrate for a few minutes before applications of a 120 mM potassium solution were made directly onto the tissue (black arrows). The third application disrupted the seal between the array and the tissue, and all signals decreased uniformly. B) A closer look at the first and second potassium applications is shown. We observed signal increases on some of the channels in response to depolarizing stimuli, especially following the first application. If these signals are due to Glu release, a 0.02 nA change in current is roughly equal to a 3.5 μM change in Glu according to the calibration slopes for the microelectrode array used in the experiment. The traces have been offset from one another for clarity.

Future Patient-Oriented Research

Our initial attempt to record Glu from a piece of excised human brain tissue represents the first of a series of steps that we may have to take to introduce our microelectrode-based Glu detection technology into the clinical setting. Our rationale unfolds in the following way. First, we would like to prove that we can record Glu from human brain tissue. Of course, the safest tissue to use is excised human brain tissue that has been removed by a neurosurgeon for a medically prescribed reason. Epileptogenic foci and brain tumors are often removed as surgical treatments of some forms of epilepsy and cancer. Once we have satisfactorily proven that we can record Glu from human brain tissue, the next step would be to target intact brain tissue. Once again, both epileptics and brain tumor patients scheduled for resections would be good candidates for our patient population. In fact, we would record the same type of brain tissue as previously described; however, we would conduct intraoperative recordings before the tissue was removed. During these studies, we would characterize Glu activity in abnormal brain tissue. Once we have demonstrated that microelectrode arrays can be used in a safe and efficient manner during neurosurgery, we would like to design similar intraoperative studies to characterize Glu regulation in normal brain tissue. The normal brain regions that we sample would not be removed following our recordings. Ultimately, we would have preliminary data to compare normal and abnormal Glu measures for each brain disorder so that we could use to propose larger studies. Furthermore, Glu measures might correlate with disease parameters so that our Glu detection technology could have an apparent therapeutical use.

Excised Abnormal Human Brain Tissue Recordings

In future attempts to record Glu from a piece of excised human brain tissue, we would benefit from gaining additional control over the tissue. Ideally, our methods would closely resemble those used for brain slice recordings. Our

first goal would be accessing adequate volumes of brain tissue in a timely manner. The size of the excised tissue should be large enough that it can be sliced very thinly (300-400 μm thick) either immediately after resection in the surgical suite using a McIllwain tissue chopper or soon thereafter using brain sectioning equipment in the recording laboratory. The tissue sample should also be large enough so that the other physical dimensions provide substantial mass for the ceramic tip of our microelectrode array to be implanted through the slice without fracturing it. One cm^3 blocks of resected brain tissue are standardly reported by groups who study human neocortical slices both in Europe and the United States (Burkhart et al., 1998, Gorji et al., 2002). Timing between removal of brain tissue and oxygenation is important to maintaining living cells within the slice. Research groups who study human neocortical slices often report preincubation procedures beginning within two to five minutes of resection. Depending on the nature of the excised tissue or the standard operating procedures of the medical center, the removed brain tissue may need to be evaluated by the Pathology department before it can be prepared for slice recordings. With proper approval by the Institutional Review Board and likely the informed consent of the patients, all or a portion of the resected brain tissue may bypass this step and immediately be entered into a research protocol.

The brain tissue slices would then be placed in oxygenated (95% O_2, 5% CO_2) artificial cerebrospinal fluid (aCSF, in mM: 124 NaCl, 5 KCl, 1.5 $MgCl_2$. 2.5 $CaCl_2$, 1.4 NaH_2PO_4, 10 D-glucose, 26 $NaHCO_3$, pH 7.3-7.4) and allowed to recover for 1-2 hours. Thereafter, a section would be placed in a recording chamber warmed to 32-34 °C and perfused with oxygenated aCSF. Microelectrode arrays configured for self-referencing Glu recordings would be prepared and calibrated beforehand. A prepared microelectrode array or microelectrode/micropipette assembly would be lowered by micromanipulator until the recording sites were positioned within the slice. Basal Glu levels could be monitored as previously described. Endogenous Glu release could be stimulated by local application (Picospritzer III via micropipette) or recording chamber perfusion (Minipuls 3 peristaltic pump, Gilson Inc., Middleton, WI) of an

appropriate high potassium solution. Volumes of 5 mM Glu could also be ejected by micropipette to further study the Glu uptake system. At this level of control, we would not only maximize our chances of successfully and definitively recording Glu from excised human brain tissue, but also have an opportunity to begin characterizing the human neocortical Glu system.

Intact Human Brain Tissue Recordings

After we accomplish Glu recordings from excised human brain, the next step is to move the recordings from the laboratory to the neurosurgical suite where we can record Glu from an intact human brain. We would enroll patients with brain disorders, such as medically refractory epileptics, who are being surgically treated by having a section of their brains removed. Risks to the patient would be minimized primarily to increased surgical and anesthetic time, as we will only record Glu from abnormal tissue targeted for resection. In some ways, the methodology becomes much simpler for these recordings because we do not have to handle the tissue and artificially keep it alive, oxygenated, or warmed. Furthermore, concerns about alterations in the chemical composition of the extracellular fluid or changes in Glu regulation created by disrupting axonal connections, tissue trauma, and secondary injury are highly reduced.

Many of our primary goals to establish Glu recordings in the intact human brain are similar to those we set during the transition to Glu recordings in the brains of chronically-used nonhuman primates (see Chapter Five). Basically we need to modify our technology and methodology to safely and efficiently record Glu in the human neurosurgical operating room setting. We started to understand the challenges of this task first-hand as part of my experiences at the Brigham hospital. I was allowed to accompany Dr. van Horne to one of his cases and study the physical layout of a standard neurosurgical suite, learn about some of the equipment and technology that already exist in the OR, and observe the work dynamics among the scrub nurses, anesthesiologists, and surgeons. This experience provided an opportunity to envision conducting Glu recordings in this

setting, specifically to imagine the logical progression of events before, during, and after the surgery and to identify the specific challenges of this endeavor.

The intraoperative recording session would be straightforward, and the major changes would be hardware modifications. Specifically, we need to create a more sophisticated version of the mobile FAST-16 (see Chapter Five) in which the computer and FAST-16 components would be efficiently housed and protected within a stable, mobile tower. All of the sensitive components including the cable connections would be behind a locked panel, and an outside user would only be able to access the computer power button, keyboard, mouse, monitor, and data ports, and the face of the FAST-16 potentiostat box. To protect the sterile field environment and avoid unnecessarily obstructing the walking workspace of the surgical suite staff, we would also need to lengthen our cable that connects the headstage (pre-amplifier) with the FAST-16 potentiostat from a few feet to 20-30 feet. Currently, a separate connector is used between the headstage and microelectrode array, but the new longer cable would likely have the headstage and microelectrode connector integrated at one end. Because we will be visualizing the brain area targeted for recordings, we will secure the connected microelectrode array onto the patient's head frame and manually advance it using existing, approved electrode implantation equipment. Finally, we would not implant a Ag/AgCl reference electrode either in the brain or under a skin flap. Instead, we would use existing skin Ag/AgCl epoxy reference electrodes (e.g. BetterSkin^{TM} Electrodes, World Precision Instruments, Inc., Sarasota, FL) that require double-sided adhesive disks and conductive recording gel to maintain good electrical contact with clean, shaven skin. Although this electrode would not be in ionic contact with the brain per se, the electrical environment of the gel on the skin simulates that of the brain extracellular fluid. We have tested this type of reference electrode on the shaven backs of Fischer 344 rats with good experimental results (Figure A.4). The background current and amplitudes of similar volumes of 5 mM Glu in the same brain area increased slightly, but many of the characteristics of Glu signaling were maintained.

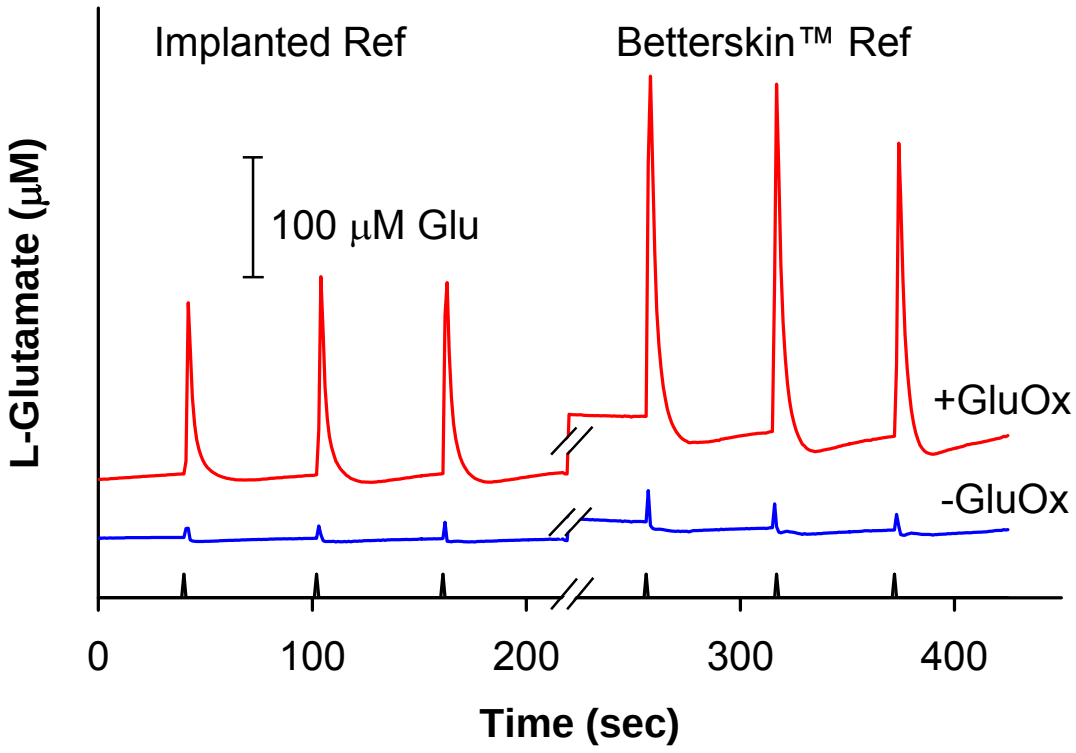

Figure A.4 Comparison of Ag/AgCl Reference Electrodes

Initial testing was carried out in the rat frontal cortex to assess the feasibility of using skin-adhered Ag/AgCl reference electrodes (Ref) during electrochemical recordings of Glu. 5 mM Glu ejections (black arrows, ~62.5 nl each) were recorded at an applied voltage of +0.7 V versus a typical bare wire, brain-implanted Ag/AgCl reference electrode (first three Glu responses). Then, the hardware's reference electrode connection was switched to the Betterskin™ Ag/AgCl epoxy reference electrode adhered to the animal's back, and the 5 mM Glu ejections were repeated (black arrows, ~62.5 nl, ~62.5 nl, 50 nl, last three Glu responses).

We also need to develop methods to efficiently conduct microelectrode calibrations within the sterile field. The intraoperative calibration might progress as follows. A side table with a non-sterile stir plate is set up and sterilely draped. A sterile cup is placed on the drape over the stir plate and filled with sterile PBS along with a small sterile stir bar. A sterilized microelectrode array is removed from its packaging and connected it to the headstage/connector cable. The recording sites are placed in the PBS using a standard clamp system. A sterile glass-bodied Ag/AgCl reference electrode is then removed from its packaging, placed in the PBS, and connected. The opposite end of the headstage/connector cable is handed off and connected to the FAST-16 potentiostat. Note that at this point the cable will have a non-sterile portion and a sterile portion that will be clearly defined to the surgical staff, which is a routine scenario in the human OR. One-step calibrations of the interferent AA, the analyte Glu, and other test molecules are conducted using sterile pipetting techniques. These procedures require at least two people, a sterilely gowned and gloved person from the surgical team and the FAST-16 user who works outside of the sterile field.

To properly complete this protocol, the headstage/connector cable, prepared microelectrode arrays, and some of the calibration equipment need to be sterile. Fortunately, many of the materials are commercially available sterilized including the cup, PBS, pipette tips, and calibration chemical storage vials. The headstage/connector cable, magnetic stir bar, and glass-bodied Ag/AgCl reference electrode would be sterilized using standard gas or heating procedures. The calibration chemicals could be prepared and sterilely filtered into the storage vials in advance. The last and possibly most important challenge that we must overcome is the sterilization of the microelectrode arrays themselves without compromising electrode performance. We hypothesized that although the enzyme GluOx might withstand heat sterilization (see Chapter Two's The Durability of L-Glutamate Oxidase subsection), the Nafion™ and/or BSA might be damaged by the high temperatures. Initial testing of gas sterilization conducted in collaboration with Dr. van Horne's team demonstrated that *in vitro* microelectrode performance suffered and the protein matrix layers were visably disrupted

following treatment. Recently, we have partnered with AdTech Medical Instruments Corporation (Racine, WI) specifically to study the physical tolerances of the microelectrode materials. With their data, we hope to devise a sterilization strategy that maintains the integrity of the layers that make our microelectrodes selective for Glu.

Final concerns relate to simplifying the experiment so that it is streamlined and straightforward. An advantage of our use of microelectrodes as research tools has been our ability to acquire kinetics data using local applications of intracranial solutions. However, these Glu recordings require time, additional preparation and equipment, and extensively trained personnel, which can be disadvantages in the human OR setting. Instead, we would concentrate on conducting passive recordings of basal Glu levels in different parts of the targeted brain tissue. Furthermore, we currently have sophisticated software written for scientists familiar with designing and performing *in vivo* electrochemical recordings. We would like to simplify this software package and make it more user-friendly, easy-to-learn, and accessible.

In addition to the acquired Glu data, we are just as interested in the safety measures for our patient population. Surgeons commonly worry about increased OR time contributing to surgical complications, so in response, we are already planning to simplify and shorten our Glu recordings. There is also a valid concern about the increased risk of infection and bleeding that might result from intraoperative recordings. By initially focusing on brain tissue that will be excised, these concerns are minimized, but still exist. We never observed a brain infection or any other poor outcome in the nonhuan primates we recorded using non-sterile implanted microelectrode arrays (Chapter Five) which supports the low risks of post-operative complications related to microelectrode use. Nonetheless, we must be extraordinarily cautious especially with respect to sterility before we implant our microelectrodes in a living human brain. We must also follow all of our patients and document any post-operative incidents to evaluate the safety of conducting intraoperative Glu recordings in the human brain. When we are

convinced of the safety to the patient, we can shift our target from abnormal to normal human brain tissue and repeat both the Glu and safety measures.

Future Clinical Applications

During the course of these initial investigations of the normal and disease-altered human cortex, significant differences in Glu regulation might be revealed that expose opportunities to use our microelectrode array technology therapeutically. The choice of both epileptic and brain tumor patients as our first subjects for Glu recordings was not simply based on neurosurgical access to brain tissue but also because there is evidence supporting that Glu regulation is altered by these diseases. Chapter One describes in detail the support for Glu alterations in epilepsy. Perhaps most importantly, extracellular Glu levels have been shown to be increased immediately before and during a seizure, and basal Glu levels are increased in the epileptogenic foci of some patients in the time period between seizures (During and Spencer, 1993, Ronne-Engstrom et al., 1992, Wilson et al., 1996, Thomas et al., 2003, Cavus et al., 2005). Furthermore, some brain tumors, specifically gliomas, have been shown to have altered, typically higher, basal Glu levels in the tumor and the adjacent brain tissue compared to normal cortex (Behrens et al., 2000, Roslin et al., 2003, Bianchi et al., 2004). In fact, Glu may connect these brain disorders because a seizure may be the first symptom of a low-grade glioma (Recht and Bernstein, 1995).

By focusing on the basal Glu levels in abnormal and normal intact human brain tissue, we are gathering information that might allow us to use Glu recording microelectrode arrays to determine the normalcy of brain tissue intraoperatively. In other words, we may be able to use our technology alone or in conjunction with other techniques to better define the borders of abnormal areas of the human brain. In epilepsy treatment, this might help the neurosurgeon determine the proper amount of brain to remove to reduce or eliminate seizure activity while preserving as much normal brain tissue and

function as possible. On the other hand, surgeons who treat patients with gliomas are most interested in removing as many of the cancerous cells as they can even at the sacrifice of normal tissue. Gliomas often have necrotic foci but are not well-circumscribed tumors, so any technology that can help locate more abnormal brain cells might benefit the care of these patients.

Another long-term goal of our laboratory is the development of brain interface devices that would be chronically implanted to monitor and interact with the intracranial environment. Once again, epileptics may be among the first patients to experience this novel approach. Because extracellular Glu levels rise immediately before seizure onset, it may be possible to use a chronically implanted Glu recording microelectrode array to determine this critical period and relay the information in real time. Upon notification, the patient or medical staff could administer interventional treatment. A similar but more sophisticated approach would require the development and use of small implantable computers and drug delivery systems. In this case, the Glu recording would be monitored by a simple computer that would control the release of medications in response to fluctuations in Glu levels. These drugs could be delivered intravenously or perhaps intraparenchymally, directly into the brain at the site of abnormal activity. Obviously, these future clinical applications require appropriate laboratory testing and clinical trials prior to federal approval; however, we have made many of the first steps and are excited by the future potential benefits to patient care that we envision.

References

1. Albin,R.L., Young,A.B., and Penney,J.B. (1989). The functional anatomy of basal ganglia disorders. Trends Neurosci. *12*, 366-375.

2. Anderson,C.M. and Swanson,R.A. (2000). Astrocyte glutamate transport: review of properties, regulation, and physiological functions. Glia *32*, 1-14.

3. Baker,D.A., Xi,Z.X., Shen,H., Swanson,C.J., and Kalivas,P.W. (2002). The origin and neuronal function of in vivo nonsynaptic glutamate. J.Neurosci. *22*, 9134-9141.

4. Balaban,R.S., Nemoto,S., and Finkel,T. (2005). Mitochondria, oxidants, and aging. Cell *120*, 483-495.

5. Bamford,N.S., Robinson,S., Palmiter,R.D., Joyce,J.A., Moore,C., and Meshul,C.K. (2004). Dopamine modulates release from corticostriatal terminals. J.Neurosci. *24*, 9541-9552.

6. Barbeito,L., Girault,J.A., Godeheu,G., Pittaluga,A., Glowinski,J., and Cheramy,A. (1989). Activation of the bilateral corticostriatal glutamatergic projection by infusion of GABA into thalamic motor nuclei in the cat: an in vivo release study. Neuroscience *28*, 365-374.

7. Behrens,P.F., Langemann,H., Strohschein,R., Draeger,J., and Hennig,J. (2000). Extracellular glutamate and other metabolites in and around RG2 rat glioma: an intracerebral microdialysis study. J.Neurooncol. *47*, 11-22.

8. Benazzouz,A. and Hallett,M. (2000). Mechanism of action of deep brain stimulation. Neurology *55*, S13-S16.

9. Bergman,H., Wichmann,T., and DeLong,M.R. (1990). Reversal of experimental parkinsonism by lesions of the subthalamic nucleus. Science *249*, 1436-1438.

10. Berners,M.O., Boutelle,M.G., and Fillenz,M. (1994). On-line measurement of brain glutamate with an enzyme/polymer-coated tubular electrode. Anal.Chem. *66*, 2017-2021.

11. Bianchi,L., De Micheli,E., Bricolo,A., Ballini,C., Fattori,M., Venturi,C., Pedata,F., Tipton,K.F., and Della,C.L. (2004). Extracellular levels of amino acids and choline in human high grade gliomas: an intraoperative microdialysis study. Neurochem.Res. *29*, 325-334.

12. Bortolotto,Z.A., Lauri,S., Isaac,J.T., and Collingridge,G.L. (2003). Kainate receptors and the induction of mossy fibre long-term potentiation. Philos.Trans.R.Soc.Lond B Biol.Sci. *358*, 657-666.

13. Brewer,G.J. (2000). Neuronal plasticity and stressor toxicity during aging. Exp.Gerontol. *35*, 1165-1183.

14. Burkhart,K.K., Beard,D.C., Lehman,R.A., and Billingsley,M.L. (1998). Alterations in tau phosphorylation in rat and human neocortical brain slices following hypoxia and glucose deprivation. Exp.Neurol. *154*, 464-472.

15. Burmeister,J.J., Moxon,K., and Gerhardt,G.A. (2000). Ceramic-based multisite microelectrodes for electrochemical recordings. Analytical Chemistry *72*, 187-192.

16. Burmeister,J.J. and Gerhardt,G.A. (2001). Self referencing ceramic based multisite microelectrodes for the detection and elimination of interferences from the measurement of L-glutamate and other analytes. Analytical Chemistry *73*, 1037-1042.

17. Burmeister,J.J., Pomerleau,F., Palmer,M., Day,B.K., Huettl,P., and Gerhardt,G.A. (2002). Improved ceramic-based multisite microelectrode for rapid measurements of L-glutamate in the CNS. Journal of Neuroscience Methods *119*, 163-171.

18. Burmeister,J.J. and Gerhardt,G.A. (2003). Ceramic-based multisite microelectrode arrays for in vivo electrochemical recordings of glutamate and other neurochemicals. Trac-Trends in Analytical Chemistry *22*, 498-502.

19. Burmeister,J.J., Palmer,M., and Gerhardt,G.A. (2005). L-lactate measures in brain tissue with ceramic-based multisite microelectrodes. Biosens.Bioelectron. *20*, 1772-1779.

20. Calabresi,P., Mercuri,N.B., Sancesario,G., and Bernardi,G. (1993). Electrophysiology of dopamine-denervated striatal neurons. Implications for Parkinson's disease. Brain *116 (Pt 2)*, 433-452.

21. Calabresi,P., Pisani,A., Mercuri,N.B., and Bernardi,G. (1996). The corticostriatal projection: from synaptic plasticity to dysfunctions of the basal ganglia. Trends Neurosci. *19*, 19-24.

22. Calabresi,P., Centonze,D., Gubellini,P., Marfia,G.A., Pisani,A., Sancesario,G., and Bernardi,G. (2000). Synaptic transmission in the striatum: from plasticity to neurodegeneration. Prog.Neurobiol. *61*, 231-265.

23. Cartmell,J. and Schoepp,D.D. (2000). Regulation of neurotransmitter release by metabotropic glutamate receptors. J.Neurochem. *75*, 889-907.

24. Cass,W.A., Gerhardt,G.A., Zhang,Z., Ovadia,A., and Gash,D.M. (1995). Increased dopamine clearance in the non-lesioned striatum of rhesus monkeys with unilateral 1-methyl-4-phenyl-1,2,3,6-tetrahydropyridine (MPTP) striatal lesions. Neurosci.Lett. *185*, 52-55.

25. Cavus,I., Kasoff,W.S., Cassaday,M.P., Jacob,R., Gueorguieva,R., Sherwin,R.S., Krystal,J.H., Spencer,D.D., and Abi-Saab,W.M. (2005). Extracellular metabolites in the cortex and hippocampus of epileptic patients. Ann.Neurol. *57*, 226-235.

26. Centonze,D., Gubellini,P., Bernardi,G., and Calabresi,P. (1999). Permissive role of interneurons in corticostriatal synaptic plasticity. Brain Res.Brain Res.Rev. *31*, 1-5.

27. Clapp-Lilly,K.L., Roberts,R.C., Duffy,L.K., Irons,K.P., Hu,Y., and Drew,K.L. (1999). An ultrastructural analysis of tissue surrounding a microdialysis probe. J.Neurosci.Methods *90*, 129-142.

28. Cooper,J.R., Bloom,F.E., and Roth,R.H. (1996). The Biochemical Basis of Neuropharmacology, 7th ed. Oxford University Press, New York.

29. Cui,G., Kim,S.J., Choi,S.H., Nam,H., Cha,G.S., and Paeng,K.J. (2000). A disposable amperometric sensor screen printed on a nitrocellulose strip: a glucose biosensor employing lead oxide as an interference-removing agent. Anal.Chem. *72*, 1925-1929.

30. Danbolt,N.C. (2001). Glutamate uptake. Prog.Neurobiol. *65*, 1-105.

31. Deumens,R., Blokland,A., and Prickaerts,J. (2002). Modeling Parkinson's disease in rats: an evaluation of 6-OHDA lesions of the nigrostriatal pathway. Exp.Neurol. *175*, 303-317.

32. Dingeldine,R. and McBain,C.J. (1994). Excitatory Amino Acid Transmitters, in Basic Neurochemistry: Molecular, Cellular, and Medical Aspects, 5th ed. (Siegel,G.J., Agranoff,B.W., Albers,R.W.,, and Molinoff,P.B., eds), 367-387. Raven Press, Ltd., New York.

33. Drew,K.L., Pehek,E.A., Rasley,B.T., Ma,Y.L., and Green,T.K. (2004). Sampling glutamate and GABA with microdialysis: suggestions on how to get the dialysis membrane closer to the synapse. J.Neurosci.Methods *140*, 127-131.

34. During,M.J. and Spencer,D.D. (1993). Extracellular hippocampal glutamate and spontaneous seizure in the conscious human brain. Lancet *341*, 1607-1610.

35. Engel,J., Jr. (1998). Research on the human brain in an epilepsy surgery setting. Epilepsy Res. *32*, 1-11.

36. Eskandar,E.N., Shinobu,L.A., Penney,J.B., Jr., Cosgrove,G.R., and Counihan,T.J. (2000). Stereotactic pallidotomy performed without using microelectrode guidance in patients with Parkinson's disease: surgical technique and 2-year results. J.Neurosurg. *92*, 375-383.

37. Feldman,R.S., Meyer,J.S., and Quenzer,L.F. (1997). The Amino Acid Neurotransmitters and Histamine, in Principles of Neuropsychopharmacology, 391-454. Sinauer Associates, Inc., Sunderland, MA.

38. Fillenz,M. (1995). Physiological release of excitatory amino acids. Behav.Brain Res. *71*, 51-67.

39. Foster,T.C. and Kumar,A. (2002). Calcium dysregulation in the aging brain. Neuroscientist. *8*, 297-301.

40. Fried,I., Wilson,C.L., Maidment,N.T., Engel,J., Jr., Behnke,E., Fields,T.A., MacDonald,K.A., Morrow,J.W., and Ackerson,L. (1999). Cerebral microdialysis combined with single-neuron and electroencephalographic recording in neurosurgical patients. Technical note. J.Neurosurg. *91*, 697-705.

41. Friedemann,M.N. and Gerhardt,G.A. (1992). Regional effects of aging on dopaminergic function in the Fischer-344 rat. Neurobiol.Aging *13*, 325-332.

42. Friedemann,M.N. and Gerhardt,G.A. (1996). In vivo electrochemical studies of the dynamic effects of locally applied excitatory amino acids in the striatum of the anesthetized rat. Exp.Neurol. *138*, 53-63.

43. Gerhardt,G.A., Oke,A.F., Nagy,G., Moghaddam,B., and Adams,R.N. (1984). Nafion-coated electrodes with high selectivity for CNS electrochemistry. Brain Res. *290*, 390-395.

44. Gerhardt,G.A., Rose,G.M., and Hoffer,B.J. (1986). Release of monoamines from striatum of rat and mouse evoked by local application of potassium: evaluation of a new in vivo electrochemical technique. J.Neurochem. *46*, 842-850.

45. Gerhardt,G.A., Cass,W.A., Henson,M., Zhang,Z., Ovadia,A., Hoffer,B.J., and Gash,D.M. (1995). Age-related changes in potassium-evoked overflow of dopamine in the striatum of the rhesus monkey. Neurobiol.Aging *16*, 939-946.

46. Gerhardt,G.A. and Burmeister,J.J. (2000). In Vivo Voltammetry for Chemical Analysis of the Nervous System, in Encyclopedia of Analytical Chemistry: Instrumentation and Applications, (Meyers,R.A., ed), 710-731. John Wiley & Sons, Ltd., Chichester.

47. Glowinski,J., Besson,M.J., and Cheramy,A. (1984). Role of the Thalamus in the Bilateral Regulation of Dopaminergic and Gabaergic Neurons in the Basal Ganglia. Ciba Foundation Symposia *107*, 150-163.

48. Gorji,A., Hohling,J.M., Madeja,M., Straub,H., Kohling,R., Tuxhorn,I., Ebner,A., Wolf,P., Panneck,H.W., Behne,F., Lahl,R., and Speckmann,E.J. (2002). Effect of levetiracetam on epileptiform discharges in human neocortical slices. Epilepsia *43*, 1480-1487.

49. Granholm,A.C., Mott,J.L., Bowenkamp,K., Eken,S., Henry,S., Hoffer,B.J., Lapchak,P.A., Palmer,M.R., van Horne,C., and Gerhardt,G.A. (1997). Glial cell line-derived neurotrophic factor improves survival of ventral mesencephalic grafts to the 6-hydroxydopamine lesioned striatum. Exp.Brain Res. *116*, 29-38.

50. Greenamyre,J.T. (2001). Glutamatergic influences on the basal ganglia. Clin.Neuropharmacol. *24*, 65-70.

51. Guilbault,G.G. and Hrabankova,E. (1970). An electrode for determination of amino acids. Anal.Chem. *42*, 1779-1783.

52. Guridi,J., Rodriguez-Oroz,M.C., Lozano,A.M., Moro,E., Albanese,A., Nuttin,B., Gybels,J., Ramos,E., and Obeso,J.A. (2000). Targeting the basal ganglia for deep brain stimulation in Parkinson's disease. Neurology *55*, S21-S28.

53. Harman,D. (1956). Aging: a theory based on free radical and radiation chemistry. J.Gerontol. *11*, 298-300.

54. Herrera-Marschitz,M., You,Z.B., Goiny,M., Meana,J.J., Silveira,R., Godukhin,O.V., Chen,Y., Espinoza,S., Pettersson,E., Loidl,C.F., Lubec,G., Andersson,K., Nylander,I., Terenius,L., and Ungerstedt,U. (1996). On the origin of extracellular glutamate levels monitored in the basal ganglia of the rat by in vivo microdialysis. J.Neurochem. *66*, 1726-1735.

55. Hu,Y., Mitchell,K.M., Albahadily,F.N., Michaelis,E.K., and Wilson,G.S. (1994). Direct measurement of glutamate release in the brain using a dual enzyme-based electrochemical sensor. Brain Res. *659*, 117-125.

56. Hudson,J.L., van Horne,C.G., Stromberg,I., Brock,S., Clayton,J., Masserano,J., Hoffer,B.J., and Gerhardt,G.A. (1993). Correlation of apomorphine- and amphetamine-induced turning with nigrostriatal dopamine content in unilateral 6-hydroxydopamine lesioned rats. Brain Res. *626*, 167-174.

57. Hudspith,M.J. (1997). Glutamate: a role in normal brain function, anaesthesia, analgesia and CNS injury. Br.J.Anaesth. *78*, 731-747.

58. Kajihara,T. and Hagihara,B. (1966). [Serum glucose measurement by oxygen electrode and glucose oxidase]. Rinsho Byori *14*, 322-327.

59. Kennedy,R.T., Watson,C.J., Haskins,W.E., Powell,D.H., and Strecker,R.E. (2002). In vivo neurochemical monitoring by microdialysis and capillary separations. Curr.Opin.Chem.Biol. *6*, 659-665.

60. Khan,S.H. and Shuaib,A. (2001). The technique of intracerebral microdialysis. Methods *23*, 3-9.

61. Kim,R. and Spencer,D. (1994). Surgery for Mesial Temporal Sclerosis, in The Surgical Management of Epilepsy (Wyler,A.R. and Hermann,B.P., eds), 1436-1444. Butterworth-Heinemann, Boston.

62. Kish,L.J., Palmer,M.R., and Gerhardt,G.A. (1999). Multiple single-unit recordings in the striatum of freely moving animals: effects of apomorphine and D-amphetamine in normal and unilateral 6-hydroxydopamine-lesioned rats. Brain Res. *833*, 58-70.

63. Korenbrot,J.I., Perry,R., and Copenhagen,D.R. (1987). Development and characterization of a polymer gel with an immobilized enzyme to measure L-glutamate. Anal.Biochem. *161*, 187-199.

64. Krack,P., Poepping,M., Weinert,D., Schrader,B., and Deuschl,G. (2000). Thalamic, pallidal, or subthalamic surgery for Parkinson's disease? J.Neurol. *247 Suppl 2*, II122-II134.

65. Krauss,J.K. and Jankovic,J. (1996). Surgical treatment of Parkinson's disease. Am.Fam.Physician *54*, 1621-1629.

66. Kulagina,N.V., Shankar,L., and Michael,A.C. (1999). Monitoring glutamate and ascorbate in the extracellular space of brain tissue with electrochemical microsensors. Anal.Chem. *71*, 5093-5100.

67. Kusakabe,H., Midorikawa,Y., Fujishima,T., Kuninaka,A., and Yoshino,H. (1983). Purification and Properties of A New Enzyme, L-Glutamate Oxidase, from Streptomyces Sp X-119-6 Grown on Wheat Bran. Agricultural and Biological Chemistry *47*, 1323-1328.

68. Lada,M.W., Vickroy,T.W., and Kennedy,R.T. (1997). High temporal resolution monitoring of glutamate and aspartate in vivo using microdialysis on-line with capillary electrophoresis with laser-induced fluorescence detection. Anal.Chem. *69*, 4560-4565.

69. Lada,M.W., Vickroy,T.W., and Kennedy,R.T. (1998). Evidence for neuronal origin and metabotropic receptor-mediated regulation of extracellular glutamate and aspartate in rat striatum in vivo following electrical stimulation of the prefrontal cortex. J.Neurochem. *70*, 617-625.

70. Lancia,A.J., Williams,E.A., McKnight,L.V., and Zahm,D.S. (2004). Vulnerabilities of ventral mesencephalic neurons projecting to the nucleus accumbens following infusions of 6-hydroxydopamine into the medial forebrain bundle in the rat. Brain Res. *997*, 119-127.

71. Lang,A.E. and Lozano,A.M. (1998). Parkinson's disease. First of two parts. N.Engl.J.Med. *339*, 1044-1053.

72. Lei,W., Jiao,Y., Del Mar,N., and Reiner,A. (2004). Evidence for differential cortical input to direct pathway versus indirect pathway striatal projection neurons in rats. J.Neurosci. *24*, 8289-8299.

73. Lindefors,N. and Ungerstedt,U. (1990). Bilateral regulation of glutamate tissue and extracellular levels in caudate-putamen by midbrain dopamine neurons. Neurosci.Lett. *115*, 248-252.

74. Linnane,A.W., Marzuki,S., Ozawa,T., and Tanaka,M. (1989). Mitochondrial DNA mutations as an important contributor to ageing and degenerative diseases. Lancet *1*, 642-645.

75. Liu,Z., Stafstrom,C.E., Sarkisian,M., Tandon,P., Yang,Y., Hori,A., and Holmes,G.L. (1996). Age-dependent effects of glutamate toxicity in the hippocampus. Brain Res.Dev.Brain Res. *97*, 178-184.

76. Marino,M.J., Awad,H., Poisik,O., Wittmann,M., and Conn,P.J. (2002). Localization and physiological roles of metabotropic glutamate receptors in the direct and indirect pathways of the basal ganglia. Amino Acids *23*, 185-191.

77. McCarthy,G., Spencer,D.D., and Riker,R.J. (1991). The Stereotaxic Placement of Depth Electrodes in Epilepsy, in Epilepsy Surgery (Luders,H., ed), 385-393. Raven Press, Ltd., New York.

78. Meldrum,B.S., Akbar,M.T., and Chapman,A.G. (1999). Glutamate receptors and transporters in genetic and acquired models of epilepsy. Epilepsy Res. *36*, 189-204.

79. Meldrum,B.S. (2000). Glutamate as a neurotransmitter in the brain: Review of physiology and pathology. Journal of Nutrition *130*, 1007S-1015S.

80. Meshul,C.K., Emre,N., Nakamura,C.M., Allen,C., Donohue,M.K., and Buckman,J.F. (1999). Time-dependent changes in striatal glutamate synapses following a 6-hydroxydopamine lesion. Neuroscience *88* , 1-16.

81. Michaelis,E.K. (1998). Molecular biology of glutamate receptors in the central nervous system and their role in excitotoxicity, oxidative stress and aging. Progress in Neurobiology *54*, 369-415.

82. Mitchell,I.J., Cooper,A.J., and Griffiths,M.R. (1999). The selective vulnerability of striatopallidal neurons. Prog.Neurobiol. *59*, 691-719.

83. Molina,H., Quinones-Molina,R., Munoz,J., Alvarez,L., Alaminos,A., Ortega,I., Ohye,C., Macias,R., Piedra,J., Gonzalez,C., and . (1994). Neurotransplantation in Parkinson's disease: from open microsurgery to bilateral stereotactic approach: first clinical trial using microelectrode recording technique. Stereotact.Funct.Neurosurg. *62*, 204-208.

84. Nakanishi,S. (1992). Molecular diversity of glutamate receptors and implications for brain function. Science *258*, 597-603.

85. Nickell,J., Pomerleau,F., Allen,J., and Gerhardt,G.A. (2005). Age-related changes in the dynamics of potassium-evoked L-glutamate release in the striatum of Fischer 344 rats. J.Neural Transm. *112*, 87-96.

86. Nieoullon,A., Cheramy,A., and Glowinski,J. (1977). Interdependence of the nigrostriatal dopaminergic systems on the two sides of the brain in the cat. Science *198*, 416-418.

87. Obrenovitch,T.P. and Zilkha,E. (2001). Microdialysis coupled to online enzymatic assays. Methods *23*, 63-71.

88. Olanow,C.W., Brin,M.F., and Obeso,J.A. (2000). The role of deep brain stimulation as a surgical treatment for Parkinson's disease. Neurology *55*, S60-S66.

89. Olivier,A. and Boling,Jr.,W. (1994). Stereotactic Intracranial Recording (Stereoelectroencephalography), in The Surgical Management of Epilepsy (Wyler,A.R. and Hermann,B.P., eds), 1511-1528. Butterworth-Heinemann, Boston.

90. Ozawa,T. (1997). Genetic and functional changes in mitochondria associated with aging. Physiol Rev. *77*, 425-464.

91. Paxinos,G. and Watson,C. (1986). The Rat Brain in Stereotaxic Coordinates. Academic Press, San Diego.

92. Parikh,V., Pomerleau,F., Huettl,P., Gerhardt,G.A., Sarter,M., and Bruno,J.P. (2004). Rapid assessment of in vivo cholinergic transmission by amperometric detection of changes in extracellular choline levels. Eur.J.Neurosci. *20*, 1545-1554.

93. Perese,D.A., Ulman,J., Viola,J., Ewing,S.E., and Bankiewicz,K.S. (1989). A 6-hydroxydopamine-induced selective parkinsonian rat model. Brain Res. *494*, 285-293.

94. Pollak,P., Krack,P., Fraix,V., Mendes,A., Moro,E., Chabardes,S., and Benabid,A.L. (2002). Intraoperative micro- and macrostimulation of the subthalamic nucleus in Parkinson's disease. Mov Disord. *17 Suppl 3*, S155-S161.

95. Pomerleau,F., Day,B.K., Huettl,P., Burmeister,J.J., and Gerhardt,G.A. (2003). Real time in vivo measures of L-glutamate in the rat central nervous system using ceramic-based multisite microelectrode arrays. Ann.N.Y.Acad.Sci. *1003*, 454-457.

96. Qu,Y., Arckens,L., Vandenbussche,E., Geeraerts,S., and Vandesande,F. (1998). Simultaneous determination of total and extracellular concentrations of the amino acid neurotransmitters in cat visual cortex by microbore liquid chromatography and electrochemical detection. J.Chromatogr.A *798*, 19-26.

97. Qureshi,A.I., Ali,Z., Suri,M.F., Shuaib,A., Baker,G., Todd,K., Guterman,L.R., and Hopkins,L.N. (2003). Extracellular glutamate and other amino acids in experimental intracerebral hemorrhage: an in vivo microdialysis study. Crit Care Med. *31*, 1482-1489.

98. Reader,T.A. and Dewar,K.M. (1999). Effects of denervation and hyperinnervation on dopamine and serotonin systems in the rat neostriatum: implications for human Parkinson's disease. Neurochem.Int. *34*, 1-21.

99. Recht,L.D. and Bernstein,M. (1995). Low-grade gliomas. Neurol.Clin. *13*, 847-859.

100. Reiner,A., Jiao,Y., Del Mar,N., Laverghetta,A.V., and Lei,W.L. (2003). Differential morphology of pyramidal tract-type and intratelencephalically projecting-type corticostriatal neurons and their intrastriatal terminals in rats. J.Comp Neurol. *457*, 420-440.

101. Riedel,G., Platt,B., and Micheau,J. (2003). Glutamate receptor function in learning and memory. Behavioural Brain Research *140*, 1-47.

102. Robinson,D.L., Venton,B.J., Heien,M.L., and Wightman,R.M. (2003). Detecting subsecond dopamine release with fast-scan cyclic voltammetry in vivo. Clin.Chem. *49*, 1763-1773.

103. Ronne-Engstrom,E., Hillered,L., Flink,R., Spannare,B., Ungerstedt,U., and Carlson,H. (1992). Intracerebral microdialysis of extracellular amino acids in the human epileptic focus. J.Cereb.Blood Flow Metab *12*, 873-876.

104. Roslin,M., Henriksson,R., Bergstrom,P., Ungerstedt,U., and Bergenheim,A.T. (2003). Baseline levels of glucose metabolites, glutamate and glycerol in malignant glioma assessed by stereotactic microdialysis. J.Neurooncol. *61*, 151-160.

105. Rossell,S., Gonzalez,L.E., and Hernandez,L. (2003). One-second time resolution brain microdialysis in fully awake rats. Protocol for the collection, separation and sorting of nanoliter dialysate volumes. J.Chromatogr.B Analyt.Technol.Biomed.Life Sci. *784*, 385-393.

106. Roth,G.S., Ingram,D.K., and Lane,M.A. (2001). Caloric restriction in primates and relevance to humans. Ann.N.Y.Acad.Sci. *928*, 305-315.

107. Rowley,H.L., Martin,K.F., and Marsden,C.A. (1995). Determination of in vivo amino acid neurotransmitters by high-performance liquid chromatography with o-phthalaldehyde-sulphite derivatisation. J.Neurosci.Methods *57*, 93-99.

108. Schober,A. (2004). Classic toxin-induced animal models of Parkinson's disease: 6-OHDA and MPTP. Cell Tissue Res. *318*, 215-224.

109. Segovia,G., Porras,A., Del Arco,A., and Mora,F. (2001). Glutamatergic neurotransmission in aging: a critical perspective. Mech.Ageing Dev. *122*, 1-29.

110. Shigeri,Y., Shimamoto,K., Yasuda-Kamatani,Y., Seal,R.P., Yumoto,N., Nakajima,T., and Amara,S.G. (2001). Effects of threo-beta-hydroxyaspartate derivatives on excitatory amino acid transporters (EAAT4 and EAAT5). J.Neurochem. *79*, 297-302.

111. Shimamoto,K., Lebrun,B., Yasuda-Kamatani,Y., Sakaitani,M., Shigeri,Y., Yumoto,N., and Nakajima,T. (1998). DL-threo-beta-benzyloxyaspartate, a potent blocker of excitatory amino acid transporters. Mol.Pharmacol. *53*, 195-201.

112. Shiraishi,M., Kamiyama,Y., Huttemeier,P.C., and Benveniste,H. (1997). Extracellular glutamate and dopamine measured by microdialysis in the rat striatum during blockade of synaptic transmission in anesthetized and awake rats. Brain Res. *759*, 221-227.

113. Smolders,I., Sarre,S., Michotte,Y., and Ebinger,G. (1995). The analysis of excitatory, inhibitory and other amino acids in rat brain microdialysates using microbore liquid chromatography. J.Neurosci.Methods *57*, 47-53.

114. Somjen,G.G. (2001). Mechanisms of spreading depression and hypoxic spreading depression-like depolarization. Physiol Rev. *81*, 1065-1096.

115. Spencer,D.D., Robbins,R.J., Naftolin,F., Marek,K.L., Vollmer,T., Leranth,C., Roth,R.H., Price,L.H., Gjedde,A., Bunney,B.S., and . (1992). Unilateral transplantation of human fetal mesencephalic tissue into the caudate nucleus of patients with Parkinson's disease. N.Engl.J.Med. *327*, 1541-1548.

116. Sreenivas,G., Ang,S.S., Fritsch,I., Brown,W.D., Gerhardt,G.A., and Woodward,D.J. (1996). Fabrication and characterization of sputtered-carbon microelectrode arrays. Analytical Chemistry *68*, 1858-1864.

117. Starr,M.S. (1995). Glutamate/dopamine D1/D2 balance in the basal ganglia and its relevance to Parkinson's disease. Synapse *19*, 264-293.

118. Starr,P.A., Vitek,J.L., and Bakay,R.A. (1998). Ablative surgery and deep brain stimulation for Parkinson's disease. Neurosurgery *43*, 989-1013.

119. Tamiya,E. and Karube,I. (1992). Ultramicrobiosensors for monitoring of neurotransmitters. Ann.N.Y.Acad.Sci. *672*, 272-277.

120. Thomas,P.M., Phillips,J.P., Delanty,N., and O'Connor,W.T. (2003). Elevated extracellular levels of glutamate, aspartate and gamma-aminobutyric acid within the intraoperative, spontaneously epileptiform human hippocampus. Epilepsy Res. *54*, 73-79.

121. Timmerman,W. and Westerink,B.H. (1997). Brain microdialysis of GABA and glutamate: what does it signify? Synapse *27*, 242-261.

122. Tossman,U., Segovia,J., and Ungerstedt,U. (1986). Extracellular levels of amino acids in striatum and globus pallidus of 6-hydroxydopamine-lesioned rats measured with microdialysis. Acta Physiol Scand. *127*, 547-551.

123. Tucci,S., Rada,P., Sepulveda,M.J., and Hernandez,L. (1997). Glutamate measured by 6-s resolution brain microdialysis: capillary electrophoretic and laser-induced fluorescence detection application. J.Chromatogr.B Biomed.Sci.Appl. *694*, 343-349.

124. Unger,J.W. (1998). Glial reaction in aging and Alzheimer's disease. Microsc.Res.Tech. *43*, 24-28.

125. Updike,S.J. and Hicks,G.P. (1967). The enzyme electrode. Nature *214*, 986-988.

126. Watkins,J.C. (2000). L-glutamate as a central neurotransmitter: looking back. Biochem.Soc.Trans. *28*, 297-309.

127. Wichmann,T. and DeLong,M.R. (2003). Pathophysiology of Parkinson's disease: the MPTP primate model of the human disorder. Ann.N.Y.Acad.Sci. *991*, 199-213.

128. Wilson,C.L., Maidment,N.T., Shomer,M.H., Behnke,E.J., Ackerson,L., Fried,I., and Engel,J., Jr. (1996). Comparison of seizure related amino acid release in human epileptic hippocampus versus a chronic, kainate rat model of hippocampal epilepsy. Epilepsy Res. *26*, 245-254.

129. Wyler,A.R. and Abson-Kraemer,D. (1994). Diagnostic Techniques in Surgical Management of Epilepsy: Strip Electrodes, Grids, and Depth Electrodes, in The Surgical Management of Epilepsy (Wyler,A.R. and Hermann,B.P., eds), 1429-1435. Butterworth-Heinemann, Boston.

130. Zhang,S., Takeda,Y., Hagioka,S., Takata,K., Aoe,H., Nakatsuka,H., Yokoyama,M., and Morita,K. (2005). Measurement of GABA and glutamate in vivo levels with high sensitivity and frequency. Brain Res.Brain Res.Protoc. *14*, 61-66.

VITA

Name:	Brian Keith Day
Birthdate:	07/19/1975
Birthplace:	Lexington, KY

Education

Fall 1999- Spring 2007	MD/PhD Candidate, University of Kentucky Lexington, KY 40536
Fall 2001- Summer 2005	Doctoral degree candidate Department of Anatomy and Neurobiology The Graduate School at the University of Kentucky
Fall 1999- Spring 2007	Medical degree candidate University of Kentucky College of Medicine
1997	AB in Biology, *Cum Laude*, Harvard University Cambridge, MA 02138
1993	Commonwealth Diploma, Boyle County High School Danville, KY 40422

Professional Positions Held

1997-1999	Head Research Associate and Laboratory Coordinator; Uniformed Services University, Bethesda, MD 20814 Geoffrey S. F. Ling, MD, PhD, Principal Investigator
1996-1997	Student researcher, Farlow Herbarium, Harvard University Donald Pfister, PhD, Supervisor
1996	Summer research associate, Department of Entomology, University of Kentucky David Wise, PhD, Supervisor

Scholastic and Professional Honors

January 2005- June 2005	Graduate Student Representative, Program in Translational Neurosciences, Department of Anatomy and Neurobiology, University of Kentucky Don M. Gash, Ph.D., Chairman
July 2004- June 2005	Morris K. Udall Fellowship, University of Kentucky, Morris K. Udall Parkinson's Disease Research Center of Excellence Greg A. Gerhardt, PhD, Director
October 2004	Invited speaker, Frontiers in Neuroscience Symposium, University of Kentucky "L-Glutamate Dynamics in the Young and Aged Brain"
March 2004	Graduate student poster award, Bluegrass Chapter, Society for Neurosciences

July 2003- June 2004	Research Challenge Trust Fund Fellowship, University of Kentucky
March 2002	Graduate student poster award, Bluegrass Chapter, Society for Neurosciences
August 2001- June 2003	Morris K. Udall Fellowship, University of Kentucky, Morris K. Udall Parkinson's Disease Research Center of Excellence
1999-2007	MD/PhD scholarship, University of Kentucky MD/PhD Program, E. Charles Snow, PhD, Director
1993-1997	Parker Browne Francis Scholarship Roy Goodman Scholarship Harvard College Scholarship Robert C. Byrd Scholarship Brotherhood Relief and Compensation Fund Scholarship WalMart Scholarship

Publications

Abstracts:

Day BK, Stephens ML, Quintero JE, Huettl P, Grondin R, Zhang Z, Luan L, Gash DM, and Gerhardt GA. Second-by-second L-glutamate measurements in cortical areas of young and aged rhesus monkeys. Annual Meeting, Society for Neurosciences, Washingotn, DC. November 2005.

Day BK, Pomerleau F, Huettl P, and Gerhardt GA. Basal measurements of L-glutamate using microelectrode arrays in the anesthetized rat brain. Annual Meeting, Society for Neurosciences, San Diego, CA. October 2004.

Day BK, Pomerleau F, Huettl P, and Gerhardt GA. Basal measurements of L-glutamate using microelectrode arrays in the anesthetized rat brain. Frontiers in Neurosciences Symposium, University of Kentucky, Lexington, KY. October 2004.

Day BK, Pomerleau FP, Huettl PF, Willis L, Granholm AC, and Gerhardt GA. Potassium-evoked glutamate release is affected bilaterally in the striatum of unilateral 6-OHDA-lesioned rats. National M.D./Ph.D. Student Conference, Keystone, CO. July 2004.

Day BK, Pomerleau FP, Huettl PF, Willis L, Granholm AC, and Gerhardt GA. Potassium-evoked glutamate release is affected bilaterally in the striatum of unilateral 6-OHDA-lesioned rats. Spring Neurosciences Day, Bluegrass Chapter, Society for Neurosciences, Lexington, KY. March 2004.

Day BK, Pomerleau FP, Huettl PF, Willis L, Granholm AC, and Gerhardt GA. Potassium-evoked glutamate release is affected bilaterally in the striatum of unilateral 6-OHDA-lesioned rats. Annual Meeting, Society for Neurosciences, New Orleans, LA. November 2003.

Day BK, Pomerleau FP, Huettl PF, Burmeister JJ, and Gerhardt GA. Pharmacological manipulation of baseline levels of L-glutamate in CNS measured using ceramic-based multisite microelectrodes. Spring Neurosciences Day, Bluegrass Chapter, Society for Neurosciences. Spring 2003.

Day BK, Pomerleau FP, Huettl PF, Burmeister JJ, and Gerhardt GA. Pharmacological manipulation of baseline levels of L-glutamate in CNS measured using ceramic-based multisite microelectrodes. Annual Meeting of the Society for Neurosciences, Orlando, FL. November 2002.

Day BK, Gerhardt GA, Huettl PF, Pomerleau FP, Palmer, MR and Burmeister JJ. Rapid measures of the dynamics of glutamate release and uptake in the rat CNS. Spring Neurosciences Day, Bluegrass Chapter, Society for Neurosciences, Lexington, KY. Spring 2002.

Manuscripts:

Day BK, Pomerleau F, Burmeister JJ, Huettl P, and Gerhardt GA. Microelectrode array studies of basal and potassium-evoked release of L-glutamate in the anesthetized rat brain. (submitted 2005).

Pomerleau F, Day BK, Huettl P, Burmeister JJ, and Gerhardt GA. Real time in vivo measures of L-glutamate in the rat central nervous system using ceramic-based multisite microelectrode arrays. Ann. N.Y. Acad. Sci. 1003:454-457, 2003.

Burmeister, JJ, Pomerleau F, Palmer M, Day BK, Huettl P and Gerhardt GA. Improved ceramic-based multisite microelectrode for rapid measurements of L-glutamate in the CNS. J Neurosci Meth 119(2):163-171, 2002.

Signed: Brian Keith Day